materials

MDPI

Review

Alanates, a Comprehensive Review

Karina Suárez-Alcántara *, Juan Rogelio Tena-Garcia and Ricardo Guerrero-Ortiz

Morelia Unit of Materials Institute Research, National Autonomus University of Mexico, 58190 Mexico City, Mexico

* Correspondence: karina_suarez@iim.unam.mx; Tel.: +52-55-5623-7300 (ext. 37889)

Received: 22 July 2019; Accepted: 21 August 2019; Published: 25 August 2019

Abstract: Hydrogen storage is widely recognized as one of the biggest not solved problem within hydrogen technologies. The slow development of the materials and systems for hydrogen storage has resulted in a slow spread of hydrogen applications. There are many families of materials that can store hydrogen; among them, the alanate family can be of interest. Basic research papers and reviews have been focused on alanates of group 1 and 2. However, there are many alanates of transition metals, main group, and lanthanides that deserve attention in a review. This work is a comprehensive compilation of all known alanates. The approaches towards tuning the kinetics and thermodynamics of alanates are also covered in this review. These approaches are the formation of reactive composites, double cation alanates, or anion substitution. The crystallographic and X-ray diffraction characteristics of each alanate are presented along with this review. In the final sections, a discussion of the infrared, Raman, and thermodynamics was included.

Keywords: alanates; metal aluminum hydrides; mechanical-milling; hydrogen storage

1. Introduction

Hydrogen storage in solid materials is a relatively new branch of hydrogen technologies. It started during the '60s of the last century with the systematic study of TiFe alloys and Mg [1–3]. The studies on hydrogen storage flourished with the spread of the use of mechanical milling to produce materials or precursors that exhibited improved properties regarding kinetics or thermodynamics [4–6]. Another breakthrough was the discovery that certain Ti-compounds made the hydrogen storage/release reversible in $NaAlH_4$ [7,8]. Certainly, there are numerous materials that are potentially useful in hydrogen storage. Among them, the family of alanates stands out because of the high hydrogen content, rich chemistry, and the possibility of reversible storage [9]. Alanates (or aluminohydrides) are robust materials; some of them are so well known that prototypes of storage tanks had been constructed (i.e., $NaAlH_4$) [10–12]. Others, such as $Ti(AlH_4)_4$ or $Zr(AlH_4)_4$, are barely known in terms of crystal structure or thermodynamics [13,14]. Figure 1 presents a "periodic table" of the known alanates with dehydrogenation temperatures.

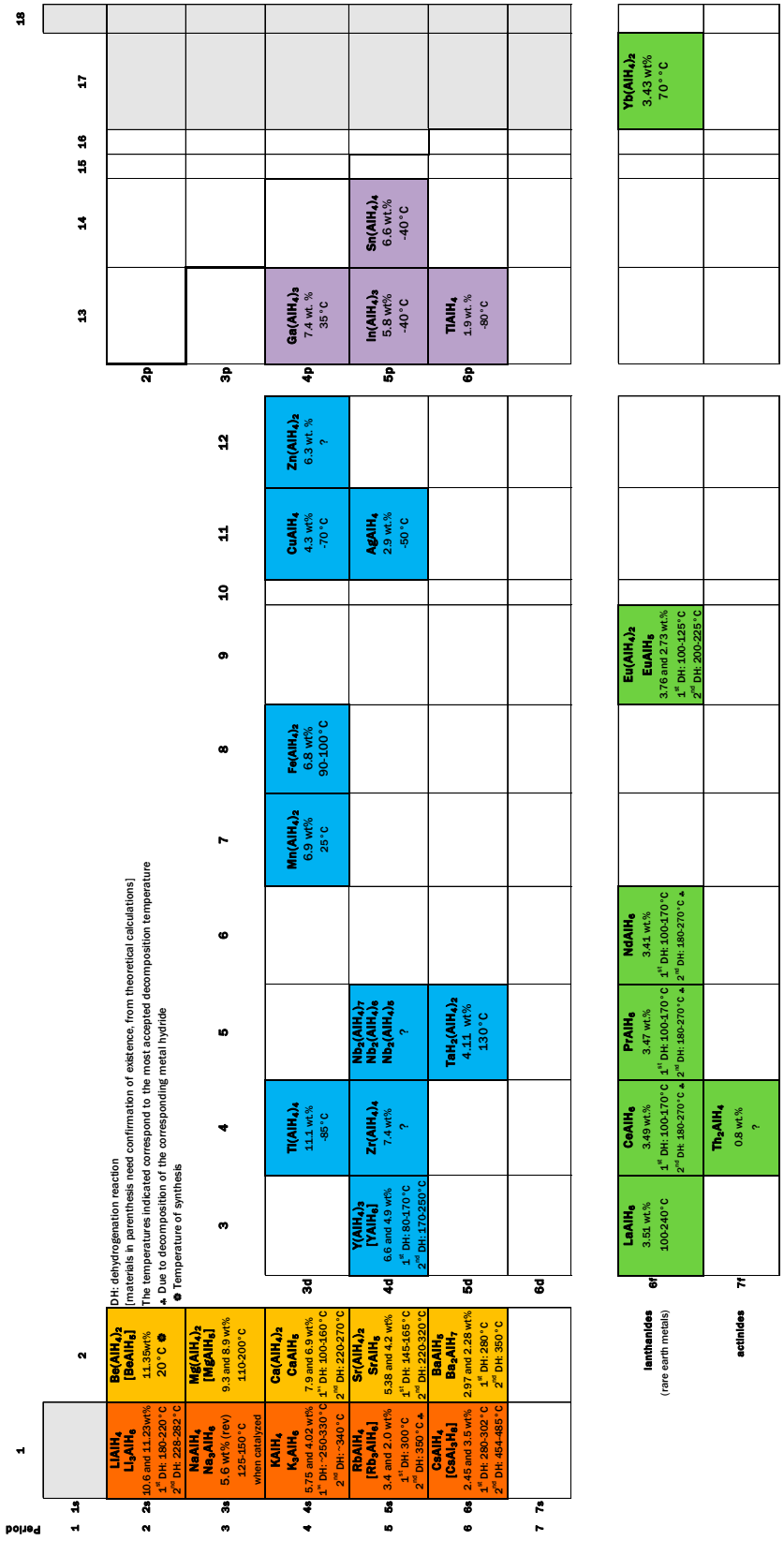

Figure 1. Periodic table of alanates. The reported alanates were collected in this "periodic table".

Alanates are like other hydrogen storage materials, in the sense that no material fulfills all of the requirements of hydrogen capacity, dehydrogenation temperatures, or reversibility. The DOE

(Department of Energy, USA [15]) had proposed along several decades the figures of merit for hydrogen storage materials and systems, specifying the type of applications (portable, light-duty vehicles, etc.). In general, high hydrogen storage capacity (6.5 wt.% [15]) and reversibility would prevail as the two fundamental characteristics of hydrogen storage materials. The exigencies of the DOE are very rigorous, particularly for light-duty vehicles applications [15], and they include (not limited to) the quantity of stored/released hydrogen (mass and volume of a complete system, 6.5 wt.% and 5 vol.%), reversibility, kinetics (optimum time to charge a hydrogen tank, 3–5 min), minimum number of cycles of hydrogen charge/discharge (1500), operational temperature (−40 to 85 °C), operational pressure (delivery pressure 5–12 bar), cost of the system (266 USD/kg H_2), safety, etc. Other factors to be careful with are the thermodynamics (related to the dehydrogenation temperature, but also to the quantity of heat added/removed to/from the system), the onboard efficiency (90%), etc. Moreover, in the future, factors such as recyclability, sustainability, or alanate production from recycled materials [16,17] must also be included as critical factors. However, niche applications for different applications [18] could be developed while using different hydrogen storage materials, including the alanates. These niche applications must meet the particular characteristics of the hydrogen production type and the needs of the final user [18,19]. Nonetheless, the alanate family would allow for the development of new materials. The present work covers the general synthesis procedures, structure, thermodynamics, and hydrogen storage capacity of the known alanates (whenever available). Additionally, double cation alanates or anion substituted materials are also presented and discussed. In the last part of the work, we present a compilation of IR (Infrared) spectroscopy, Raman spectroscopy, and thermodynamics data, along with some general tendencies.

2. General Syntheses Procedures

In this section, the synthesis routes are enumerated, describing them in a general way. Further along in this review, more details are presented for each particular alanate. However, all of the alanates have the need for protective atmospheres during handling, synthesis, and actual hydrogenation or dehydrogenation reactions in common. All of the the alanates can be classified as dangerous materials due to their flammability when exposed to oxygen or humidity. Definitely, they ignite and release hydrogen in contact with water, some more violently than others. Thus, great precautions and security measures must be taken when working with alanates.

2.1. Syntheses in Organic Solvents

2.1.1. Direct Synthesis

Alanates are frequently synthesized by the reaction of metals or metallic hydrides (e.g., NaH) with Al, H_2, and a catalyst in organic solvents, such as toluene, hexane, n-octane, ether, diglyme, ether, or tetrahydrofuran (THF) (Equations (1)–(4)) [20,21]. Frequently, a Ti-compound is used as a catalyst. Typically, an excess of Al is used. This method needs the use of moderate to high hydrogen pressure (100–150 bar) and moderate temperatures (120–150 °C); except for $LiAlH_4$, which requires a higher pressure (350 bar) [21]. This method can be considered to be highly dangerous due to the explosive mixture of organic solvents, metal hydride, and Al with oxygen and humidity. The materials thus produced require further steps of purification and drying. Frequently, the alanates are kept and sold in THF solution.

$$M + {}^1/_2\, H_2 \rightarrow MH, \quad (1)$$

$$MH + Al + 3/2\, H_2 \leftrightarrow MAlH_4,\ M = Li\ (\text{low conversion}),\ Na,\ K,\ Cs \quad (2)$$

Frequently, Equation (2) is expanded as a two-step reaction with M_3AlH_6 as an intermediary [22]:

$$MH + 1/3\ Al + 1/2\, H_2 \leftrightarrow 1/3\, M_3AlH_6, \text{ and} \quad (3)$$

$$1/3\ M_3AlH_6 + 2/3\ Al + H_2 \leftrightarrow MAlH_4 \quad (4)$$

2.1.2. Reaction of Metal Hydrides and Aluminum Salts

Another example of lithium alanate synthesis is the reaction of LiH with $AlCl_3$ in refluxing ether under an atmosphere of dry nitrogen [23]:

$$4LiH + AlCl_3 \rightarrow LiAlH_4 + 3LiCl. \quad (5)$$

This type of reaction is known as "the Schlesinger method". Despite the simplicity of this reaction, it requires the use of milled LiH (finer than 100 mesh). Additionally, this reaction requires an excess of LiH. Substitution of $AlCl_3$ by $AlBr_3$ can also be effective [24]. The same reaction outline of Equation (5) can be used with NaH or KH, and $AlCl_3$, to produce $NaAlH_4$ and $KAlH_4$, respectively [24]. However, these reactions need the use of $Al(C_2H_5)_3$ as a catalyst for the reaction with NaH, and C_6H_6-$(C_2H_5)_2O$ as the solvent; and $Al(C_2H_5)_3$ or $(i\text{-}C_4H_9)_2AlH$ as a catalyst for the reaction with KH [24].

The same type of reaction can be applied to M^{+2} alanates, such as $Mg(AlH_4)_2$ (Equation (6)) [25–27] or $Ca(AlH_4)_2$ [28], for example:

$$4MgH_2 + 2AlCl_3 \rightarrow Mg(AlH_4)_2 + 3MgCl_2. \quad (6)$$

No catalyst is used in the last example.

Some materials are obtained rather as THF adducts when this solvent is used [29]. Frequently, the THF adducts cannot be purified (elimination of THF) without the decomposition of the alanate. The use of protective atmospheres during synthesis can improve the yield of the reactions [29]. A general reaction could be described as:

$$nMH_x + xAlCl_3 \rightarrow M(AlH_4)_x + (n-1)MCl_x \quad (7)$$

Some of the references for this kind of synthesis are rather old. Initially, this synthesis procedure was not considered for hydrogen storage purposes.

2.1.3. Metathesis of Alanates

Several alanates having one cation or bi-cation have been produced by the metathesis reaction between $NaAlH_4$ or $LiAlH_4$ and metal halides in organic solvents, such as THF or Et_2O [30]. One practical reason for this is that $NaAlH_4$ and $LiAlH_4$ are the only commercially available alanates. This type of reaction dates back from 1950, from the work of Wiberg and Bauer [27], and the reaction can be summarized as:

$$nM1AlH_4 + M2X_n \rightarrow M2(AlH_4)_n + nM1X_n, \quad (8)$$

where M1 = Na or Li, M2 = Mg, Ca, or other metals, and X = Cl, Br, I [27,30,31].

Reactions of this type normally are conducted under refluxing conditions from cryogenic to room temperature for several hours or even days. The products usually are adducts of the solvent used, and subsequent operations of purification and drying are required.

2.2. Syntheses Assisted by Mechanical Milling

During the 80s of the last century, the mechanical milling sped up the development of hydrogen storage. We refer both to the study of materials (number of new materials), and the materials themselves towards the storage/release of hydrogen (kinetics of reactions) [5,6]. There are many parameters of mechanical milling. Figure 2 summarizes some of the most important ideas around the mechanical milling that are relevant for the hydrogen storage.

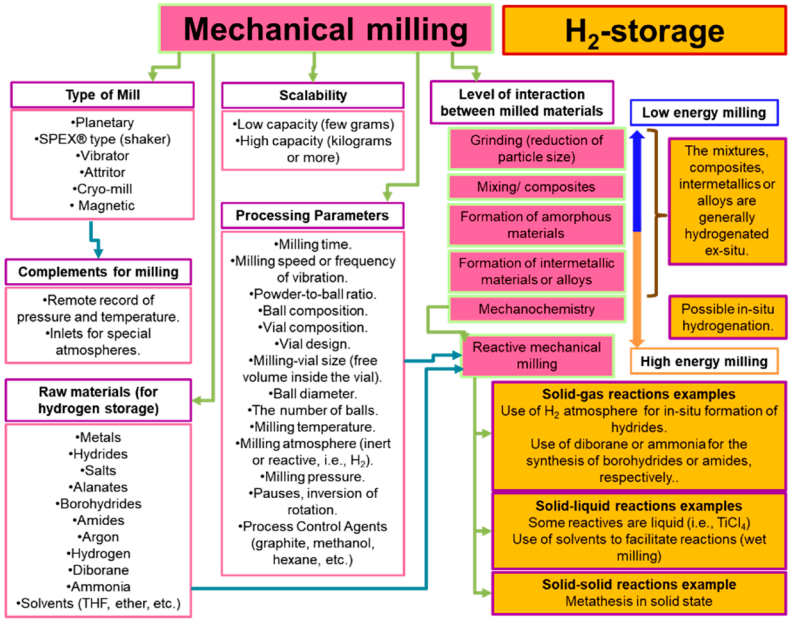

Figure 2. Mechanical milling main concepts.

By means of mechanical milling, the same reactions that are described in Section 2.1 can be performed. In most of the cases, the mechanically assisted reactions are faster than the same reactions in solvents. Additionally, the need for solvents is reduced or eliminated. However, some possible problems such as the elimination of side-products (purification) or the contamination by abrasion of balls and vials must be considered. The abrasion of the balls and vial can affect the performance of alanates. Although, an experienced "miller" will know that and would take actions to reduce contamination. These actions can be: (i) Not over-milling. Extended times of milling sometimes can be prejudicial by destroying the alanate, increasing the possibility of abrasion and is a waste of energy. (ii) Check the status of the balls and vial before every milling. (iii) Replace the balls and seals periodically. (iv) Keep the milling vial in good condition. (v) Use compatible materials; there are balls and vials of other materials beyond iron-alloys.

2.2.1. Direct Synthesis by Mechanical Milling

The mechanical milling of the corresponding metal hydride and aluminum and further ex-situ hydrogenation can produce some alanates. Or in-situ by means of a hydrogen atmosphere during the milling. In the ex-situ approach, the hydrogenation of the milled precursors is performed in a specialized reactor (Sieverts type apparatus) to complete Equations (1) and (2). The typical example is the $NaAlH_4$ synthesis by means of mechanical milling of NaH and Al, or Na and Al, and further hydrogenation facilitated by additives, dopants, or catalysts. In the in-situ approach (or reactive mechanical milling), the production of alanates can be attained by the solid-gas reaction between the metal hydride, aluminum, additives, and hydrogen. Again, the typical example is the one-step synthesis of $NaAlH_4$ [32]. The direct synthesis assisted by mechanical milling is an improvement towards "green chemistry", including solvent free-synthesis [33,34]. Despite the relative simplicity of this method, it is usually performed only in lab-scale for studies of hydrogen storage.

A third approach is the use of solvents (i.e.; wet ball milling) to obtain a precursor mixture of the alanate [35] or the alanate of interest if a hydrogen atmosphere is used. This methodology requires a drying step.

2.2.2. Reaction of Metal Hydrides and Aluminum Salts under Mechanical Milling

Few examples of Equation (7) by mechanical milling have been reported. This absence of data can be related to the instability of some alanates and the consequent difficulty of their synthesis. Among

the examples is the work of Hlova et al. [36–38]. They produced the reaction of LiH with $AlCl_3$ or NaH with $AlCl_3$ in several molar proportions, with the objective of forming AlH_3. Besides forming AlH_3, they formed mixtures of $LiAlH_4$-$LiAlCl_4$-Li_3AlH_6 or $NaAlH_4$-$NaAlCl_4$-Na_3AlH_6, respectively, under 345–350 bar of hydrogen pressure. In another example, Dymova et al. reacted $2MgH_2$-$AlCl_3$ to form $Mg(AlH_4)_2$ and $MgCl_2$ [39].

However, it must be considered that the mechanochemical version of Equation (5), and Equation (7), in general, or any similar reaction that involves hydrides or alanates plus aluminum salts, would compete with the formation of Al, for example [36]:

$$3MH + AlCl_3 \rightarrow Al + 3MCl + 1.5H_2, (M = Li, Na). \quad (9)$$

Milling under cryogenic conditions, i.e., with liquid-nitrogen cooling, could be effective in reducing Al formation.

2.2.3. Reaction of Metal Hydrides and Alane under Mechanical Milling

Another disadvantage of the reaction of metal hydrides and aluminum salts is the loss in hydrogen capacity. This is the result of the formation of salts, such as LiCl, NaCl, or $MgCl_2$, which usually are not separated from the products. Alternatively, to avoid the formation of these salts, a reaction of a metal hydride with AlH_3 has been proposed [40–42], for example:

$$MgH_2 + 2AlH_3 \rightarrow Mg(AlH_4)_2 \quad (10)$$

In some cases, the reaction did not go to completion, and the formation of intermediaries, such as $CaAlH_5$, was reported [41]. However, the general, complete, reaction would be:

$$MH_x + xAlH_3 \rightarrow M(AlH_4)_x \quad (11)$$

The main drawback of this synthesis method is that alane is not a commercial reagent, as such it must be produced in a preliminary step.

2.2.4. Metathesis of Alanates under Mechanical Milling

Several alanates have been produced by metathesis promoted by mechanical milling, Equation (8). Once the milling parameters are well established, this method can be very simple and has many advantages. The main advantages include (i) total elimination of solvents and (ii) significant reduction of the reaction time [43]. However, the main disadvantage is that the produced alanate is impure; the product of milling is a mixture of the alanate and salt. The final result is a drastic reduction of the hydrogen capacity. Examples are the production of $Mg(AlH_4)_2$-$2NaCl$ from $2NaAlH_4$-$MgCl_2$ [43], $Ca(AlH_4)_2$-$2LiCl$ from $2LiAlH_4$-$CaCl_2$ [40], or $Eu(AlH_4)_2$-$2NaCl$ from $EuCl_2$-$2NaAlH_4$ [44].

3. The "Single Metal" Alanates

In this section, experimental and theoretical "single metal" alanates are described. They are ordered in groups according to the periodic table. Alane was also included. At the end of this section, the binary (double cations) alanates are presented. Some of them are well-known, while others are barely developed. This section presents the essential characteristics of synthesis, dehydrogenation reactions, and temperatures, crystallographic data, crystal structures, expected X-ray diffraction patterns, and, in some cases, phase diagrams.

3.1. AlH_3

The aluminum hydride or alane is a material with high hydrogen content (10 wt.%). A 10 wt.% of hydrogen is very attractive; it meets the DOE targets of 6.5 wt.% of hydrogen for mobile applications. Even more, the low dehydrogenation temperature makes the alane, in principle, compatible with

polymer exchange membrane fuel cells (PEMFC) applications. AlH_3 is typically produced by the reaction of $LiAlH_4$ with $AlCl_3$ in an organic solvent, such as THF or Et_2O [45]:

$$3LiAlH_4 + AlCl_3 + nEt_2O \rightarrow 4AlH_3{\cdot}nEt_2O + 3LiCl\downarrow. \quad (12)$$

Instead of $LiAlH_4$, LiH was used in the early studies of this reaction [45]. The product is an adduct that must be separated from the solvent. An excess of $LiAlH_4$ or some $LiBH_4$ is added to the reaction mixture to improve the time and temperature of desolvation [45,46]. The solvent-free mechanosynthesis of AlD_3 was performed while using cryomilling $3LiAlD_4 + AlCl_3$ at a low temperature (−196 °C). This conditions eliminated the competing reaction towards the formation of Al and LiCl [47,48]. This synthesis allowed for the determination of the structures of α-AlD_3 and α'-AlD_3. Mechanical milling of $3LiAlH_4 + AlCl_3$ at room temperature also can produce the alane by using high pressures of hydrogen (210 bar) or inert gas (125 bar of He or 90 bar of Ar) [49]. Alternatively, the alane can be produced by the electrochemical reaction of $LiAlH_4$ or $NaAlH_4$ with or without LiCl as an electrocatalytic additive and with or without hydrogen atmosphere. The general reactions involved are [50–52]:

$$3AlH_4^- + Al + n\text{THF} \rightarrow 4AlH_3{\cdot}n\text{THF} + 3e^-, \text{ anode of Al} \quad (13)$$

$$3(M^+ PdH + e^- \rightarrow MH + Pd), \text{ cathode of Pd, } PdH_2 \quad (14)$$

According to reports, the alane has seven polymorphs, and here we present the four most frequently reported (Table 1) [46]. The energy of phase transition between these polymorphs is low: around −1 to −2 kJ/mol H_2; thus, the phase transitions occur spontaneously at room temperature (adding complications to the crystal structure determination) [53]. The common structure of the alanes is corner-shared (AlH_6) octahedra [54].

The reported formation enthalpy of alane is around −6 to −9 kJ/mol H_2; thus, an equilibrium pressure of the order of 10^5 bar at room temperature is expected [53]. However, the minimum hydrogen pressure, experimentally observed and calculated, which is necessary for the formation of the alane from the elements is about 7000 bar at room temperature [55]. Thus, on-board regeneration of alane for hydrogen storage in automotive applications is definitely out of the picture. Recently, a report on nanoconfined AlH_3 indicates partial re-hydrogenation at 150 °C and 60 bar [56]. Nanoconfinement reduces the hydrogen content; however, it must be explored as a way to reach reversibility.

Dehydrogenation enthalpies range from −5 to 6 kJ/mol H_2 for the different polymorphs [57], thus near room temperature decomposition would be expected. Dehydrogenation temperatures are observed in the range of 150–200 °C [53,58]; however, ball milling has reduced the dehydrogenation temperature below 100 °C [59]. Alane is considered as a metastable hydride, due to the formation of surface oxides, which protect against to further oxidation or decomposition. The surface oxides impose a kinetic barrier to decomposition [58,60]. In particular, for the alane, the passivation is somehow beneficial, reducing decomposition during its storage and handle in the laboratory. However, in general, passivating surface oxidation is a problem. It is challenging to reduce the oxygen and humidity content of protective atmospheres (argon) until acceptable values (<10 ppm) for hydrogen storage applications. This means that a hydrogen storage system that is based on alanates (and hydrides in general) must have proper filtering, trapping, or regenerative systems to reduce oxygen and humidity content, which can be costly. Ball milling of alane exposes new, fresh, and non-oxidized surfaces that improve the kinetics of the dehydrogenation reaction [61]. The dehydrogenation pathways, as proposed by Sartory et al., are presented in Figure 3 [62].

The thermal dehydrogenation of alane was improved by the use of simple hydrides, such as LiH [63]; otherwise, AlH_3 is useful in reducing dehydrogenation temperature or improving dehydrogenation kinetics when added to MgH_2 or $LiBH_4$ [64,65].

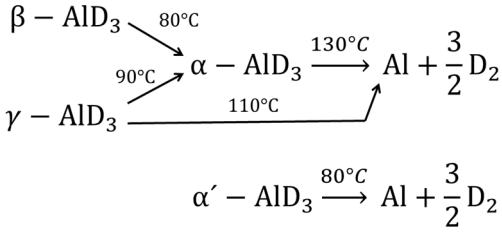

Figure 3. Dehydrogenation pathway of several deuterated alanes (adapted from [62]).

Table 1. Crystallographic data of alanes.

Compound	Space Group, Cell Dimensions [Å] and Angles [°]	Atomic Coordinates
α-AlD_3	*(R-3c)* No. 167 [66] a = 4.227; b = 4.227; c = 11.244 α = β = 90; γ = 120	Al: 0, 0, 0 D: 0.63, 0, 1/4
α′-AlD_3	*(Cmcm)* No. 63 [47] a = 6.470(3); b = 11.117(5); c = 6.562(2) α = β = 90; γ = 90	Al1: 0, 1/2, 0 Al2: 1/4, 1/4, 0 D1: 0, 0.197(2), 0.451(4) D2: 0.312(2), 0.1000(14), 0.047(3) D3: 0, 0.465(3), 1/4 D4: 0.298(4), 0.277(2), 1/4
β-AlD_3	*(Fd-3m)* No. 227 [67] a = 9.0037(1); b = 9.0037(1); c = 9.0037(1) α = β = γ = 90	Al1: 1/2, 0, 0 D1: 0.4301(1); 0.125; 0.125
γ-AlD_3	*(Pnnm)* No. 58 [68] a = 7.3360(3); b = 5.3672(2); c = 5.7562(1) α = β = γ = 90	Al1: 0, 0, 0 Al2: 0.4174(5), 0.7127(6), 0 D1: 0.2044(9), 0.8269(11), 0 D2: 0.3668(10), 0.3931(13), 0 D3: 0, 1/2, 1/2 D4: 0.4174(6), 0.7038(8), 0.3009(6)

In the present review, the crystal structures and the calculated X-ray diffraction powder patterns (powder cell 2.3 and mercury software 3.8) are presented for visual comparison. The first of them correspond to the alane polymorphs (Figure 4).

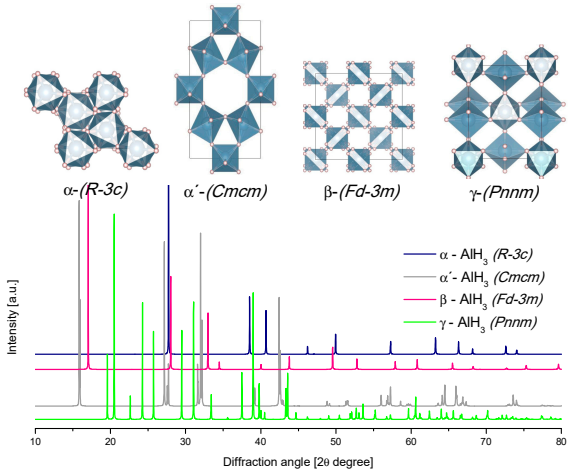

Figure 4. Crystal structure of several alanes and their calculated diffraction patterns (λ = $Cu_{k\alpha 1}$).

3.2. *Alanates of Group 1*

3.2.1. Lithium Alanate

The $LiAlH_4$ has the highest hydrogen content of all alanates, 10.6 wt.%; this is due to the lightness of Li atoms. $LiAlH_4$ and $NaAlH_4$ are the only commercially available alanates; their cost, of course, is not low enough for massive applications. Both of them are currently produced while using direct synthesis in an organic solvent. Mechanochemical production of $LiAlH_4$ by the milling of LiH and Al under hydrogen atmosphere has given minimal results [69].

Pure and not milled $LiAlH_4$ undergoes a melting transition, at 160–180 °C before undergoing a first dehydrogenation reaction to give Li_3AlH_6 and Al at 180–220 °C, Equation (15). A second dehydrogenation reaction is observed to occur at 228–282 °C to give LiH and Al, Equation (16) [70,71]:

$$LiAlH_4 \rightarrow 1/3\ Li_3AlH_6 + 2/3\ Al + H_2 \quad (15)$$

$$1/3\ Li_3AlH_6 \rightarrow LiH + 1/3Al + \frac{1}{2}\ H_2 \quad (16)$$

$$\text{Global reaction: } LiAlH_4 \rightarrow LiH + Al + 3/2\ H_2 \quad (17)$$

Together, both reactions provide for a hydrogen release of 7.9 wt.%. The third dehydrogenation step, i.e., the LiH decomposition is beyond any practical hydrogen storage operational temperature. Ball milling and the use of additives have reduced the dehydrogenation temperature of $LiAlH_4$ [72]. The list is extensive among the additives. However, the use of Ti-salts, $TiCl_3{\cdot}1/3AlCl_3$, [73], or NbF_5 [74] stands out. Data on apparent activation energies indicate an effective reduction of this parameter upon the use of additives [74]. Blanchard et al. proposed a reduction or elimination of an induction period (slow production rate of Al or Li_3AlD_6 nuclei) during the decomposition of $LiAlD_4$ as the action mode of the additives [75].

A common characteristic of all alanates is the covalent character of the Al–H bond, while the interaction between $[AlH_4]^-$ or $[AlH_6]^{3-}$ and M^{n+} is ionic [76]. The crystal structure of α-$LiAlH_4$ (α-$LiAlD_4$) and Li_3AlH_6 (Li_3AlD_6) is well-known, as determined both experimentally and by first-principles (Table 2 and Figure 5) [77–79]. Additionally, two high-pressure phases, β-$LiAlH_4$, and γ-$LiAlH_4$, have been described [76,80]. The α-$LiAlH_4$ to β-$LiAlH_4$ transition is expected to occur between 26,000 [76] −71,500 [69] bar. The β-$LiAlH_4$ to γ-$LiAlH_4$ transition is expected at 338,000 bar [69]. These pressures are far away from any application in hydrogen storage.

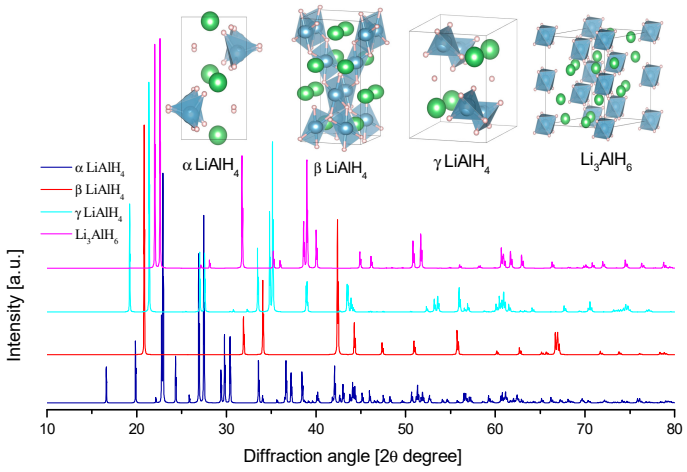

Figure 5. Crystal structure of lithium alanates and their calculated diffraction patterns (λ = $Cu_{k\alpha 1}$).

Table 2. Crystallographic data of Li-alanates.

Compound	Space Group, Cell Dimensions [Å] and Angles [°]	Atomic Coordinates
α-$LiAlD_4$	(P21/c) No. 14 [78] a = 4.8254(1); b = 7.8040(1); c = 7.8968(1) α = 90; β = 112.268(1); γ = 90	Al: 0.1428(2), 0.2013(1), 0.9311(1) Li: 0.5601(12), 0.4657(6), 0.8236(6) D1: 0.1902(10), 0.0933(8), 0.7710(6) D2: 0.3526(10), 0.3726(7), 0.9769(6) D3: 0.2384(11), 0.0840(7), 0.1141(7) D4: 0.8024(14), 0.2644(7), 0.8689(8)
β-$LiAlH_4$	(I 41/a) No. 88 [76] a = 4.6611; b = 4.6611; c = 10.5219 α = β = γ = 90	Li: 0, 1/4, 0.625 Al: 0, 1/4, 0.125 H: 0.2527, 0.4237, 0.5413
γ-LiAlH4	(Pnma) No. 62 [76] a = 6.4667; b = 5.3478; c = 6.5931 α = β = γ = 90	Li: 0.2428, 1/4, 0.2467 Al: 0.513, 1/4, 0.8221 H1: 0.3067, 1/4, 0.9617 H2: 0.7162, 1/4, 0.9631 H3:0.4889, 0.9833, 0.2943
Li_3AlH_6	(R-3) No. 148 [81] a = 8.0389(2); b = 8.0389(2); c = 9.4755(5) α = β = 90, γ = 120	Al1: 0, 0, 0 Al2: 0, 0, 1/2, Li: 0.966(2), 0.236(3), 0.3007(17) D1: 0.8325(11), 0.8030(7), 0.1008(6) D2: 0.1593(10), 0.1799(8), 0.3884(6)

$LiAlH_4$ is a well-known hydrogen storage material due to its facile dehydrogenation, but practically impossible complete rehydrogenation at moderate conditions. Few examples of successful rehydrogenation were observed by transferring the dehydrogenated products to an organic solvent and then exposing them to a hydrogen atmosphere. Among the examples is the rehydrogenation in Me_2O at room temperature, 100 bar hydrogen pressure, and 24 h stirring [82,83]. Another reported approach was performing the hydrogenation/dehydrogenation reactions in organic solvent [84]. The experiments and calculations indicate that the $LiAlH_4$ rehydrogenation is thermodynamically restricted [85]. The theoretical (*ab-inito*) calculations indicate that the dehydrogenation products of $LiAlH_4$ are thermodynamically favored [86]. Ke et al. give the (T, p) stability diagram of LiH and Al versus Li_3AlH_6; these data indicate the need for very high pressures to produce Li_3AlH_6 from 3LiH + Al + 3/2H_2 (Figure 6). In a (T, p) phase diagram for LiH/Li_3AlH_6 and Li_3AlH_6/$LiAlH_4$, Jang et al. demonstrated an equilibrium pressure of about 10^5 bar for Li_3AlH_6/$LiAlH_4$ in a wide range of temperatures [87]. Unfortunately, no equation was given to reproduce that equilibrium line. On the other hand, the equilibrium pressure of the direct and reverse reaction in THF;

$$LiH + Al + 3/2H_2 \overset{THF}{\leftrightarrow} LiAlH_4{\cdot}4THF, \quad (18)$$

is in the range of 1–2 bar at 80–90 °C [84]. This equilibrium has been studied in a very limited way. Perhaps, a liquid system of hydrogen storage based on $LiAlH_4$ deserves more attention.

3.2.2. Reactive Mixtures (Composites) with $LiAlH_4$

Reactive mixtures of hydrides have been proposed as a way to tailor the dehydrogenation temperature or improve rehydrogenation in borohydrides [89]. In this approach, two (or recently more) hydrides (simple or complex) are mixed; and, under suitable dehydrogenation conditions, they react with each other. The dehydrogenation is modified, including the dehydrogenation pathway, temperature, kinetics, and reversibility. Notably, the dehydrogenation temperature of composites is sensitive to the way of mixing of materials and the history of the composite; i.e., time and conditions of mixing, purity of reagents, cycling, etc. In the past decade, the research on $LiAlH_4$ has extended, intentionally or not, to the formation of reactive mixtures (composites). Relevant published work is compiled in the next sections.

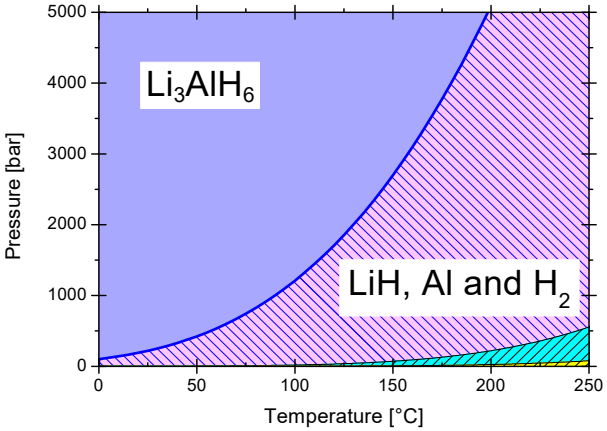

Figure 6. Phase diagram of LiH/Al/H_2 and Li_3AlH_6. The blue line represents the equilibrium. Data adapted from reference [86]: $\ln(p) = -\frac{0.22}{RT} + 13.89$; where (in the original formula) p is in atm, T in Kelvin and $\Delta H_R = 0.22$ eV. For visual reference (bottom and right) the equilibrium of Ti-doped Na_3AlH_6 (blue zone) and NaH + Al (yellow zone) phases were included [88].

Composites of $LiAlH_4$-MgH_2

Along the last decade, several $LiAlH_4$-MgH_2 composites have been studied for hydrogen storage [90–95]. The main results coincide in that the dehydrogenation pathway is marked by three steps, the usual two of $LiAlH_4$ and one of MgH_2. The temperature of these dehydrogenation steps is somewhat reduced compared to the pure components. Even more, the use of additives, such as TiH_2 [96], TiF_3 [90], $MnFe_2O_4$ [91], or $HfCl_4$ [93], reduced approximately up to 60 °C the dehydrogenation temperatures as compared to the mixture without additives. The role of the additives is to reduce the activation energy of dehydrogenation [93]. Other points of coincidence are the formation of Mg-Al and Li-Mg compounds of relatively varied stoichiometry after dehydrogenation and the occurrence of partial reversibility dominated by MgH_2 rehydrogenation without indications of $LiAlH_4$ rehydrogenation.

Composites of $LiAlH_4$-$LiBH_4$

$LiBH_4$ is as a potential hydrogen storage material due to its high hydrogen content. However, the dehydrogenation/hydrogenation high temperature and pressure prevent its use in a pure form. Thus, $LiBH_4$ has been mixed with a variety of chemicals, including $LiAlH_4$, for the formation of binary composites [97–100]. Additionally, ternary composites of the type $LiAlH_4$-$LiBH_4$-MgF_2 have been proposed [101]. In this regard, the possibilities of ternary composites are almost infinite. There are a lot of factors to consider, such as the selection of the composites, the relative composition, milling conditions, etc. Systematic studies are missing, noticeably by the difficulty and enormous of the task. The $LiAlH_4$ did not survive the milling process in many catalyzed mixtures, resulting in a mixture of $LiBH_4$, LiH, and Al [97]. Mao et al. proposed that $LiAlH_4$-$LiBH_4$ doped with TiF_3 has a reduced dehydrogenation enthalpy as compared with pure $LiBH_4$ [99]. The reported studies coincide in a two-step dehydrogenation pathway and a reduction of the dehydrogenation temperatures, especially if a catalyst, such as TiF_3, is used [99]. The first reaction is the decomposition of $LiAlH_4$ at temperatures around 100 °C. The second step is the decomposition of $LiBH_4$. However, the presence of Al directs the formation of AlB_2 [98]:

$$2LiBH_4 + Al \leftrightarrow 2LiH + AlB_2 + 3H_2 \quad (19)$$

The rehydrogenation of the $LiAlH_4$-$LiBH_4$ mixtures was proven to occur at various conditions of pressure and temperature, among them 40, 70, and 85 bar, and 350, 400, and 600 °C [97–99]. The rehydrogenation is directed to the formation of $LiBH_4$, since no rehydrogenation of $LiAlH_4$ has reported. While using $NaBH_4$ instead of $LiBH_4$ conduces to similar conclusions; a two-step

dehydrogenation with reduced temperature as compared with pure materials, the presence of AlB_2 after dehydrogenation, and partial hydrogenation due to the formation of $NaBH_4$ [102].

However, Xia et al. [103] reported the formation of Li_3AlH_4 and $LiBH_4$ in successive rehydrogenations of $2LiBH_4$-$LiAlH_4$ confined in mesoporous carbon scaffolds (up to 8.5 wt.% content, rehydrogenation at 500 °C, 100 bar, 10 h, seven cycles). Confinement in meso or nanoporous materials is another strategy for reducing the dehydrogenation temperature and improving the reversibility. However, a reduction in the hydrogen capacity is expected. Other confinement effects are [104–107]: (i) The reduction or total elimination of the loss of critical elements, such as B in the borohydrides. (ii) Reduction of the diffusion pathways of several species. (iii) Interaction with the meso or nanomaterials supports (can be of catalytic type). (iv) Large surface areas. (v) Reduction of the activation energies. The confinement as a strategy for improving hydrogen storage properties depends on several factors, such as: (i) the material used for confinement (carbons, nanocarbons, zeolites, graphene, silica, etc.) (ii) The history of the confined material. (iii) The way of infiltration (and drying if necessary). (iv) The size of the porous. (v) Functionalization of the surface of the support material. Confinement is a universe of possibilities, and it deserves a mayor review that is beyond the scope of the present report on alanates.

Composites of $LiAlH_4$-$LiNH_2$

The $LiAlH_4$-$LiNH_2$ composites have also been studied [108–113]. The first dehydrogenation steps are the decomposition of $LiAlH_4$ to Al and LiH. Then its dehydrogenation products react with $LiNH_2$. Here, less consensus can be found (compared to the previous examples of $LiAlH_4$ composites), and several reactions, mechanisms, and intermediaries have been proposed, for example:

Chen et al. proposed the reaction of $LiNH_2$ with Al as [108]:

$$LiNH_2 \rightarrow {}^1/_2\, Li_2NH + {}^1/_2\, NH_3 \quad (20)$$

$$Al + NH_3 \rightarrow AlN + 3/2\, H_2 \quad (21)$$

Evidently, due to NH_3 production, this method cannot be intended for proton-exchange membrane (PEM) fuel cells.

Dolotko et al. [111] indicated that reaction (21) has a minor contribution to the dehydrogenation reaction, instead, they proposed that $LiNH_2$ reacts with both LiH and Al:

$$2LiNH_2 + LiH + Al \rightarrow Li_3AlN_2 + 5/2\, H_2, \quad (22)$$

and the overall reaction was proposed as:

$$LiAlH_4 + LiNH_2 \rightarrow {}^1/_2\, Li_3AlN_2 + {}^1/_2\, Al + {}^1/_2\, LiH + 11/4\, H_2 \quad (23)$$

Lu et al. proposed that the overall reaction is [112]:

$$2LiAlH_4 + LiNH_2 \rightarrow 2Al + Li_2NH + LiH + 4H_2 \quad (24)$$

Jepsen et al. studied $LiAlH_4$-$LiNH_2$ composites in several molar proportions [113]. The intermediary $Li_{4-x}Al_x(NH)_{2-2x}N_2$ formed when the $LiAlH_4$-$LiNH_2$ ratio was 1:1.5, 1:2, and 1:2.5. This study supports that the $LiNH_2$ reacts with LiH to form Li_2NH and H_2. The main differences among the studies are mainly the molar proportions and milling conditions. This last parameter ranged from some minutes of manual milling in a mortar to several hours of mechanical milling. The use of additives, such as transition metal chlorides reduced, approximately 30 °C, the dehydrogenation temperature [114]. Regarding the reversibility, partial reversibility was proven while using rather hard conditions, i.e., 180 bar and 275 °C [111] or 100 bar and 425 °C [113]. However, the reversibility does not rely on the formation of $LiAlH_4$.

3.2.3. Sodium Alanate

$NaAlH_4$ is the most important and studied alanate. $NaAlH_4$ is used as a reducing agent in many reactions unrelated to the hydrogen storage. Due to the work of Bogdanović et al. on the use of catalysts or additives, the regeneration of $NaAlH_4$ is possible in the solid-state. Thus, this material has been seriously considered for hydrogen storage [7,88,115]. The dehydrogenation and rehydrogenation reactions are [7,116]:

$$NaAlH_4 \rightarrow 1/3\ Na_3AlH_6 + 2/3\ Al + H_2 \quad (25)$$

$$1/3\ Na_3AlH_6 \rightarrow NaH + 1/3Al + 1/2\ H_2 \quad (26)$$

$$\text{Global reaction: } NaAlH_4 \rightarrow NaH + Al + 3/2\ H_2 \quad (27)$$

Reactions (25) and (26) account for 5.6 wt.% of reversible hydrogen storage. Uncatalyzed $NaAlH_4$ experiences a solid to liquid phase transition before dehydrogenation. Meanwhile, in catalyzed $NaAlH_4$, the dehydrogenation temperature is generally lower than the melting point [117]. The first dehydrogenation step occurs at 210–220 °C. Meanwhile, the second step occurs at approximately 250 °C [117].

The crystal structure of $NaAlH_4$ was determined in 1979 (Table 3 and Figure 7) [118]. The $NaAlH_4$ consists of $[AlH_4]^-$ tetrahedra, with the Na atoms that are surrounded by eight $[AlH_4]^-$ tetrahedra in a distorted square antiprism geometry [119,120].

Table 3. Crystallographic data of Na-alanates.

Compound	Space Group, Cell Dimensions [Å] and Angles [°]	Atomic Coordinates
$NaAlH_4$	($I\ 4_1/a$) No. 88 [118] a = b = 5.020(2); c = 11.330(3) α = β = γ = 90	Al: 0, 0, 0 Na: 0, 0, 1/2 H: 0.228(1) 0.117(2) 0.838(9)
Na_3AlH_6	($P\ 2_1/c$) No. 14 [121] a = 5.4145(3); b = 5.5402(3); c = 7.7620(4) α = 90; β = 89.871(4), γ = 90	Al: 0, 0, 0 Na1: 0, 0, 1/2 Na2: −0.00129(5), 0.46129(4), 0.25008(4) H1: 0.0918, 0.0352, 0.2207 H2: 0.222, 0.3283, 0.5454 H3:0.1649, 0.2689, 0.95
Na_3AlD_6	($P\ 2_1/c$) No. 14 [122] a = 5.390(2); b = 5.514(2); c = 7.725(3) α = 90; β = 89.86(3), γ = 90	Na1: 0, 0, 1/2 Na2: −0.006(5), 0.461(4), 0.252(5) Al: 0, 0, 0 D1:0.091(3), 0.041(3), 0.215(3) D2: 0.234(3), 0.328(3), 0.544(3) D3: 0.165(3), 0.266(3), 0.944(3)

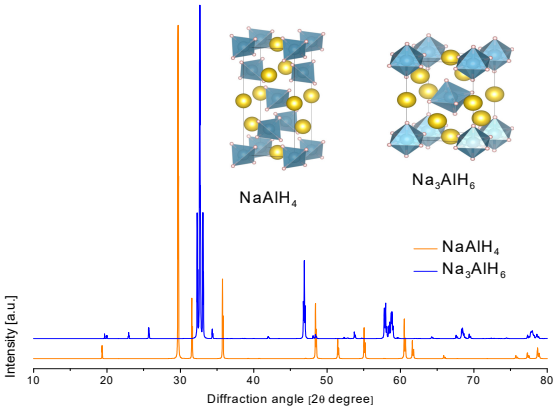

Figure 7. Crystal structure of sodium alanates and their calculated diffraction patterns (λ = $Cu_{k\alpha 1}$).

The $NaAlH_4$ and Na_3AlH_6 dehydrogenation enthalpies are well known (37 and 47 kJ/mol H_2, respectively, Ti-doped) [88]. These values mainly indicate a kinetic restrain for hydrogenation/dehydrogenation reactions, rather than a thermodynamic difficulty (see Section 7 for details on dehydrogenation enthalpies). A phase diagram NaH + Al/Na_3AlH_4/$NaAlH_4$ can be constructed from these data (Figure 8), [88] which indicates that equilibrium pressures at moderate temperatures are technically achievable, particularly if a catalyst is used. Since the work of Bogdanović, literally, thousands of papers have been published about different catalysts, variations in compositions or variations of the synthesis procedure [123]. $NaAlH_4$ can be produced by all of the methods that are described in Section 2 in several conditions of pressure and temperature at laboratory scale by the use of a catalyst [32,35]. Among the catalysts, dopants, or additives, the list includes, but is not limited to: chlorides of the first and second row of transition metals [124], lanthanide-oxides, such as La_2O_3, CeO_2, Sm_2O_3, and Gd_2O_3 [125], titanium compounds, such as $Ti(OBu)_4$ [88], $TiCl_3$ [7], TiF_3, $TiCl_4$ [117], TiB_2 [126,127], TiN [128], $TiCl_3$-1/3$AlCl_3$ [129], chlorides of Sc and Ce [130], or carbon nanomaterials [131]. The effectiveness of these materials as reaction accelerators is related to the additive level, the addition technique (milling, impregnation with solvent, CVD, etc.), structure, and morphology [127,132].

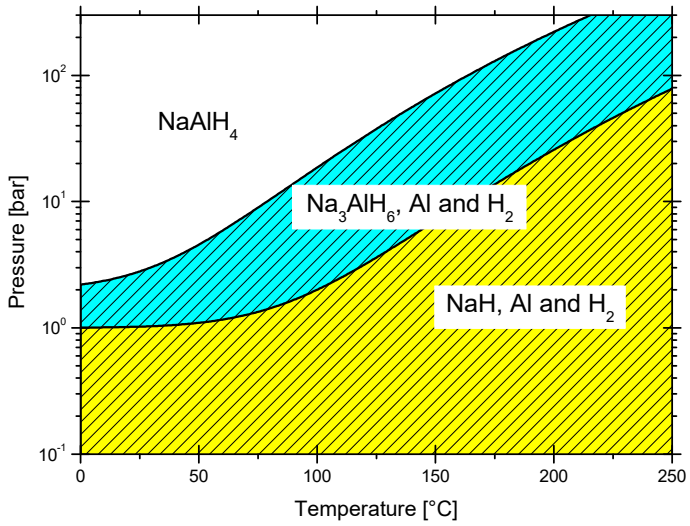

Figure 8. Phase diagram of Ti-doped ($Ti(OBu)_4$) $NaAlH_4$, Na_3AlH_6, and NaH + Al. Na_3AlH_6/$NaAlH_4$: $\ln\left(\frac{p_{eq}}{p}\right) = -\frac{37\ \text{kJ·mol}^{-1}}{RT} + \frac{122\ \text{J·mol}^{-1}\ \text{K}^{-1}}{R}$. NaH and Al/$Na_3AlH_4$: $\ln\left(\frac{p_{eq}}{p}\right) = -\frac{47\ \text{kJ·mol}^{-1}}{RT} + \frac{126\ \text{J·mol}^{-1}\ \text{K}^{-1}}{R}$ [88,133].

Role of Catalyst

Among the extensive list of materials tested as catalysts, dopants, or additives for improving hydriding and dehydriding reactions of $NaAlH_4$, the Ti, Sc, and Ce compounds stand out due to their effectiveness [132]. However, most of the theoretical and experimental studies to unravel the action mode of the catalyst have focused on Ti-compounds [134]. Nevertheless, after almost 20 years of the discovery of the benefits of using a catalyst, some fundamental questions are still not adequately addressed. Here are some points to consider:

1. Morphology/particle size effects. Beattie et al. demonstrated that Ti-doped $NaAlH_4$ particles presented few morphological changes as compared with un-doped materials [135]. By-products of the addition of materials, such as $TiCl_3$, i.e., Ti-Al alloys, and NaCl, can act as grain refiners for Al and NaH phases, keeping particle sizes small [136]. In general, much effort is put to reduce particle sizes and to avoid the sintering of particles, and thus maintaining the hydriding/dehydriding performance.
2. Location of Ti and substitution of atoms. The Ti atoms can be located in the bulk, in interstitial positions, at the subsurface, or the surface. The Ti preferred position depends on the doping

level and synthesis technique (impregnation vs. ball milling), or in theoretical calculations, the choice of reference states. The Ti atoms can be located in NaH, Al, Na_3AlH_6, or $NaAlH_4$ phases. Theoretical studies have been performed basically to include all of these possibilities. Some studies have unraveled the interactions of Ti (or Ti-compounds) with NaH and Al. Other reports indicated interactions of Ti (or Ti-compounds) with Na_3AlH_6 and $NaAlH_4$. Contradictory results/conclusions frequently come across. Additionally, many studies point to atom substitution and formation of defects. The replacement of Al by Ti in $NaAlH_4$ could be possible, yet this configuration is metastable [137,138]. Løvvik situates the substitution in the second metal layer from the surface [137,138]. Other DFT calculations suggest that the most frequent Ti-defect in $NaAlH_4$ is a defect that is formed by the substitution of Al by Ti and the addition of two hydrogen ions; this defect has a −1 charge [139]. The substitution of Na by Ti and other metal atoms also has been investigated. Marashdeh et al. classified the catalysts as "good" (Sc, Ti, Zr) and "bad" (Pt, Pd) according to their ability to exchange places with a Na atom on a (001) surface of $NaAlH_4$ [140]. In the "zipper model", Ti-species, at the surface or at a grain-boundary, displace subsurface Na atoms and eject them to the $NaAlH_4$ surface. Subsequently, the Na atoms react quickly with other species and destabilize the surface, which returns the Ti-species to a surface location [134,140]. For Na_3AlH_6, Michel et al. found a competition between Ti substitution on the Na sites (+1 charge defect) and Ti substitution on the Al site, with an additional bound to H atom (neutral site) [139]. For the hydrogenation reaction, the reports indicate that Ti near an Al surface (subsurface) promotes H_2 dissociation and H spillover on the Al surface [141]. Wang et al. remind us, in favor of this role of subsurface Ti, that metallic aluminum does not absorb diatomic hydrogen from the gas phase by itself. Meanwhile, atomic hydrogen strongly reacts with aluminum surfaces to form alanes [142]. Thus, subsurface Ti would promote H_2 dissociation and enhance H mobility and adsorption [142]. These effects constitute essentially the "hydrogen pump" action mechanism that was proposed for Ti [134]. Theoretical calculations of subsurface Sc, V or Nb substitution of Al indicate that these materials could also perform as a catalyst [143]. Wang et al. also remind us that Ti, Zr, V, Fe, Ni, Nb, Y, La, Ce, Pr, Nd, and Sm are expected to be good catalysts based on their ability to "mix" well with Al [142].

3. Progressive changes of the oxidation state of Ti-species. While Ti^{+3} species is the most recurrent initial oxidation state of the Ti-catalyst, several reports conclude that the oxidation state changes to Ti^0, followed by the formation of Ti_x-Al_y alloys, and finally the formation of Al_3Ti [134,144–146]. However, Al_3Ti seems to be an inefficient catalyst, as compared to other Ti or Ti-compounds [134,147]. Perhaps the formation of Ti_x-Al_y alloys and Al_3Ti is the reason for the long-term (after hydriding/dehydriding cycling) decay of hydrogen storage capacity [148].
4. Formation of Ti-Al-H complexes. Theoretical calculations suggest that the replacement of Na by Ti near o connected with $[AlH_4]^-$ would lead to the formation of Ti-Al-H complexes that can help during the dehydrogenation/rehydrogenation reactions [149–151]. $TiAl_2H_7$ and $TiAl_2H_2$ are two optimized structures of the Ti-Al-H complexes [150]. The effect of the Ti-Al-H complexes would be to reduce the desorption energy of hydrogen [149,151] and to break H-H and Al-H bonds as a result of balanced electron-accepting/back-donation [151].
5. Additional effects. Other effects, such as the formation of mobile species or vacancies, the changes in the Fermi level of reacting species, or the destabilization of Al–H bonds, can also influence the hydrogenation/dehydrogenation reactions [134].

3.2.4. Reactive Mixtures (Composites) with $NaAlH_4$

Composites of $NaAlH_4$-MgH_2

Composites of $NaAlH_4$ and MgH_2 in several proportions (4:1, 2:1, and 1:1) have been studied in the past years [152,153]. In some cases, catalysts, such as TiF_3 [154], TiO_2 [155], or TiH_2 [156], have been used. The composites in general present four dehydrogenation reactions [152,154]:

$$NaAlH_4 + MgH_2 \rightarrow NaMgH_3 + Al + 1.5H_2 \text{ (170–212 °C)} \quad (28)$$

$$17MgH_2 + 12Al \rightarrow Mg_{17}Al_{12} + 17H_2 \text{ (280–330 °C)} \quad (29)$$

$$NaMgH_3 \rightarrow NaH + Mg + H_2 \text{ (330–360 °C)} \quad (30)$$

$$NaH \rightarrow Na + 1/2\ H_2 \text{ (375 °C and higher)} \quad (31)$$

Only the first three reactions are relevant for hydrogen storage purposes. The reported values of hydrogen released in the first cycle of dehydrogenation ranged between 6.7–7.2 wt.% [152,154,155]. However, these values consider the decomposition of NaH. Prolonged ball milling or the use of catalysts produced a decrement of the activation energy and dehydrogenation temperatures in all steps [152–156]. Nano-confinement in carbon aerogel scaffolds reduced the dehydrogenation steps from four to only two [157]. Regarding the reversibility, up to six hydrogenation/dehydrogenation cycles have been demonstrated when the composite is mixed with carbon nanotubes and graphene nanosheets. In this case, the hydrogen storage level is around 3.5 wt.% at 275 °C and 76 bar [158]. Reaction (28) occurs before $NaAlH_4$ decomposes to Na_3AlH_6. Thus, a mutual destabilization between $NaAlH_4$ and MgH_2 was proposed as the reaction drive force [152,154]. Ismail et al. mixed MgH_2 and Na_3AlH_6 (4:1) [159]; in this composite, the dehydrogenation pathway is initiated by the following reaction:

$$Na_3AlH_6 + 3MgH_2 \rightarrow 3NaMgH_3 + Al + 3/2\ H_2 \text{ (120–250 °C)} \quad (32)$$

The rest of the steps are similar to the reaction sequence (29)–(31).

Other Composites with $NaAlH_4$

The $LiBH_4$-$NaAlH_4$ system was studied in two stoichiometric proportions, 1:0.5 and 1:1.15, with theoretical hydrogen storage capacity of 11.9 and 9.8 wt.%, respectively [160]. A metathesis reaction can occur during ball milling or during heating (~95 °C) depending on the amount of reactants and the energetics of the mixing (mortar vs. ball milling) [160]:

$$LiBH_4 + NaAlH_4 \rightarrow LiAlH_4 + NaBH_4 \quad (33)$$

The first dehydrogenation reaction is the decomposition of $LiAlH_4$ to produce Li_3AlH_6, Al and H_2 (~105–110 °C). The dehydrogenation pathway differs according to the excess of initial $NaAlH_4$. If an excess of $NaAlH_4$ is present, it reacts with Li_3AlH_6 to form $LiNa_2AH_6$, LiH, Al, and H_2 (~200 °C). $LiNa_2AH_6$ decomposes at ~290 °C. Without excess of $NaAlH_4$, Li_3AlH_6 decomposes at ~180 °C. $NaBH_4$ (diffraction peaks) disappear at ~340 °C in both cases. Further heating can lead to the formation of Li-Al alloys and AlB_2 phases [160].

Rehydrogenation was confirmed at ~110 bar hydrogen pressure and 400 °C. The rehydrogenation product was $LiBH_4$, as confirmed by in-situ synchrotron radiation powder X-ray diffraction.

3.2.5. Potassium Alanate

$KAlH_4$ has an acceptable total hydrogen content of 5.75 wt.% and a reversible hydrogen storage capacity of 4.3 wt.% (through reactions (34) and (35)). These values are comparable to $NaAlH_4$ and, additionally, $KAlH_4$ does not need a catalyst to undergo re-hydrogenation at a hydrogen pressure

as low as 10 bar [161]. $KAlH_4$ can be produced by direct synthesis in organic solvent from KH, Al, and hydrogen [21], or in powder form under high pressure of hydrogen (>175 bar) and heating [162], or by mechanical milling, followed by hydrogen exposure [161], or by the reactive mechanical milling in hydrogen atmosphere [163,164], or by the metathesis of $NaAlH_4$ or $LiAlH_4$ with KCl promoted by ball milling [165].

The dehydrogenation ad re-hydrogenation reactions most "commonly accepted" are [166]:

$$KAlH_4 \rightarrow 1/3\ K_3AlH_6 + 2/3\ Al + H_2\ (\sim 250–330\ ^\circ C) \quad (34)$$

$$1/3K_3AlH_6 \rightarrow KH + 1/3Al + {}^1/_2\ H_2\ (\sim 340\ ^\circ C) \quad (35)$$

$$\text{Global reaction: } KAlH_4 \rightarrow KH + Al + 3/2H_2 \quad (36)$$

A third reaction is the decomposition of KH; however, this reaction is not of interest in hydrogen storage applications. An explanation of "commonly accepted" is required; for $KAlH_4$ dehydrogenation and rehydrogenation reactions pathways are still not fully understood. Dehydrogenation pathway involving reactions (34) and (35) are similar to $LiAlH_4$ and $NaAlH_4$, and it is supported by pressure –composition isotherm (PCI) curves that present two plateaus (1 bar and 10 bar) at 355 °C [166,167]. Additionally, some DFT calculations indicate that K_3AlH_6 is sufficiently thermally stable to behave as an intermediary [168]. Santhanam et al. reported the synthesis of K_3AlH_6 by 12 h of the mechanical milling of $KAlH_4$ and 2KH [169]. However, a number of experimental reports indicate the presence of other reaction intermediaries, such as $KAlH_2$ [170], AlH_3 [171], K_xAlH_y [167], or other phases with partially known crystallography [172]. Some of them were observed during the in-situ synchrotron radiation powder X-ray diffraction experiments; however, they have not been isolated [172]. The controversial results indicate a possible dependency of the dehydrogenation path of $KAlH_4$ on the operating conditions, as pointed out by Ares et al. [164]. Additives, such as $TiCl_3$ [164,167], or salts, such as NaCl and LiCl (the other product of the ball milling metathesis) [165], could modify the reaction kinetics.

The structure of $KAlD_4$ was reported by Hauback et al. in 2005 (Table 4, Figure 9) [173]. $KAlD_4$ takes the same structure as $BaSO_4$ and $KGaD_4$, i.e., the space group *Pnma* [173,174]. The experimental and theoretical studies coincide on a small distortion of the $[AlH_4]^-$ ion from the ideal tetrahedron [173,174]. More interesting is the case of the K_3AlH_6 structure; Vajeeston et al. reported three different K_3AlH_6 structures according to first-principles studies (Table 4, Figure 9) [175]. The α-K_3AlH_6 phase is isostructural with α-Na_3AlF_6, and it transforms into the high-pressure structures β-K_3AlH_6 and γ-K_3AlH_6:

$$\alpha - K_3AlH_6 \xrightarrow{534\ kbar} \beta - K_3AlH_6 \xrightarrow{602\ kbar} \gamma - K_3AlH_6 \quad (37)$$

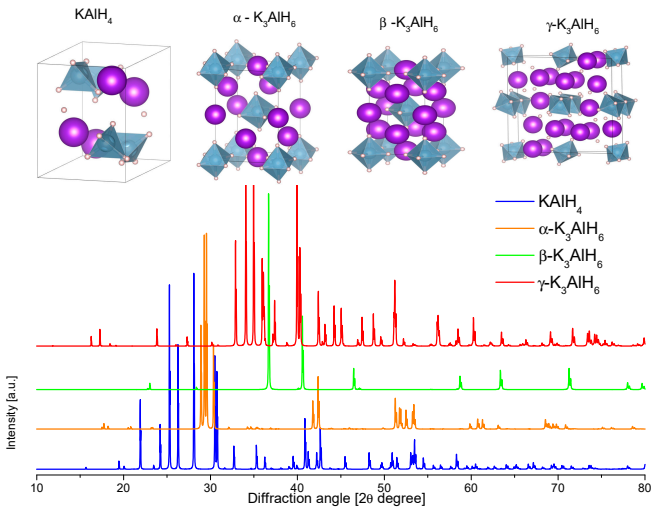

Figure 9. Crystal structure of potassium alanates and their calculated diffraction patterns (λ = $Cu_{k\alpha 1}$).

Table 4. Crystallographic data of K-alanates.

Compound	Space Group, Cell Dimensions [Å] and Angles [°]	Atomic Coordinates
$KAlD_4$	(*Pnma*) No. 62 [173] a = 8.8514(14); b = 5.8119(8); c = 7.3457(11) α = β = γ = 90	K: 0.1839(12), 1/4, 0.1522(17) Al: 0.5578(11), 1/4, 0.8209(13) D1: 0.4018(10), 1/4, 0.9156(9) D2: 0.7050(9), 1/4, 0.9630(12) D3: 0.4209(6), 0.9741(8), 0.3098(7)
α-K_3AlH_6	($P\ 2_1/c$) No. 14 [175] a = 6.1771; b = 5.8881; c = 8.6431 α = 90; β = 89.3, γ = 90	K1: 0, 0, 1/2 K2: −0.0058, 0.4828, 0.2544 Al: 0, 0, 0 H1: 0.0617, 0.0089, 0.2042 H2: 0.2799, 0.3136, 0.5349 H3: 0.1786, 0.2281, 0.9652
β-K_3AlH_6	(*I 4/mmm*) No. 139 [175] a = b = 4.4441; c = 7.8098 α = β = γ = 90	K1: 0, 0, 1/2 K2: 0, 1/2, 1/4 Al1: 0, 0, 0 H1: 0, 0, 0.2128 H2: 0.3429, 0, 0
γ-K_3AlH_6	(*Pnnm*) No. 58 [175] a = 10.8885; b = 10.2576; c = 2.5538 α = β = γ = 90	K1: 0.2347, 0.03444, 0 K2: 0.55047, 3/4, 0 K3: 0.691, 0.2178, 0 Al1: 1/2, 1/2, 0 Al2: 0, 1/2, 0 H1: 0.9388, 0.0715, 0 H2: 0.5928, 0.3931, 0 H3: 0.3085, 0.3814, 0 H4: 0.0632, 0.3708, 0 H5: 0.4194, 0.0352, 0 H6: 0.8387, 0.3512, 0

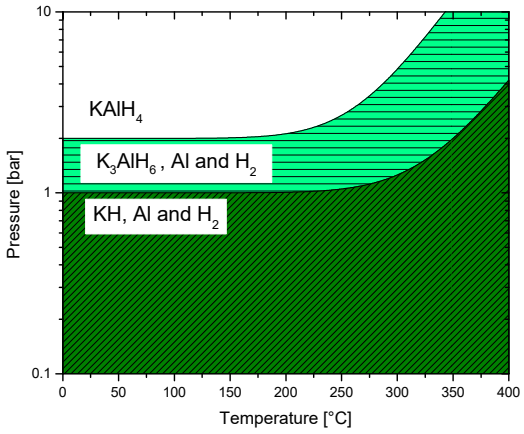

Figure 10. Phase diagram of $KAlH_4$, K_3AlH_6, and KH + Al. Constructed with data of reference [167] $K_3AlH_6/KAlH_4$: $\ln\left(\frac{p_{eq}}{p}\right) = -\frac{70\ \text{kJ·mol}^{-1}}{RT} + \frac{130\ \text{J·mol}^{-1}\ \text{K}^{-1}}{R}$. KH and Al/$K_3AlH_4$: $\ln\left(\frac{p_{eq}}{p}\right) = -\frac{81\ \text{kJ·mol}^{-1}}{RT} + \frac{130\ \text{J·mol}^{-1}\ \text{K}^{-1}}{R}$.

The experimental dehydrogenation enthalpies for reactions (34) and (35) are 70 ± 2 and 81 ± 2 kJ/mol H_2, respectively [167]. A phase diagram was generated with these values (Figure 10). In this diagram, the feasibility of hydrogenation at low pressure is evident and it justifies the rehydrogenation without the need for a catalyst or additives.

3.2.6. Rubidium Alanate

$RbAlH_4$ has a hydrogen content of 3.4 wt.%. If this material follows the group 1 tendency regarding dehydrogenation reactions, $RbAlH_4$ could reach a 2.5 wt.% of reversible hydrogen storage. Weidenthaler et al. reported the synthesis of $RbAlH_4$ from the metals Al, Rb, and with $TiCl_3$ as an additive; milling was performed in a hydrogen atmosphere (200 bar) [176]. Adkis et al. reported the synthesis of $RbAlH_4$ by the reaction between $LiAlH_4$ and metallic Rb [177]. Bestide et al. reported the metathesis between $LiAlH_4$ and rubidium halides that are assisted by triethylaluminum ($AlEt_3$) in toluene, hexane, and diethyl ether [178]. A stoichiometric reaction (99% product) was almost obtained in the latter work. This reaction yield was explained by the formation of a complex between the halide salts and the triethylaluminum, i.e., a Ziegler-type complex. $RbAlH_4$, and the deuterated species were also produced by the metathesis reaction between $NaAlH_4$, $LiAlH_4$, or $LiAlD_4$ with RbCl or RbF promoted by ball milling [176]. $RbAlH_4$ or $RbAlD_4$ were further heated in an autoclave and then purified [176].

$RbAlH_4$ decomposes in two steps at 300 °C and 350 °C (peak temperatures in TG-DCS curves) [176]. However, no complete dehydrogenation and full reversibility have been demonstrated. There is no consensus regarding the dehydrogenation pathway. Weidenthaler et al. proposed that the two dehydrogenation events are related to the formation of RbH plus Al, and the decomposition of RbH, respectively [176]. For its part, Dymova el at. proposed a first decomposition that is associated with the formation of Rb_3AlH_6 at 317–334 °C and a second dehydrogenation step by the formation of RbH at 390–417 °C [176,179]. Further confirmation of the dehydrogenation pathway and the formation of Rb_3AlH_6 is needed.

The structure of $RbAlH_4$ was calculated by Vajeeston et al. [180] and then further confirmed by Weidenthaler et al. (Table 5 and Figure 11) [176]. By means of ab-initio calculations, two high-pressure $RbAlH_4$ phases are anticipated [181]:

$$RbAlH_4\ (Pmma) \xrightarrow{32\ kbar} RbAlH_4\ (I41/a) \xrightarrow{68\ kbar} RbAlH4\ (Cmc21) \quad (38)$$

However, no further details regarding the experimental crystallographic data were reported [181]. Ravindran et al. reported the structure of $RbAlH_4$ obtained by theoretical calculations. This structure corresponds to a high-pressure phase above ~55 kbar [182].

Table 5. Crystallographic data of Rb-alanates.

Compound	Space Group, Cell Dimensions [Å] and Angles [°]	Atomic Coordinates
α-$RbAlD_4$	(*Pnma*) No. 62 [176] a = 9.2862(6); b = 5.9392(3); c = 7.5784(6) α = β = γ = 90	Rb: 0.1813(4), 1/4, 0.1574(7) Al: 0.5639(6), 1/4, 0.8121(7) D1: 0.4045(7), 1/4, 0.9073(7) D2: 0.6884(7), 1/4, 0.9615(8) D3: 0.4204(4), 0.9691(6), 0.3080(6)
α-$RbAlD_4$	($Cmc2_1$) No. 36 [176] a = 3.9933; b = 14.6472; c = 6.4933 α = β = γ = 90	Rb: 1/2, 0.6206, 0.2833 Al: 1/2, 0.1154, 0.7607 D1: 1/2, 0.7996, 0.0670 D2: 1/2, 0.1717, 0.9990 D3: 1/2, 0.5992, 0.7814 D4: 1/2, 0.9888, 0.1074

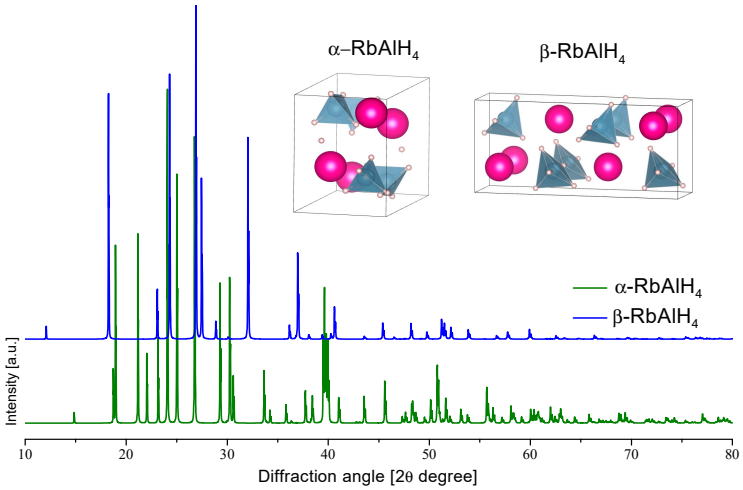

Figure 11. Crystal structure of rubidium alanates and their calculated diffraction patterns ($\lambda = Cu_{k\alpha 1}$).

3.2.7. Cesium Alanate

$CsAlH_4$ has a hydrogen content of 2.4 wt.%; thus, the interest in $CsAlH_4$ is pure chemistry research and is hardly relevant for hydrogen storage. $CsAlH_4$ has been prepared by mechanical milling or solvent metathesis of $NaAlH_4$ and CsCl, with subsequent purification [183,184]. Previously, Bestide et al. reported the metathesis between $LiAlH_4$ and cesium halides assisted by triethylaluminum ($AlEt_3$) in toluene, hexane, and diethyl ether [178]. $CsAlH_4$ decomposition is marked by four endothermic events [180]:

1. 210–229 °C: polymorphic transition, the material gets an intense yellow color.
2. 280–302: hydrogen evolution due to the proposed reaction:

$$3CsAlH_4 \rightarrow 2CsH + CsAl_3H_8 + H_2 \quad (39)$$

3. 454–485 °C: further decomposition reaction of $2CsH + CsAl_3H_8$:

$$2CsH + CsAl_3H_8 \rightarrow 3Cs + 5H_2 + 3Al \quad (40)$$

4. 666–672 °C: melting of Al. This reaction pathway does not follow the same decomposition and formation of intermediaries as the rest of the alanates of group 1. In-situ diffraction data is missing for further confirmation of this proposed decomposition pathway. Krech et al. [183] demonstrated a reversible polymorphic transformation between orthorhombic and tetragonal $CsAlH_4$; the transformation can be activated by ball-milling or by thermal treatment:

$$CsAlH_4(o) \underset{\text{thermal treatment at 200 °C}}{\overset{\text{ball–milling at 200 bar } H_2}{\rightleftharpoons}} CsAlH_4(t) \quad (41)$$

Table 6 lists the collected experimental crystallographic data of cesium alanates (Figure 12).

3.3. Alanates of Group 2

In group 2, in principle, the expected alanates would be $M(AlH_4)_2$ and $MAlH_5$. The alanates of group 2 will be discussed in the following sections.

Table 6. Crystallographic data of Cs-alanates.

Compound	Space Group, Cell Dimensions [Å] and Angles [°]	Atomic Coordinates
$CsAlD_4$ (o)	(*Pnma*) No. 62 [185] a = 9.8847(5); b = 6.15949(29); c = 7.9182(4) α = β = γ = 90	Al: 0.55462(33), 1/4, 0.80887(30) D1: 0.5755(4), 0.04042(31), 0.69536(32) D2: 0.6641(6), 1/4, 0.9620(5) D3: 0.4017(5), 1/4, 0.8868(6) Cs: 0.1847(4), 1/4, 0.1652(8)
$CsAlD_4$ (t)	($I\,4_1/a$) No. 88 [185] a = b = 5.67231(9); c = 14.2823(5) α = β = γ = 90	Al: 0, 3/4, 0.875 Cs: 1/2, 3/4, 0.125 D1: 0.19658(31), 0.7115(9), 0.95567(12) D2:0.25993(26), 0.7644(19), 0.92159(17)

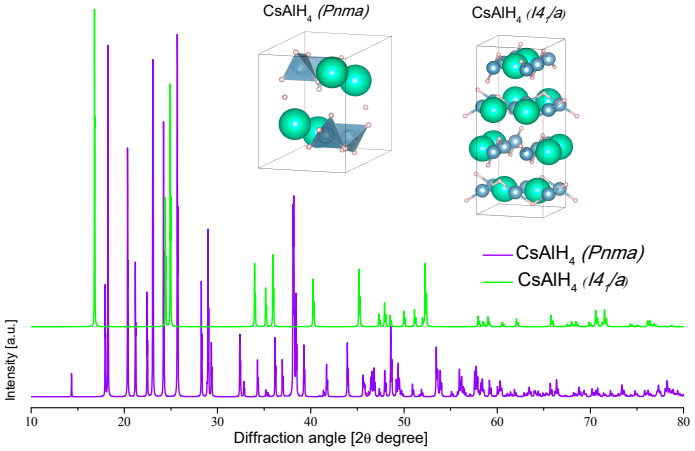

Figure 12. Crystal structure of cesium alanates and their calculated diffraction patterns (λ = $Cu_{k\alpha 1}$).

3.3.1. Beryllium-Alanate

The existence of $Be(AlH_4)_2$ is questionable. Some reviews list the $Be(AlH_4)_2$ phase with a dehydrogenation temperature of 20 °C [186]. The cited reference of these reviews is a book of relatively difficult access [187], whih in turn refers to a series of published works on borohydrides and other boron compounds [188,189]. However, these references dealt with the synthesis of $Be(BH_4)_2$, not $Be(AlH_4)_2$ [188,189]. In 1973, Ashby et al. attempted to produce $Be(AlH_4)_2$ from $LiAlH_4$, or $NaAlH_4$, and $BeCl_2$ in diethyl ether and THF without success [190]. In favor of the existence of $Be(AlH_4)_2$ is the report of Wiberg et al. (1951) [191]. In this work, the reaction between $BeCl_2$ and $LiAlH_4$ was proposed to produce $Be(AlH_4)_2$ in ether at 20 °C. However, no further details were presented.

Only a few theoretical works on $BeAlH_5$ have been published. Klaveness et al. reported two calculated structures of $BeAlH_5$; the low and high-pressure phases, namely, the α and β phases [192]. However, these calculations were estimated at 0 K, and it was not clear whether $BeAlH_5$ could be stable at ambient conditions in that work. Later, Santhosh et al., also by first-principle calculations, found that the α-$BeAlH_5$ phase could be stable at ambient (*p* and *T*) conditions [193]. The calculated α-$BeAlH_5$ phase consisted of alternating sheets of corner-sharing (AlH_6) octahedra and chains of corner-sharing (BeH_4) tetrahedra. On the other hand, the calculated β-$BeAlH_5$ phase only consisted of chains of corner-sharing (AlH_6) octahedra (Table 7 and Figure 13) [192].

Table 7. Calculated crystallographic data of Be-alanates.

Compound	Space Group, Cell Dimensions [Å] and Angles [°]	Atomic Coordinates
α-$BeAlH_5$	($P2_1$) No. 4 [192] a = 4.790; b = 4.324; c = 6.227 α = γ = 90; β = 89.408	Be: 0.002, 0.230, 0.623 Al: 0.243, 0.990, 1.000 H1: 0.247, 0.162, 0.749 H2: 0.001, 0.740, 0.902 H3: 0.501, 0.740, 0.914 H4: 0.240, 0.821, 0.251 H5: 0.890, 0.965, 0.515
β-$BeAlH_5$	(*C2/c*) No. 15 [192] a = 5.959; b = 7.008; c = 6.241 α = γ = 90; β = 116.205	Be: 0, 0.333, 0.250 Al: 0,0,0 H1: 0, 0.904, 0.250 H2: 0.902, 0.777, 0.881 H3: 0.688, 0.044; 0.913

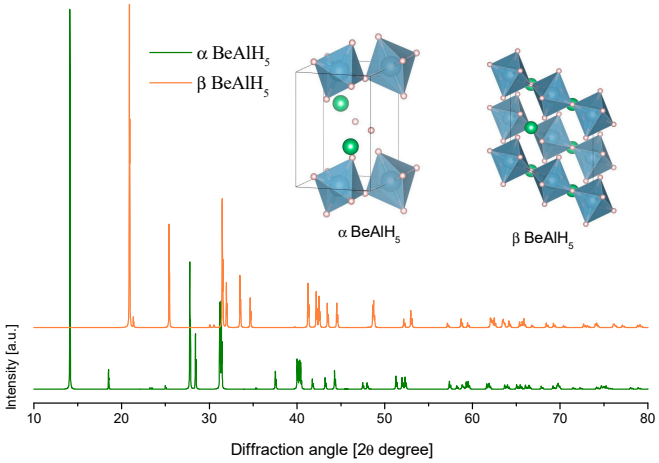

Figure 13. Crystal structure of beryllium alanates and their calculated diffraction patterns (λ = $Cu_{k\alpha 1}$).

3.3.2. Magnesium Alanate

$Mg(AlH_4)_2$ has been known since the 1950s [25,27]. At that time, magnesium alanate was synthesized in an organic solvent by the reaction between magnesium hydride and aluminum tri-halides, Equation (6). After almost 50 years, the solid state version of reaction (6) was reported on by Dymova et al. [39] and others [194]. Additionally, roughly at the same time, the metathesis reaction between $NaAlH_4$ and $MgCl_2$ in organic solvent was reported [30]. In the synthesis that involves organic solvents, the formation of adducts, and the purification (drying without decomposing the alanates), is a frequent problem. Thus, more recently, the metathesis reaction between $NaAlH_4$ (or $LiAlH_4$) and $MgCl_2$, as assisted by mechanical milling, was published and frequently used [43,195].

$Mg(AlH_4)_2$ has a hydrogen content of 9.3 wt.%; however, dehydrogenation studies report values in the range of 6–7 wt.% in the first dehydrogenation step [196]. The most accepted dehydrogenation pathway assumes that $Mg(AlH_4)_2$ decomposes in the temperature range of 110–200 °C, according to the reaction [196,197]:

$$Mg(AlH_4)_2 \rightarrow MgH_2 + 2Al + 3H_2. \quad (42)$$

Subsequently, further dehydrogenation of MgH_2 in the presence of Al leads to the formation of Mg-Al compounds of several reported stoichiometries [197,198]. Reports indicate that the dehydrogenation temperature can be reduced by additional milling [199], the addition of materials, such as TiF_4, TiF_3 [200], and $TiCl_3$ [31], or the reduction of particle size [196,198]. Possibly, the other metathesis product, i.e., LiCl or NaCl, can also produce a change in the dehydrogenation temperatures [195]. Rehydrogenation is partially achieved by the formation of MgH_2 instead of $Mg(AlH_4)_2$ [31,195,200].

However, Gremaud et al. reported the formation of $Mg(AlH_4)_2$ at 1 bar, and 100 °C from thin films of Mg-Al covered with a thin layer of Ti [201].

The crystal structure of $Mg(AlH_4)_2$ was determined by a combination of X-ray and neutron diffraction at 295 K (Table 8 and Figure 14.) [202]. The crystallographic information is consistent with other experimental and theoretical reports [203–205]. The structure consists of $[AlH_4]^-$ tetrahedra that formed double layers that were perpendicular to the **c** axis of the trigonal cell and alternating with Mg layers (Figure 14) [205].

Table 8. Crystallographic data of magnesium alanates.

Compound	Space Group, Cell Dimensions [Å] and Angles [°]	Atomic Coordinates
$Mg(AlH_4)_2$	*(P −3 m 1)* No. 164 [202] a = b = 5.1949(2); c = 5.8537(2) α = 90; β = 90; γ = 120	Mg: 0, 0, 0 Al: 0.3333, 0.6667, 0.7057(5) H1: 0.3333, 0.6667, 0.439(2) H2: 0.1589(14), −0.1589(14), 0.804(2)
$MgAlH_5$	*(P 2_1 2_1 2_1)* No. 19 [206] a = 4.55; b = 4.26; c = 13.024 α = 90; β = 90; γ = 90	Mg: −0.2504, −0.2466, −0.3204 Al: 0.2486, 0.2528, −0.4083 H1: −0.4756, −0.0559, 0.4069 H2: −0.03, 0.0912, 0.3051 H3: 0.4719, −0.0516, −0.4063 H4: 0.0284, 0.0975, −0.3045 H5: −0.0024, 0.0916, −0.4994
α-$MgAlH_5$	*(P* 21 */c)* No. 14 [207] *a* = 4.7499; *b* = 8.8127; *c* = 6.6281 α = 90; β = 90; γ = 109.75	Mg: 0.527, 0.985, 0.253 Al: 0.092, 0.245, 0.395 H1: 0.400, 0.121, 0.444 H2: 0.349, 0.390, 0.495 H3: 0.121, 0.592, 0.201 H4: 0.197, 0.862, 0.142 H5: 0.130, 0.305, 0.156
β-$MgAlH_5$	*(Cc)* No. 9 [207] *a* = 7.8033; *b* = 5.7251; *c* = 6.7393 α = 90; β = 90; γ = 115.39	Mg: 0.542, 0.025, 0.257 Al: 0.000, 0.000, 0.000 H1: 0.008, 0.924, 0.256 H2: 0.201, 0.289, 0.034 H3: 0.771, 0.969, 0.882 H4: 0.027, 0.299, 0.979 H5: 0.246, 0.031, 0.130

$MgAlH_5$ was originally proposed by Dymova et al. as a reaction intermediary of the decomposition of $Mg(AlH_4)_2$ [39]. However, further experimental reports did not confirm this. Other elements of group 2 (M) indeed form $MAlH_5$ compounds. On the other hand, theoretical calculations indicate the possible crystals structures of $MgAlH_5$ (Table 8).

The few available kinetic studies indicate that the dehydrogenation reaction is ruled by the diffusion of MgH_2, Al, or hydrogen in the TiF_4 doped samples [197,208]. In any case, the activation energy of dehydrogenation reaction (42) is high: 117.5 [206]–123 [197] kJ/mol. Theoretical studies indicate that $Mg(AlH_4)_2$ is metastable at room temperature with a formation enthalpy of −21 kJ/mol H_2 [209]. By ab-initio calculations, Spanò et al. determined, that the dehydrogenation temperature at atmospheric pressure must be 111 °C [210]. Thus, despite the interesting high hydrogen content and low dehydrogenation temperatures, $Mg(AlH_4)_2$ can be classified as a one-way hydrogen storage material.

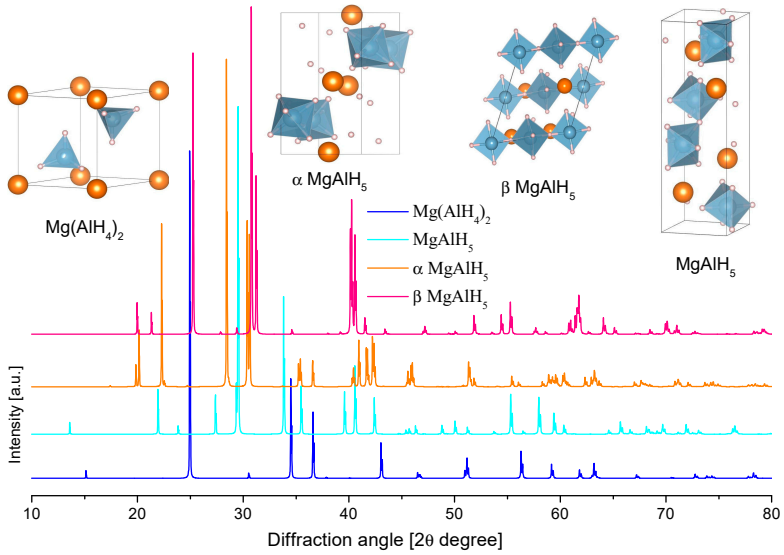

Figure 14. Crystal structure of magnesium alanates and their calculated diffraction patterns ($\lambda = Cu_{k\alpha 1}$).

3.3.3. Reactive Mixtures (Composites) with $Mg(AlH_4)_2$

Few examples of the composites of $Mg(AlH_4)_2$ were found during the preparation of this review; they are, in summary: $Mg(AlH_4)_2$-$NaAlH_4$ [211,212], $Mg(AlH_4)_2$-MgH_2 [213], $Mg(AlH_4)_2$-$LiBH_4$ [214,215], and $Mg(AlH_4)_2$-$Ca(BH_4)_2$ [216]. The original reports include several stoichiometries and preparation procedures. However, they have the reduction of dehydrogenation temperature as compared with the individual components and a relatively high amount of hydrogen released during the first dehydrogenation step in common. In many cases, the role of $Mg(AlH_4)_2$ is classified as a catalyst of the other components of the mixture. Usually, the first dehydrogenation step corresponds to the decomposition of $Mg(AlH_4)_2$, i.e., reaction (42). Afterwards, MgH_2 reacts with other components of the mixture. For example, in the $Mg(AlH_4)_2$-$NaAlH_4$ composite, $NaMgH_3$ was formed, and the proposed reaction is [211]:

$$2Na_3AlH_6 + 6MgH_2 \rightarrow 6NaMgH_3 + 2Al + 3H_2 \quad (43)$$

Further decomposition of $NaMgH_3$ in the presence of Al leads to the formation of Mg-Al alloys.

For the $Mg(AlH_4)_2$-$LiBH_4$ composite, Liu et al. proposed as a second step the formation of Mg_2Al_3 from the reaction of MgH_2 and Al. Subsequently, Mg_2Al_3 reacts with $LiBH_4$ [214]:

$$6LiBH_4 + 0.5Mg_2Al_3 + 0.5Al \rightarrow 6LiH + MgAlB_4 + AlB_2 + 9H_2 \quad (44)$$

The formation of $MgAlB_4$ was also proposed by Pang et al. [215]. Two main drawbacks are observed for the composites of $Mg(AlH_4)_2$:

1. Despite the reduction in dehydrogenation temperatures, the "ideal" dehydrogenation temperature—compatible with PEM fuel cells—is not attained.
2. Re-hydrogenation is only partially achieved through the formation of MgH_2, not $Mg(AlH_4)_2$.

3.3.4. Calcium Alanate

Reports on the synthesis of $Ca(AlH_4)_2$ dates from the 1950s [28]; back then, the synthesis was performed in an organic solvent by the reaction between CaH_2 and $AlCl_3$ [28] or $AlBr_3$ [217]. As other alanates, the synthesis of $Ca(AlH_4)_2$ evolved towards the metathesis reaction between $NaAlH_4$ or $LiAlH_4$ and $CaCl_2$ in an organic solvent [31], to finally take advantage of the use of mechanical milling to perform direct or metathesis synthesis. As for other alanates, the synthesis in organic solvents,

such as THF, produced adducts of complicated purification without decomposition of the alanate. Thus, the synthesis that is assisted by mechanical milling is nowadays popular [218].

Calcium alanate has a total hydrogen content of 7.9 wt.%. Its complete decomposition occurs in four steps; the first two steps liberate 5.2–5.9 wt.% hydrogen of the theoretical 7.15 wt.% [165,219,220]. The dehydrogenation reactions are [220]:

$$Ca(AlH_4)_2 \rightarrow CaAlH_5 + Al + 3/2H_2 \text{ (100–160° C)} \quad (45)$$

$$CaAlH_5 \rightarrow CaH_2 + Al + 3/2H_2 \text{ (220–270 °C)} \quad (46)$$

$$CaH_2 + 4Al \rightarrow Al_4Ca + H_2 \text{ (~350 °C)} \quad (47)$$

$$CaH_2 + Al_4Ca \rightarrow 2Al_2Ca + H_2 \text{ (~400 °C)} \quad (48)$$

Adding TiF_3 led to a decrease in the activation energy and the dehydrogenation temperature [219]. Li et al. suggest that the F atoms from TiF_3 substitutes H atoms in $Ca(AlH_4)_2$ and that TiF_3 initiates the decomposition of calcium alanate [219]:

$$Ca(AlH_4)_2 + \frac{x}{3}TiF_3 \rightarrow CaAlF_xH_{5-x} + Al + \frac{x}{3}Ti + \frac{x+3}{2}H_2. \quad (49)$$

The crystal structure of $Ca(AlH_4)_2$ and $CaAlH_5$ were determined in 2009 (Table 9 and Figure 15) [221]. However, theoretical predictions and partial experimental reports were published as early as 2005–2006 [222–224]. $Ca(AlD_4)_2$ takes an orthorhombic $Ca(BF_4)_2$-type structure [221]. Meanwhile, the crystal structure of $CaAlD_5$ was found to be a monoclinic α-$SrAlF_5$-type structure [221]. $CaAlH_5$ consists of corner-sharing (AlH_6) octahedra [224].

Table 9. Crystallographic data of calcium alanates.

Compound	Space Group, Cell Dimensions [Å] and Angles [°]	Atomic Coordinates
$Ca(AlD_4)_2$	*(Pbca)* No. 61 [221] a = 13.4491(27); b = 9.5334(19); c = 9.0203(20) $\alpha = \beta = \gamma = 90$	Ca: 0.8958(1), 0.4662(2), 0.2818(3) Al1: 0.4389(3), 0.7757(5), −0.0011(8) Al2: 0.8460(3), 0.1060(4), 0.1839(5) D1: 0.3710(9), 0.6842(11), 0.1087(12) D2: 0.5280(8), 0.8546(12), 0.0825(14) D3: 0.4877(9), 0.6706(12), −0.1183(13) D4: 0.3647(8), 0.8817(11), −0.0835(13) D5: 0.8264(10), 0.0829(11), 0.0086(8) D6: 0.8094(8), 0.2610(8), 0.2337(14) D7: 0.9590(5), 0.0702(12), 0.2407(16) D8: 0.7762(9), −0.0075(10), 0.2636(16)
$CaAlD_5$	*(P 2_1/c)* No. 14 [221] a = 9.8000(19); b = 6.9081(13); c = 12.4503(23) $\alpha = 90$; $\beta = 137.936(4)$; $\gamma = 90$	Ca1: 0.7845(16), 0.2166(19), 0.7382(13) Ca2: 0.3275(14), 0.2676(16), 0.1816(11) Al1: 0.8017(15), 0.3097(16), 0.4907(12) Al2: 0.2071(14), 0.2175(14), 0.8706(11) D1: 0.0058(17), 0.3009(19), 0.5190(14) D2: 0.6406(16), 0.4242(18), 0.3076(12) D3: 0.6070(14), 0.2725(17), 0.4696(13) D4: 0.7010(18), 0.3865(14), 0.8592(15) D5: 0.9589(14), 0.1915(15), 0.6767(10) D6: 0.1259(17), 0.0329(14), 0.9070(13) D7: 0.1154(19), 0.3773(14), 0.9139(15) D8: 0.2848(16), 0.0634(15), 0.8156(14) D9: 0.2612(19), 0.4064(13), 0.8154(13) D10: 0.4470(13), 0.1884(16), 0.0707(12)

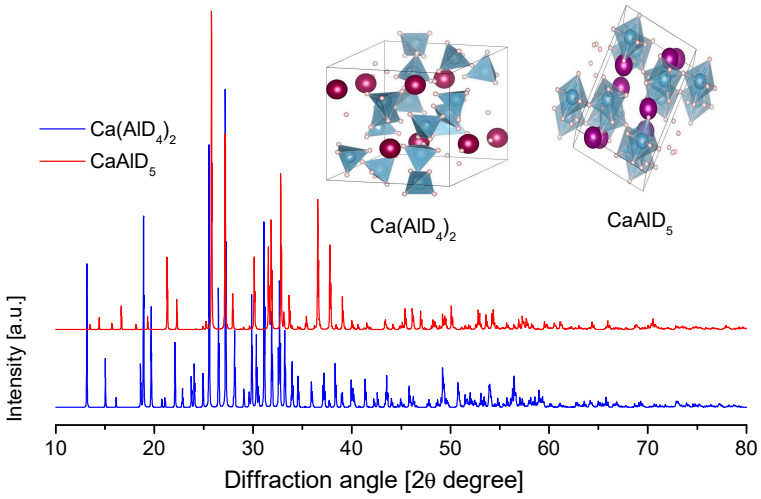

Figure 15. Crystal structure of calcium alanates and their calculated diffraction patterns ($\lambda = Cu_{k\alpha 1}$).

$Ca(AlH_4)_2$ decomposition is slightly exothermic [224], with the enthalpy of reaction (45) being about −7 [220] to −9 kJ/mol H_2 [224]. The second dehydrogenation step (reaction (46)) is endothermic with an enthalpy of 32 kJ/mol H_2 [224]. The reversibility of Equations (45) and (46) was not reported. The enthalpy values indicate that the first reaction is not suitable for hydrogen storage for mobile applications. However, the second reaction, in principle, could be suitable for mobile hydrogen storage. The enthalpy value of reaction (46) was used to generate the phase diagram of Figure 16. The diagram indicates that $CaAlH_5$ could be produced at temperatures and pressures that are compatible with fuel cells, perhaps with the help of a proper catalyst. In this scenario, the reversible hydrogen storage capacity would be 4.19 wt.%.

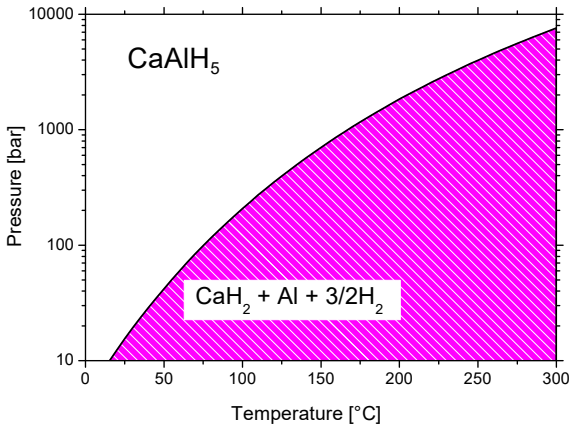

Figure 16. Phase diagram of $CaAlH_5$, CaH_2, and Al. CaH_2 and Al/$CaAlH_5$: $\ln\left(\frac{p_{eq}}{p}\right) = -\frac{32\ \text{kJ·mol}^{-1}}{RT} + \frac{130\ \text{J·mol}^{-1}\ \text{K}^{-1}}{R}$ [224].

3.3.5. Reactive Mixtures (Composites) with $Ca(AlH_4)_2$

Scarce examples of reactive mixtures with $Ca(AlH_4)_2$ were found during the redaction of this review. One of them was the mixture of $LiBH_4$ and $Ca(AlH_4)_2$, giving the best results with a molar ratio of 6:1, respectively [225]. In that system, the released hydrogen was 8.2 wt.% up to 450 °C. Reactions (45) and (46) initiate the dehydrogenation pathway. Subsequently, $LiBH_4$ reacts as: [225]

$$8LiBH_4 + CaH_2 + Al \rightarrow CaB_6 + AlB_2 + 8LiH + 13H_2. \quad (50)$$

The last step is the reaction (47) of the remaining materials. Rehydrogenation was demonstrated at 450 °C and 40 bar to produce $LiBH_4$ and $Ca(BH_4)_2$ and 4.5 wt.% hydrogen storage.

Hanada et al. reported the dehydrogenation of $Ca(AlH_4)_2$ + Si, $Ca(AlH_4)_2$ + $2MgH_2$, $Ca(AlH_4)_2$ + 2LiH, and $Ca(AlH_4)_2$ + $2LiNH_2$ mixtures that were produced by manual or ball milling [226]. In their work, $Ca(AlH_4)_2$ was produced by a metathesis reaction and it was used without purifying, i.e., with the load of NaCl. The weight losses were 6.1 wt.% for $Ca(AlH_4)_2$ + $2MgH_2$ and 5.5 wt.% for manually milled $Ca(AlH_4)_2$ + $2LiNH_2$. These values were reported without taking the load of NaCl into account. The rest of the hydrogen release values were not clearly specified. For the $Ca(AlH_4)_2$ + Si mixture, the first two reactions are the usual $Ca(AlH_4)_2$ dehydrogenation reactions, Si does not react with CaH_2 or Ca-containing phases [226]. For the $Ca(AlH_4)_2$ + $2MgH_2$ mixture, after the usual first two dehydrogenation reactions, MgH_2 decomposes at around 270–350 °C and then reacts with Al to form $Al_{12}Mg_{17}$ [226]. Alapati et al., by means of first-principle calculations, arrived at the same reactions, plus a high-temperature reaction [227]:

$$6CaH_2 + Al_{12}Mg_{17} \rightarrow 17Mg + 6Al_2Ca + 6H_2 \ (\sim 600\ ^\circ C) \quad (51)$$

For the $Ca(AlH_4)_2$ + 2LiH mixture, $CaAlH_5$ is generated during ball milling due to the solid-state reaction between $Ca(AlH_4)_2$ and LiH [226]. Meanwhile, Li_3AlH_6 appears after heating to 150 °C under 3 bar of He. Subsequently, at 250 °C, the CaH_2 and Al phases arise and Li_3AlH_6 disappears [226]. For the $Ca(AlH_4)_2$ + $2LiNH_2$ mixture, a reaction of decomposition of $Ca(AlH_4)_2$ with $LiNH_2$ occurs during ball milling. A similar hand-milled mixture produced the same two dehydrogenation reactions of $Ca(AlH_4)_2$, plus the reaction:

$$CaH_2 + 2LiNH_2 \rightarrow Li_2NH + CaNH + 2H_2 \quad (52)$$

The last reaction is reported to simultaneously occur with Equation (47) in this system [226]. The re-hydrogenation reactions are not reported.

3.3.6. Strontium Alanates

The system Sr-Al-H presents a richness of chemistry and compounds. Here, we present the most representative characteristics reported for them. $Sr(AlH_4)_2$ has a hydrogen content of 5.3 wt%. It was first produced by the reaction between SrH_2 and AlH_3 by mechanochemical activation in 2000 [228]. After that, $Sr(AlH_4)_2$ was produced by the metathesis reaction between $SrCl_2$ and $2NaAlH_4$, being assisted by mechanical milling [44]. The decomposition of $Sr(AlH_4)_2$ initiated at about 130 °C. Subsequently, a second dehydrogenation step occurred at about 240 °C to achieve a total of 2.1 wt.% of released hydrogen with both reactions (0.8 and 1.3 wt.%, respectively, including the NaCl load) [44]. $SrAlH_5$ (4.21 wt.% of total hydrogen content) is proposed as a reaction intermediary of the decomposition of $Sr(AlH_4)_2$ [192,228]:

$$2Sr(AlH_4)_2 \rightarrow 2SrAlH_5 + 2Al + 3H_2 \ (145–165\ ^\circ C) \quad (53)$$

$$2SrAlH_5 \rightarrow 2SrH_2 + 2Al + 3H_2 \ (220–320\ ^\circ C) \quad (54)$$

$$2SrH_2 + 4Al \rightarrow Al_4Sr + SrH_2 + H_2 \ (355–390\ ^\circ C) \quad (55)$$

$$SrH_2 \rightarrow Sr + H_2 \ (890–950\ ^\circ C) \quad (56)$$

Partial rehydrogenation was achieved by (re)milling at high hydrogen pressure (300 bar). Further dehydrogenation demonstrated a drastic reduction of the hydrogen release (about 0.8 wt.%) [44].

$SrAlD_5$ was produced by the mechanical milling of SrD_2 and AlD_3 and further heating at 154 °C for 1 h in Ar [229]. $SrAlD_5$ was studied by synchrotron and neutron diffraction in detail; the resolved structure consists of (AlD_6) octahedra that share corner D atom forming a chain (Figure 17) [229]. This was the first complete experimental report on the crystallography of $SrAlD_5$ (Table 10). Previously,

the partial crystal structure (no H positions given) [44] and first-principle crystallographic data of $SrAlH_5$ were reported [192]. The calculated and the experimental data appreciably differ (Figure 17).

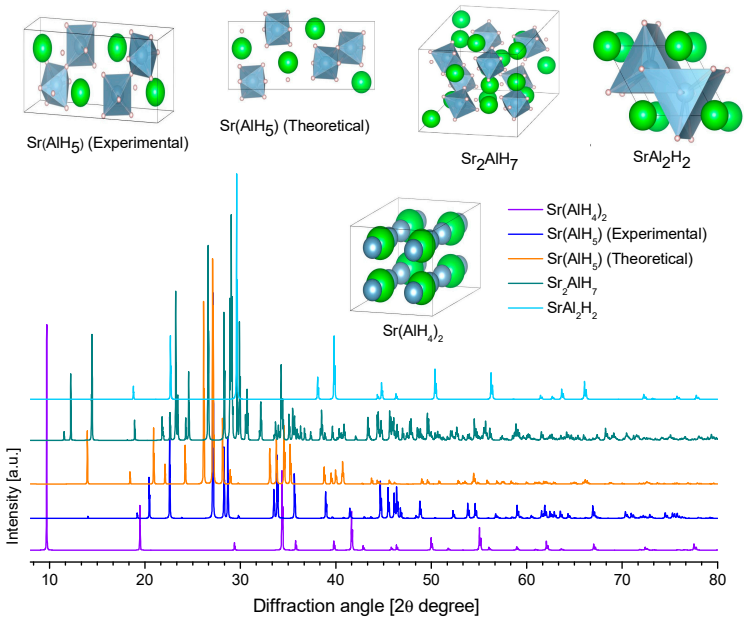

Figure 17. Crystal structure of strontium alanates and their calculated diffraction patterns ($\lambda = Cu_{k\alpha 1}$).

Sr_2AlH_7 (3.37 wt.% of hydrogen content) was produced by the mechanical milling of $SrAl_2$ and further hydrogenation at 70 bar and 270 °C for ten days. The arc melting of Sr and Al previously prepared $SrAl_2$ [230]. Zhang et al. reported that the crystal structure of Sr_2AlD_7 consisted of isolated (AlD_6) units and one-dimensional chains of edge-sharing (DSr_4) tetrahedra [230].

The proposed formation pathway is [231–233]:

$$SrAl_2 + H_2 \rightarrow SrAl_2H_2 \text{ (190 °C, 50 bar)} \quad (57)$$

$$4SrAl_2H_2 + 3H_2 \rightarrow 2Sr_2AlH_7 + 6Al \text{ (240 °C, 70 bar)} \quad (58)$$

The milling of $SrAl_2$ in hydrogen atmosphere led to the formation of SrH_2 and Al. The milled materials were further hydrogenated at 260 °C (no pressure indicated) for two days to give Sr_2AlH_7 [231]:

$$4SrH_2 + 2Al + 3H_2 \rightarrow 2Sr_2AlH_7. \quad (59)$$

On the other hand, Sr_2AlH_7 decomposes to SrH_2, Al, and H_2 at 290 °C [231,232]. However, attempts to hydrogenate mixtures of $4SrH_2 + 2Al$ (70 bar, 260 °C, two days) did not succeed. In this last case, stearic acid was used as a process control agent (PCA) to avoid the cold welding of Al during mechanical milling. Possibly, another PCA might lead to successful hydrogenation. Unfortunately, the dehydrogenation curves of Sr_2AlH_7 were not presented in these studies.

Table 10 lists the collected crystallographic information of Sr-Al-H compounds.

3.3.7. Barium Alanates

For Barium, two barium-aluminum-hydride compounds have been reported: $BaAlH_5$ (2.97 wt.% hydrogen content) and Ba_2AlH_7 (2.28 wt.% hydrogen content). They have been prepared from Ba_7Al_{13} or Ba_4Al_5 alloys, followed by ball-milling and several days in hydrogenation conditions (70 bar, ~200 °C). The Ba_7Al_{13} and Ba_4Al_5 alloys were previously prepared by arc melting [234–236]. Alternatively, the reactive ball milling of the mixture of BaH_2 and Al can produce the $BaAlH_5$ and Ba_2AlH_7 [237]. The formation of $BaAlH_5$ or Ba_2AlH_7 can be directed by the choice of precursor or

by the selection of the temperature (Figure 18) [234–236]. $BaAlH_5$ and Al were produced by the hydrogenation of Ba_7Al_{13} (dark pink reaction, Figure 18). Meanwhile, $BaAlH_5$, $BaAl_4$, and BaH_2 were produced by the hydrogenation of Ba_4Al_5 (green reaction, Figure 18). The further heating of $BaAlH_5$ (black reaction, Figure 18) or high-temperature synthesis from Ba_7Al_{13} (blue reaction, Figure 18) can produce Ba_2AlH_7 along with some by-products [234–236].

Table 10. Crystallographic data of strontium-aluminum hydrides.

Compound	Space Group, Cell Dimensions [Å] and Angles [°]	Atomic Coordinates
$Sr(AlH_4)_2$	*Pmmn* (No. 59) [44] a = 9.1165(18); b = 5.2164(11); c = 4.3346(8) α = β = γ = 90	Sr: 0.1958(3), 1/4, 3/4 Al1: 0.9665(11), 1/4, 1/4 Al2: 0.37309(11), 3/4, 1/4
$SrAlD_5$ (experimental)	*Pbcm* (No. 57) [229] a = 4.6226(10); b = 12.6213(30); c = 5.0321(10) α = β = γ = 90	Sr: 0.2532(7), 0.8925(3), 1/4 Al: 0.3296(11), 0.1597(3), 1/4 D1: 0.4366(13), 1/4, 0 D2: 0.3461(13), 0.5790(5), 1/4 D3: 0.0311(13), 0.7146(3), 1/4 D4: 0.1914(7), 0.0718(3), 0.4986(9)
$SrAlH_5$ (theoretical)	*P* $2_12_12_1$ (No. 19) [192] a = 12.679; b = 5.200; c = 4.508 α = β = γ =90	Sr: 0.908, 0.104, 0.036 Al: 0.165, 0.117, 0.071 H1: 0.763, 0.859, 0.278 H2: 0.078, 0.337, 0.918 H3: 0.093, 0.860, 0.945 H4: 0.079, 0.114, 0.374 H5: 0.254, 0.116, 0.768
Sr_2AlD_7	*I2* (No. 5) [230] a = 12.552(1); b = 9.7826(8); c = 7.9816(7) α = γ = 90; β = 100.286(4)	Sr1: 0.0935(3), 0.3289(4), 0.3195(6) Sr1′: 0.9065(3), 0.6711(4), 0.3195(6) Sr2: 0.8609(4), 0.0684(4), 0.0882(6) Sr2′: 0.1391(4), 0.9316(4), 0.4118(6) Al1: 0.671(1), 0.847(1), 0.232(2) Al1′: 0.329(1), 0.153(1), 0.268(2) D1: 0.7494(7), 0.8594(7), 0.077(1) D1′: 0.2506(7), 0.1406(7), 0.423(1) D2: 0.6014(7), 0.7106(7), 0.117(1) D2′: 0.3986(7), 0.2894(7), 0.383(1) D3: 0.7658(6), 0.7378(8), 0.341(1) D3′: 0.2342(6), 0.2622(8), 0.159(1) D4: 0.5885(6), 0.8298(8), 0.379(1) D4′: 0.4115(6), 0.1702(8), 0.121(1) D5: 0.7395(6), 0.9919(7), 0.3291(9) D5′: 0.2605(6), 0.0081(7), 0.1709(9) D6: 0.5748(6), 0.9558(7), 0.1157(8) D6′: 0.4252(6), 0.0442(7), 0.3843(8) D7: 0.4375(6), 0.6037(7), 0.3189(9) D7′: 0.5625(6), 0.3963(7), 0.1811(9)
$SrAl_2D_2$	*P-3m1* (No. 164) [233] a = b = 4.5253(1); c = 4.7214(2) α = γ = 90; β = 120	Sr: 0,0,0 Al: 0.3333, 0.6667, 0.4589(7) D: 0.3333, 0.6667, 0.0976(4)

Liu et al. reported a clear effect of the initial stoichiometry of the mixture on the product when a mixture of BaH_2 and Al was used as the precursor. The 2:1 and 1:1 mixtures directed the product to Ba_2AlH_7. Meanwhile, a 1:2 mixture directed the product to $BaAlH_5$ [237]. However, none of the mixtures produced a complete reaction.

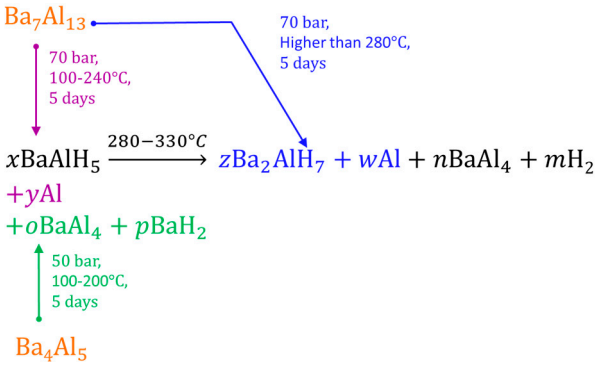

Figure 18. Production of $BaAlH_4$ or B_2AlH_7 from hydrogenation of Ba_7Al_{13} or Ba_4Al_5.

Liu et al. proposed the following reactions for the decomposition of $BaAlH_5$ and Ba_2AlH_7 [236]:

$$5BaAlH_5 \rightarrow Ba_2AlH_7 + 2BaH_2 + BaAl_4 + 7H_2 \text{ (280 °C, Argon)} \quad (60)$$

$$4BaAlH_5 \rightarrow 3BaH_2 + BaAl_4 + 7H_2 \text{ (350 °C, Vacuum)} \quad (61)$$

$$4Ba_2AlH_7 \rightarrow 7BaH_2 + BaAl_4 + 7H_2 \text{ (350 °C, Vacuum)} \quad (62)$$

Table 11 and Figure 19 present the crystal structures of the barium-aluminum hydrides. The crystal structure of $BaAlH_5$ is composed of corner-sharing (AlH_6) octahedra that form zigzag chains along the crystallographic *c* axis [207]. Meanwhile, Ba_2AlD_7 is composed of isolated (AlD_6) octahedra and infinite one-dimensional chains of edge-sharing (DBa_4) tetrahedra [235].

Table 11. Crystallographic data of barium-aluminum hydrides.

Compound	Space Group, Cell Dimensions [Å]	Atomic Coordinates
$BaAlH_5$	Pna21 (No. 33) [207] a = 9.1568; b = 7.0718; c = 5.1039 α = β = γ = 90	Ba: 0.686, 0.156, 0.256 Al: 0.041, 0.846, 0.229 H1: 0.008, 0.946, 0.905 H2: 0.584, 0.844, 0.025 H3: 0.578, 0.786, 0.504 H4: 0.357, 0.695, 0.233 H5: 0.708; 0.545, 0.214
Ba_2AlD_7	I2/a (No. 15) [235] a = 13.197(3); b = 10.237(2); c = 8.509(2) α = γ = 90; β = 101.290(9)	Ba1: 0.3459, 0.5848, 0.3249 Ba2: 0.1084, 0.3247, 0.0852, Al1: 0.927, 0.096, 0.235 D1: 0.004(1), 0.116(1), 0.077(2) D2: 0.846(1), 0.974(1), 0.135(2) D3: 0.023(1), 0.999(2), 0.325(2) D4: 0.844(1), 0.104(2), 0.387(2) D5: 0.983(1), 0.249(2), 0.324(2) D6: 0.832(1), 0.207(1), 0.115(2) D7: 0.693(1), 0.864(1), 0.322(2)

3.4. Alanates of Transition Metals

The alanates of the transition metals date from the 1950s–1960s. Although most of them have decomposition temperatures too low for hydrogen storage purposes, some of them can be of interest. However, almost all of the reported materials have been poorly characterized. Normally, the old reports did not present the basic characterization of materials, for example, X-ray diffraction or infrared spectroscopy. On the other hand, some of them have only been theoretically discussed. In the following sections, the most important (experimental and/or theoretical) characteristics of this family of alanates are presented.

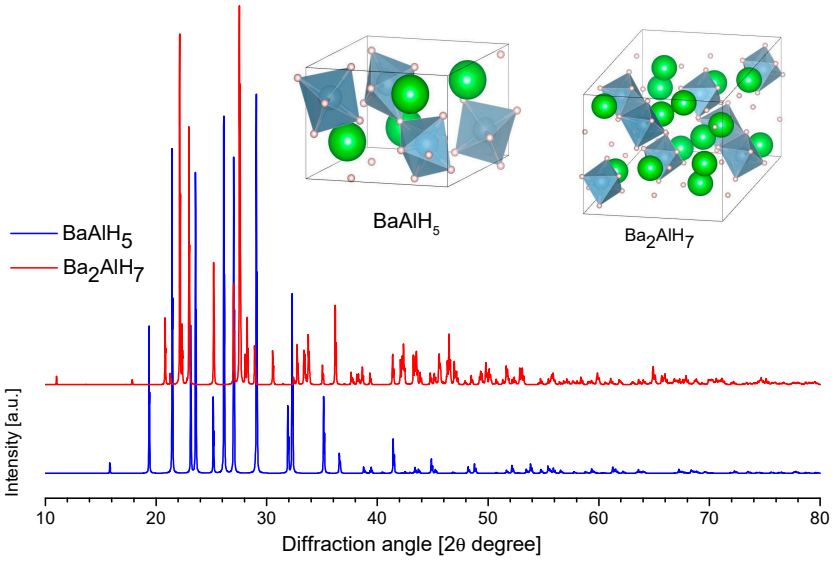

Figure 19. Crystal structure of barium alanates and their calculated diffraction patterns ($\lambda = Cu_{k\alpha 1}$).

3.4.1. Scandium Alanate

Charkin et al., in a theoretical study, proposed the decomposition of a hypothetical $Sc(AlH_4)_3$ to provide the following products: a) $HSc(AlH_4)_2 + AlH_3$, b) $H_2Sc(AlH_4) + 2AlH_3$, or c) $ScH_3 + 3AlH_3$. This latter route will give the highest dissociation energy [238]. $Sc(AlH_4)_3$ deserves more research to estimate, for example, formation energy or crystal structure. Experimentally, $Sc(AlH_4)_3$ has not been synthesized, despite a possible and interesting 8.7 wt.% of hydrogen content.

3.4.2. Yttrium Alanate

$Y(AlH_4)_3$ was first described by Kost et al. in 1978 [239]. Later, in 2017, Cao et al. demonstrated the partial reversibility of hydrogen storage [240]. $Y(AlH_4)_3$ has a hydrogen content of 6.6 wt.% and it can be produced by the metathesis reaction between $3LiAlH_4 + YCl_3$ [240].

Kost et al. reported the beginning of decomposition of $Y(AlH_4)_3$ at 50 °C [239]. However, they did not present additional details. Cao et al., based on different characterization techniques, proposed that the decomposition of $Y(AlH_4)_3$ occurs as:

$$Y(AlH_4)_3 \rightarrow YAlH_6 + 2Al + 3H_2 \text{ (80–170 °C)} \quad (63)$$

$$YAlH_6 \rightarrow YH_3 + Al + 1.5H_2 \text{ (170–250 °C)} \quad (64)$$

$$YH_3 \rightarrow YH_2 + 0.5H_2 \text{ (250–350 °C)} \quad (65)$$

$$YH_2 + 3Al \rightarrow YAl_3 + H_2 \text{ (>350 °C)} \quad (66)$$

In reaction (63), at 140 °C, 3.4 wt.% of hydrogen was released. 2.6 wt.% of hydrogen was re-adsorbed at 145 °C and 100 bar. However, no direct hydrogenation from YH_3 +Al at 145 °C and 100 bar occurred [240]. $Y(AlH_4)_3$, and $YAlH_6$ are reported as amorphous materials [240]. However, no direct evidence of $YAlH_6$ was presented [240]; thus, further characterizations of these materials are needed.

3.4.3. Titanium Alanate

Wiberg et al. reported the formation of $Ti(AlH_4)_4$ (11.1 wt.% hydrogen content) in 1951 [14]. The synthetic route was the metathesis reaction between $TiCl_4$ and $LiAlH_4$ in ether at −110 °C [14]. Later, in 1975, Kost et al. reported a similar synthesis while using $LiAlH_4$ and $TiBr_4$ or $TiCl_4$. The product was separated from the solution in a filter cooled with dry ice [241]. The reported stoichiometries

indicted that the metathesis reaction was not completed or that partial substitution of Cl^- by $[AlH_4]^-$ was achieved [241]. Wiberg reported that $Ti(AlH_4)_4$ was decomposed at −85 °C [14]; for its part, Kost reported the evolution of "two g-atom of H per g-atom of Ti" at −70 °C [241]. The decomposition of $Ti(AlH_4)_4$ was proposed as [241]:

$$Ti(AlH_4)_4 \rightarrow TiH_2 + 4AlH_3 + H_2. \quad (67)$$

Further decomposition of AlH_3 was observed at 110 °C [241]. No more characteristics of this material have been reported. However, $Ti(AlH_4)_4$ can be a very interesting material in regards to its hydrogen content, perhaps tailoring the dehydrogenation temperature with some structural or chemical modification could be explored. Another point to discuss is that Ti can work in other oxidation states besides Ti^{4+}; for example, Ti^{3+} or Ti^{2+}. The Ti^{3+} and Ti^{2+} compounds are generally more stable than the Ti^{4+} compounds, i.e., the liquid and volatile $TiCl_4$ versus solid TiF_3 or $TiCl_2$. Alternatively, other compositions of Ti-Al alloys or intermetallics could be explored. For example, Ramzan et al. explored employing DFT calculations, the structural stability, and other properties of Ti_4AlH_3 and Ti_3AlH_2 phases [242]. Maeland et al., some time ago, reported the reversible hydrogenation of Ti_3Al at 9.2 bar of deuterium pressure and 200 °C to form Ti_3AlD_x (x = 5.9–8) [243].

3.4.4. Zirconium Alanate

The first report on $Zr(AlH_4)_4$ was the work of Reid et al. in 1957 [13]. $Zr(AlH_4)_4$ (7.49 wt.% hydrogen content) was produced by the metathesis reaction between $Zr(BH_4)_4$ and $LiAlH_4$ in ether solution and He atmosphere [13]. $Zr(BH_4)_4$ was formerly prepared by metathesis of $LiBH_4$ and $ZrCl_4$ [13]. In 2008, $Zr(AlH_4)_4$ was produced by the reaction between $LiAlH_4$ and $ZrCl_4$ in ether solution [244]. No clear indication of the reaction temperature was found in this work. No reports regarding the characteristics of dehydrogenation or on the characterization of this material were found. Other compositions of the Zr-Al-H system deserve further research; for example, Matsubara et al. achieved the hydrogenation of the intermetallic Zr_3Al to give Zr_3AlH_4 [245].

3.4.5. Vanadium Alanate

Charkin et al. also proposed the decomposition of a hypothetical $V(AlH_4)_3$ to provide the following products: (a) $HV(AlH_4)_2$ + AlH_3, (b)$H_2V(AlH_4)$ + $2AlH_3$, or (c) VH_3 + $3AlH_3$ [238]. Experimental confirmation of the existence of $V(AlH_4)_3$ is missing.

3.4.6. Niobium Alanates

Wiberg et al., in 1965, reported the reaction between $NbCl_5$ and $LiAlH_4$ in several proportions and temperatures in ether at low temperature [246]. Wiberg et al. concluded that the products were a function of the temperature and the excess of $LiAlH_4$ used; the first family of products was [246]:

$$NbCl_5 + 5LiAlH_4 \rightarrow Nb(AlH_4)_n + (5 - n)AlH_3 + \frac{5-n}{2}H_2 + 5LiCl, \quad (68)$$

when n = 3.5 at −70 °C the product was $Nb_2(AlH_4)_7$, for n = 3.0 at −40 °C the product was $Nb_2(AlH_4)_6$, and for n = 2.5 at 20 °C the product was $Nb_2(AlH_4)_5$.

The other family of products was:

$$NbCl_5 + (5 + m)LiAlH_4 \rightarrow Li_mNb(AlH_4)_{n+m} + (5 - n)AlH_3 + \frac{5-n}{2}H_2 + 5LiCl, \quad (69)$$

$LiNb_2(AlH_4)_7$ was formed at −70 °C; meanwhile, $LiNb_2(AlH_4)_5$ and $LiNb(AlH_4)_3$ were formed at 25 °C [246]. Wiberg et al. wonderfully described the synthesis procedure and the changes in the color that are associated with each Nb or LiNb- alanates. However, a detailed characterization is needed,

particularly the characterization of the material obtained at room temperature $Nb_2(AlH_4)_5$ (5.9 wt.% hydrogen content).

3.4.7. Tantalum Alanates

$TaH_2(AlH_4)_2$ was reported by Kost et al. in 1978 [239]. The compound has a hydrogen content of 4.11 wt.%. It was produced in cold ether by the reaction between LiH, Al and a metal halide. Kost et al. reported that $TaH_2(AlH_4)_2$ is a red powder that decomposes at 130 °C. $TaH_2(AlH_4)_2$ and AlH_3 are the decomposition products of a very unstable $Ta(AlH_4)_n$ [239].

3.4.8. Manganese Alanate

The reports on $Mn(AlH_4)_2$ are rather diffuse, as in the case of $Be(AlH_4)_2$. The first compilation where $Mn(AlH_4)_2$ appeared, is the book of Mackay [187]. In that book, $Mn(AlH_4)_2$ was reported to be prepared from a halide complex (no mention of which halide) and $LiAlH_4$ in Et_2O, and to decompose at 25 °C. The book refers, in turn, to two reports of Monnier et al. [247,248]. No further reports on $Mn(AlH_4)_2$ were found. $Mn(AlH_4)_2$ would have a hydrogen content of 6.89 wt.%.

3.4.9. Iron Alanate

$Fe(AlH_4)_2$ can be an interesting material for hydrogen storage, due to the 6.84 wt.% of hydrogen content. However, contradictory reports on the decomposition temperature are published. In favor of the near-room temperature stability of $Fe(AlH_4)_2$ is the report of Neumaier et al. [249]. $Fe(AlH_4)_2$ was prepared by means of metathesis of $FeCl_3 + 3LiAlH_4$ in ether at low temperature (−116 °C) [249]. Once formed, the iron easily decomposed. Neumaier et al. presented a *p*-T diagram of the decomposition reaction; around 20 °C a continuous partial decomposition was observed. Meanwhile, a fast decomposition was observed at 90–100 °C. Two comments can be mentioned: (1) The quantity of released hydrogen was not reported despite a detailed thermolysis study being presented. (2) The fast decomposition at 90–100 °C is near to the temperature of α-, and α'-alane decomposition [186], which is one by-product of iron alanate formation. This leave doubts about who is decomposing $Fe(AlH_4)_2$ or AlH_3. Despite that, Neumaier et al. considered $Fe(AlH_4)_2$ to be stable at room temperature. The proposed reactions of formation and decomposition are [249]:

$$FeCl_3 + 3LiAlH_4 \rightarrow Fe(AlH_4)_2 + AlH_3 + 3LiCl + 0.5H_2, \quad (70)$$

$$Fe(AlH_4)_2 \rightarrow Fe + 2Al + 4H_2 \quad (71)$$

Against the near-room temperature stability of $Fe(AlH_4)_2$ is the report of Schaeffer et al. [250]. They also produced $Fe(AlH_4)_2$ by means of metathesis of $FeCl_3$ and an excess of $LiAlH_4$. However, Schaeffer et al. considered $Fe(AlH_4)_2$ to be unstable at room temperature.

3.4.10. Copper Alanate

$CuAlH_4$ (4.2 wt.% hydrogen content) was reported as a product of the reaction between CuI and $LiAlH_4$ in ether at −78 °C by Ashby et al. [251]. $CuAlH_4$ is unstable and it reacts quickly, with the proposed product being Cu_3AlH_6 [251]:

$$CuAlH_4 \rightarrow CuH + AlH_3 \quad (72)$$

$$2CuH + CuAlH_4 \rightarrow Cu_3AlH_6 \quad (73)$$

Both of the alanates decomposed with a slight heating. Wiberg et al. reported that the reaction between CuI and $LiAlH_4$ in pyridine at room temperature did not produce Cu-alanates; it produced LiI, AlI_3, and CuH [252].

3.4.11. Silver Alanate

$AgAlH_4$ (2.9 wt.% hydrogen content) was produced by the following reaction in ether at −80 °C [253]:

$$AgClO_4 + LiAlH_4 \rightarrow AgAlH_4 + LiClO_4 \quad (74)$$

$AgAlH_4$ decomposed at −50 °C to the elements Ag, Al, and H_2 [253].

3.4.12. Zinc Alanate

Zhizhin et al. (and references wherein) summarized the production of ZnH_2; one of the reactions is [254]:

$$2LiAlH_4 + ZnI_2 \rightarrow 2LiI + 2AlH_3 + ZnH_2 \quad (75)$$

However, depending on the reaction conditions (solvent composition, mainly), admixtures of Zn-AlH_4 can be present:

$$LiAlH_4 \overset{ZnI_2}{\rightarrow} Zn(AlH_4)_2 \overset{ZnI_2,LiAlH_4}{\rightarrow} Zn[ZnI_2(AlH_4)_2] \overset{ZnI_2,LiAlH_4}{\rightarrow} Zn[ZnI_3(AlH_4)] \quad (76)$$

3.5. Alanates of the Main Group

As in the case of transition metals alanates, the alanates of the main group elements are scarce, with most of them being unstable, even at low temperatures.

3.5.1. Gallium Alanate

$Ga(AlH_4)_3$ (7.4 wt.% hydrogen content) was produced by the reaction between $GaCl_3$ and $LiAlH_4$ in ether at 0 °C [255,256]:

$$GaCl_3 + 3LiAlH_4 \rightarrow Ga(AlH_4)_3 + 3LiCl \quad (77)$$

However, at 35 °C, the $Ga(AlH_4)_3$ decomposes into GaH_3 and AlH_3 [256].

3.5.2. Indium Alanate

$In(AlH_4)_3$ (5.8 wt.% hydrogen content) was produced by the reaction between $InCl_3$ and $LiAlH_4$ in ether at −70 °C [256]:

$$InCl_3 + 3LiAlH_4 \rightarrow In(AlH_4)_3 + 3LiCl \quad (78)$$

The $In(AlH_4)_3$ decomposed at −40 °C. However, in a similar reaction at room temperature:

$$InCl_3 + LiAlH_4 \rightarrow InCl_2(AlH_4) + LiCl, \quad (79)$$

the product $InCl_2(AlH_4)$ is stable up to 100 °C [256].

3.5.3. Thallium Alanate

The synthesis of $TlAlH_4$ was reported in 1967, the reaction was performed in ether at −100 °C [257,258]:

$$TlClO_4 + LiAlH_4 \rightarrow TlAlH_4 + LiClO_4. \quad (80)$$

$TlAlH_4$ decomposed at −80 °C (1.9 wt.% hydrogen content). Wiberg et al. tried the metathesis reaction between $TiCl_3$ and $LiAlH_4$ in ether at −115 °C [258]. However, no Tl^{+3}-alanate could be isolated from the reaction of $TlCl_3$ and $LiAlH_4$, with the product spontaneously decomposing at −110 °C [258,259]. A marginal stabilization was achieved when a Cl^- substituted an $[AlH_4]^-$ ion: $TlCl(AlH_4)_2$ was produced by the reaction between $TlCl_3$ and AlH_3 in ether at −115 °C in the presence of $AlH_3{\cdot}AlCl_3$ [259]. $TlCl(AlH_4)_2$ decomposed at −95 °C [259].

3.5.4. Tin Alanate

$Sn(AlH_4)_4$ (6.6 wt.% hydrogen content) was produced by the reaction between $SnCl_4$ and $LiAlH_4$ in ether at −80 °C [260]:

$$SnCl_4 + 4LiAlH_4 \rightarrow Sn(AlH_4)_4 + 4LiCl. \quad (81)$$

$Sn(AlH_4)_4$ decompose at −40 °C. The decomposition products are Sn, Al and H_2.

3.6. Alanates of Lanthanides and Actinides

3.6.1. Lanthanum, Cerium, Praseodymium and Neodymium Alanates

La, Ce, Pr, and Nd alanates were produced by metathesis that was assisted by mechanical milling of the corresponding trichlorides and $NaAlH_4$ (in excess 1:3) under hydrogen pressure (1–15 bar) [261]. The expected products, $M(AlH_4)_3$, M = La, Ce, Pr, and Nd, are unstable and decompose during ball milling. Instead of $M(AlH_4)_3$, alumino-hydrides of stoichiometry MAl_xH_y were obtained (very close to $MAlH_6$ stoichiometry). Thermolysis of the $MAlH_6$ (M = Ce, Pr, and Nd) materials demonstrated two-steps of decomposition, except for $LaAlH_6$ [261]. The first step is associated with the decomposition of the alanate. Meanwhile, the second step can be associated with the decomposition of the corresponding metal hydride and the formation of M-Al alloys. Although the decomposition pathway was proposed for Nd, based on the in-situ X-ray diffraction data that were presented by Weidenthaler et al., the reaction can be extrapolated for Ce and Pr [261]:

$$NdAlH_6 \rightarrow NdH_3 + Al + 3/2H_2 \quad (82)$$

$$NdH_3 + 4Al \rightarrow NdAl_4 + 3/2H_2 \quad (83)$$

Table 12 summarizes the hydrogen content, hydrogen released, decomposition temperatures, and crystal structure data [261]. The experimental X-ray diffraction patterns of MAl_xH_y were compared to the DFT calculations of hypothetical $MAlH_6$ materials. Figure 20 presents the expected X-ray diffraction patterns and the structures.

Table 12. Lanthanides-Aluminum Hydrides ($MAlH_6$) relevant data [261].

Material	Hydrogen Content	Hydrogen Release *	Decomposition Temperature [°C]	Crystal Structure (*R-3m*, No.166) [Å]	
	[wt.%]			Experimental	DFT **
$LaAlH_6$	3.51	0.98	Beginning 100, ending 240	a = 6.4732 c = 6.2765	a = 6.5272(4) c = 6.3212(7) H: 0.2149, 0.7851, 0.4904
$CeAlH_6$	3.49	0.80	First step: Beginning 100, ending 170 Second step: Beginning 180, ending 270	a = 6.4711 c = 6.2527	a = 6.4637(4) c = 6.2609(7) H: 0.2147, 0.7853, 0.4910
$PrAlH_6$	3.47	0.78		a = 6.4217 c = 6.2028	a = 6.4106(7) c = 6.2118(11) H: 0.2139, 0.7861, 0.4894
$NdAlH_6$	3.41	0.78		a = 6.3796 c = 6.1616	a = 6.3846(7) c = 6.1741(10) H: 0.2132, 0.7868, 0.4883

* (including NaCl load) ** M = La, Ce, Pd, Nd on 0, 0, 1/2, and Al on 0, 0, 0.

3.6.2. Europium Alanate

$Eu(AlH_4)_2$ was produced by the metathesis reaction of $EuCl_2$ + $2NaAlH_4$ or $EuCl_3$ + $3NaAlH_4$. The reaction was performed by means of mechanical milling in a hydrogen atmosphere (1–15 bar) and different milling times (180 min seems enough time) [44]. Independently of the initial oxidation state of Eu ion, Eu^{2+}, or Eu^{3+}, the final alanate was Eu^{2+}, i.e., $Eu(AlH_4)_2$. Additionally, $NaEu_2Cl_6$ was observed as an intermediary. $Eu(AlH_4)_2$ has a hydrogen content of 3.76 wt.%. Pommerin et al. demonstrated a hydrogen release of about 1.8 wt.% (including the NaCl load) in two steps [44]. The first step occurred at about 100–125 °C with the formation of $EuAlH_5$. The second step occurred at about 200–225 °C. Further heating led to the formation of $EuAl_4$. Rehydrogenation was achieved by milling at high hydrogen pressure (50, 200, or 300 bar). Unfortunately, the rehydrogenation was not achieved under 1000 bar of static H_2 pressure; i.e., the temperature of rehydrogenation was not clearly indicated without milling. Further dehydrogenation demonstrated that the two-step reactions and temperature range are kept. However, a drastic reduction of the hydrogen release was found (about 0.8 wt.%) [44]. Partial crystallographic information was reported, i.e., no H position was determined (Table 13) [44]. Figure 20 presents the expected X-ray diffraction patterns and structures.

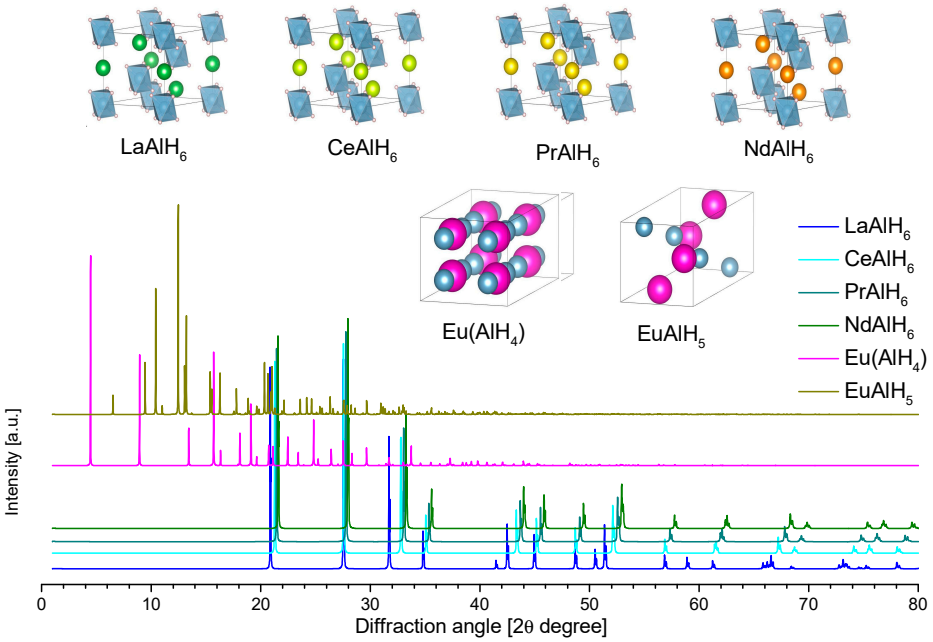

Figure 20. Crystal structure of lanthanides alanates and their calculated diffraction patterns (λ = $Cu_{k\alpha 1}$).

Table 13. Crystallographic data of Europium alanates [44].

Compound	Space Group, Cell Dimensions [Å]	Atomic Coordinates
$Eu(AlH_4)_2$	*Pmmn* (No. 59) a: 9.1003(13); b: 5.1912(8); c: 4.2741(5)	Eu: 0.1966(3), 0.25, 0.75 Al: 0.9625(12), 0.25, 0.25 Al: 0.3821(5), 0.75, 0.25
$EuAlH_5$	*Pnma* (No. 62) a: 12.481(3); b: 5.0103(12); c: 4.5887(11)	Eu: 0.6517(3), 0.25, 0.2016(12) Al: 0.4105(14), 0.25, 0.586(4)

3.6.3. Ytterbium Alanate

$Yb(AlH_4)_2$ was reported by Kost et al. in 1978 [239]. The compound has a hydrogen content of 3.43 wt.%. It was produced in cold ether by the metathesis reaction between LiH, Al, and a metal halide. Kost et al. reported that $Yb(AlH_4)_2$ is a yellow powder that decomposes at 70 °C.

The decomposition products of $Yb(AlH_4)_2$ are the hydrides of Al and Yb [239]. The YbH_2 is metastable at room temperature [262].

3.6.4. Thorium-Aluminum Hydride

No records of thorium alanate were found; however, an intermetallic hydride of Th was found: Th_2AlH_4. The thorium-aluminum hydride can be easily obtained by the hydrogenation of the intermetallic Th_2Al [263]. Th_2Al needs activation at 450 °C in vacuum, followed by deuterium absorption at 0.15 bar and iced-water cooling [264]. The products were Th_2AlD_x, x = 3.9 ± 0.1, 2.7, and 2.3 [264]. Experimental and theoretical crystal structure of Th_2AlH_4 reasonably agreed on a *I4/mcm* space group with lattice parameters a = 7.626 Å, and c = 6.515 Å, and atomic positions Th (0.1656, 0.6656, 0), Al (0, 0, 0.25), and H (0.377, 0.8707, 0.1512) [265].

4. Cation-Mixed Alanates

Cation substitution has demonstrated utility in the tailoring of the thermodynamic and kinetic properties in borohydrides [22,266]. A similar approach has been applied to alanates, for which $LiAlH_4$ or $NaAlH_4$ are frequently used as starting materials due to their reactivity. These alanates react with other metal hydrides to form mixed cation alanates. The reactions can be generalized as [267]:

$$M'AlH_4 + 2MH \rightarrow M_2M'AlH_6, \quad (84)$$

$$MAlH_4 + MH + M'H \rightarrow M_2M'AlH_6, M \neq M'. \quad (85)$$

Theoretical calculations had predicted the stability of alanates, such as $LiNa_2AlH_6$, K_2LiAlH_6, K_2NaAlH_6, $K_{2.5}Na_{0.5}AlH_6$, $LiMgAlH_6$, $LiCaAlH_6$, $NaCaAlH_6$, and $KCaAlH_6$ [268,269]. Some of them have been successfully synthesized, as presented below.

4.1. Li-Na Alanates

Na_2LiAlH_6 can be obtained by the reaction of 2NaH and $LiAlH_4$ in an organic solvent [270], in the solid-state at very high hydrogen pressure [270], by means of a mechanically activated reaction between NaH, LiH, and $NaAlH_4$ (Equation (86)) [271], or 2NaH + $LiAlH_4$ [272–274], or NaH + $LiAlH_4$ [275], or $2NaAlH_4$ + LiH [276], or by the reactive mechanical milling of 2NaH+LiH+Al that was catalyzed with TiF_3 under 30 bar of hydrogen pressure [277]. Wang et al. produced Na_2LiAlH_6 by the reaction between 2NaH and $LiAH_4$ [274]. However, detailed study of the synthesis reaction pathway by X-ray diffraction demonstrated that, during mechanical milling, a metathesis reaction occurred to produce a mixture of LiH, $NaAlH_4$, and residual NaH, i.e., the same reactants of Equation (86).

$$NaH + LiH + NaAlH_4 \rightarrow Na_2LiAlH_6. \quad (86)$$

$LiNa_2AlH_6$ was also observed during the electrochemical decomposition of $NaAlH_6$ in the presence of Li [278]:

$$NaAlH_4 + 3/2\ Li \rightarrow \frac{1}{2}\ Na_2LiAlH_6 + \frac{1}{2}\ Al + LiH. \quad (87)$$

Na_2LiAlH_6 has a total hydrogen content of 7.03 wt.% and a theoretical reversible hydrogen storage of 3.51 wt.% (Equation (88)). Na_2LiAlH_6 has demonstrated reversibility (Equation (88)) [274,277], which is enhanced by the use of a catalysts, such as TiF_3, $TiFe_3$, $TiCl_3$, CeO_2, $ZrCl_4$, $TiBr_4$, $CrCl_3$, $AlCl_3$, TiO_2, Y_2O_3, or $MnCl_2$ [276,277,279,280].

$$Na_2LiAlH_6 \leftrightarrow 2NaH + LiH + Al + 3/2\ H_2. \quad (88)$$

Dehydrogenation reaction (Equation (88)) without additives occurs between 190–250 °C and it releases about 3.35 wt.%. Further reactions involve NaH decomposition at 320–380 °C and finally the reaction of LiH with Al at 380–480 °C, with the formation of LiAl and H_2. Wang et al. demonstrated

a release of 6.73 wt.% and a re-hydrogenation level of 6.6 wt.% when heating up to 530 °C under vacuum, and 285 °C and 135 bar, respectively. Small amounts of Na_3AlH_6 have been observed during the dehydrogenation of Na_2LiAlH_6 [274,281]. Additives, such as TiF_3, resulted in a low-temperature beginning of Na_2LiAlH_6 decomposition (~50 °C) [276,277,280]. Additionally, Al_3Ti was found after dehydrogenation when Na_2LiAlH_6 is mixed with TiF_3 [279,280].

First principle studies (before experimentation, i.e., synthesis and crystal structure determination) indicated that Na_2LiAlH_6 would have *P* $2_1/n$ [282] or *P* $2_1/c$ [283] symmetry, which is very close to *Fm-3m* symmetry [283]. Brinks et al. determined the group symmetry of Na_2LiAlD_6 as *Fm-3m*. This material consists of corning-sharing (AlD_6) and (LiD_6) octahedra, where each octahedron is surrounded by six octahedra (Table 14 and Figure 21) [284]. The deuterated Na_2LiAlD_6 was produced by the ball milling of $NaAlD_4$ and $LiAlD_4$ [284].

Table 14. Crystallographic data of Li-Na mixed alanates.

Compound	Space Group, Cell Dimensions [Å]	Atomic Coordinates
Na_2LiAlD_6 (experimental)	*Fm-3m* (No. 225) [284] a: 7.38484 (5)	Na: 0.25, 0.25, 0.25 Li: 0.5, 0.5, 0.5 Al: 0, 0, 0 D: 0.238(4), 0, 0
Na_2LiAlH_6 (calculated)	*P* $2_1/c$ (No. 14) [282] a = 5.165; b = 5.251; c = 7.339 α = 90, β = 90.03, γ = 90	Li: 0, 0, 0.5 Na: 0.99, 0.47, 0.25 Al: 0, 0, 0 H: 0.07, 0.02, 0.23 H: 0.23, 0.3, 0.53 H: 0.2, 0.27, 0.96

The research group of Prof. Q. Wang performed a complete study regarding the determination of the (*p*, T) equilibrium of reaction (88) with and without TiF_4 as a catalyst (Figure 22) [274,285]. The results indicate that the catalyst moves to higher pressure the equilibrium towards Na_2LiAlH_6 formation at a given temperature; or conversely a reduction of the equilibrium temperature at a given pressure. Fonneløp et al. revealed that the addition of 10 mol% of TiF_3 to Na_2LiAlH_6 induced hydrogen release at temperatures as low as 50 °C [281]. In such a case, the dehydrogenation pathway changes from a one-step process (Equation (88)) to a two-step process, with the formation of Na_3AlH_6 as the intermediary. Between 50–180 °C, the decomposition reaction was described as:

$$Na_2LiAlH_6 \rightarrow 2/3\ Na_3AlH_6 + LiH + 1/3\ Al + 1/2\ H_2. \quad (89)$$

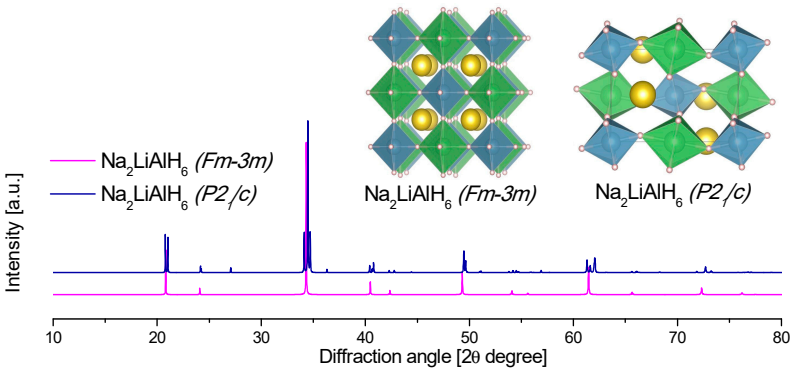

Figure 21. Crystal structure of Na-Li alanate and its calculated diffraction patterns ($\lambda = Cu_{k\alpha 1}$).

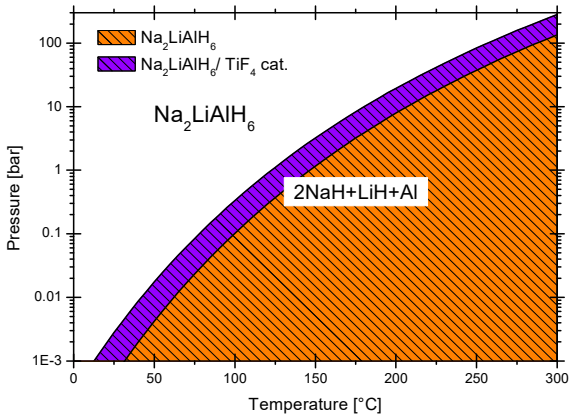

Figure 22. Phase diagram of 2NaH + LiH + Al vs. Na_2LiAlH_6. Data adapted from references [274,285], $\ln(p) = -\frac{7685.3}{T} + 18.3$ for un-catalyzed material, and $\ln(p) = -\frac{6894.9}{T} + 17.0$ for material catalyzed with TiF_4. In the original formulae, p is in atm, and T in Kelvin.

Further heating (180–225 °C) leads to the usual decomposition reaction of Na_3AlH_6.

Finally, the other possible combination of Li, Na, Al, and H would be as Li_2NaAlH_6. However, attempts to synthesize this material have been unsuccessful. The attempts involve the synthesis in organic solvents, such as Me_2O (160 °C, 12 h), or by ball-milling [267]. As proposed by Santhanam et al. [169], Li_2NaAlH_6 is not formed at all under the tested conditions, or it disproportionates Na_2LiAlH_6, LiH and $LiAlH_4$.

4.2. Li-K Alanates

K_2LiAlH_6 was reported in 2005 by Graetz et al. [267]. K_2LiAlH_6 was produced by the ball-milling of 2KH + $LiAlH_4$ [267]. Graetz et al. determined an *Fm-3m* structure for K_2LiAlH_6. However, in their paper, they recognized that the diffraction pattern was not suitable for Rietveld analysis [267]. Briefly, after that, Rönnebro et al. performed the mechanical milling of the same precursors followed by a heating treatment of the pelletized sample at 320–330 °C and 700 bar for 1–2 days. By doing this, K_2LiAlH_6 was crystallized, and its crystal structure was determined to have *R3m* symmetry (Table 15) [286]. As in the case of Na_2LiAlH_6, theoretical calculations (predating synthesis and crystal structure determination) predicted that K_2LiAlH_6 would have *P* $2_1/n$ symmetry (Table 15 and Figure 23) [282,283]. The differences between the calculated and the experimental data could be related to the temperature of calculation (0 K) versus the temperature of synthesis and testing (near room temperature).

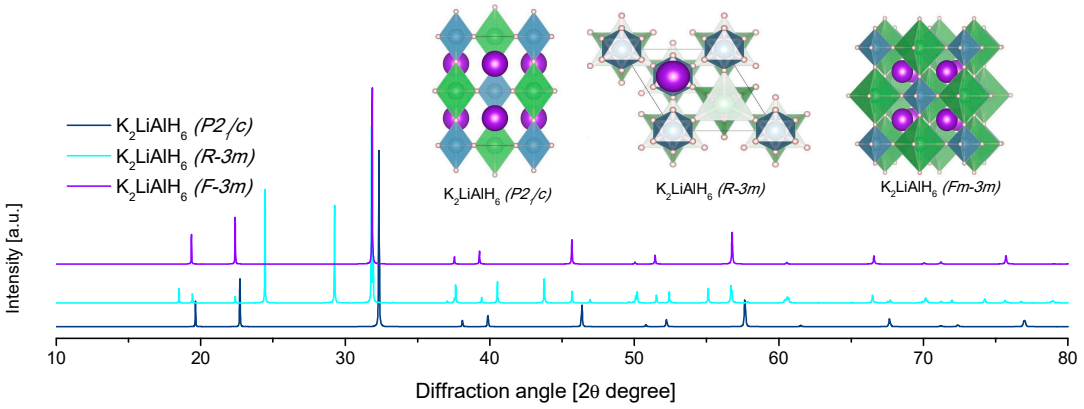

Figure 23. Crystal structure of Li-K alanate and its calculated diffraction patterns ($\lambda = Cu_{k\alpha 1}$).

Table 15. Crystallographic data of Li-K mixed alanates.

Compound	Space Group, Cell Dimensions [Å]	Atomic Coordinates
K_2LiAlH_6	*R-3m* (No. 166) [286] a: 5.62068(8) c: 27.3986(6)	Li: 0, 0, 0.4036(8) Al: 0, 0, 0 Al: 0, 0, 1/2 K: 0, 0, 0.1270(1) K: 0, 0, 0.2853 (1) H: 0.096(7), −0.096(7), 0.466(3) H: 0.205(5), −0.205(5), 0.638(2)
K_2LiAlH_6	*Fm-3m* (225) [267] a = 7.9383	K: 1/4, 1/4, 1/4 Li: 1/2, 1/2, 1/2 Al: 0, 0, 0 H: 0.216, 0, 0
K_2LiAlH_6 (calculated)	*P* $2_1/n$ (No. 14) [282] a = 5.528 b = 5.536 c = 7.832 α = 90, β = 90.03, γ = 90	K: 0, 1/2, 1/4 Li: 0, 0, 1/2 Al: 0, 0, 0 H: 0, 0, 0.23 H: 0.27, 0.27, 1/2 H: 0.23, 0.23, 0

K_2LiAlH_6 has a total hydrogen content of 5.11 wt.% and a possible reversible hydrogen storage of 2.56 wt.%. The dehydrogenation of K_2LiAlH_6 was performed at 227 °C, while rehydrogenation was performed at 300 °C and up to 10 bar [267]. The rehydrogenation achieved 2.3 wt.% hydrogen storage, i.e., approximately 90% of the theoretical value. However, the reaction time was very long, around 280 h; and, perhaps a higher hydrogenation pressure would improve kinetics.

Regarding other Li-K alanates and similar to the Li_2NaAlH_6 case, no Li_2KAlH_6 has been produced so far [169].

4.3. Li-Mg Alanates

The mixed alanate $LiMg(AlH_4)_3$ has a hydrogen content of 9.7 wt.%; $LiMg(AlH_4)_3$ is known since 1979 by the work of Bulychev et al. [287]. It can be produced by the metathesis reaction between $LiAlH_4$ and $MgCl_2$ [165,220,288]:

$$3LiAlH_4 + MgCl_2 \rightarrow LiMg(AlH_4)_3 + 2LiCl. \quad (90)$$

Reaction (90) can be performed in an organic solvent or assisted by mechanical milling. The decomposition of $LiMg(AlH_4)_3$ is a two-step process [289,290]:

$$LiMg(AlH_4)_3 \rightarrow LiMgAlH_6 + 2Al + 3H_2 \text{ (100–130 °C)} \quad (91)$$

$$LiMgAlH_6 \rightarrow LiH + MgH_2 + Al + 3/2\ H_2 \text{ (150–180 °C)} \quad (92)$$

The addition of graphitic nanofibers can reduce the dehydrogenation temperatures [291]. Addition of TiF_3 leads to the decomposition of the mixed alanate even during ball-milling [290]. Attempts of re-hydrogenation were unsuccessful, even at high pressures [289,290]. The structure of $LiMg(AlH_4)_3$ consists of a corner-sharing network of alternating $[AlH_4]^-$ tetrahedra and (LiH_6) and (MgH_6) octahedra (Table 16 and Figure 24) [288]. The structure of $LiMgAlH_6$ consists of alternating $AlMg_3$ and Al_2Li_3 layers; in the Al_2Li_3 layer, the $[AlH_6]^-$ octahedra share edges with three (LiD_6) octahedra [206,290].

Table 16. Crystallographic data of Li-Mg mixed alanates.

Compound	Space Group, Cell Dimensions [Å]	Atomic Coordinates
$LiMg(AlD_4)_3$	*P* $2_1/c$ (No. 14) [288] a = 8.37113(16) b = 8.73910(17) c = 14.3012(3) α = γ = 90, β = 124.8308(8)	Mg: 0.6305(6), 0.5292(4), 0.8833(3) Li: 0.127(3), 0.4720(19), 0.3822(14) Al1: 0.7615(5), 0.6282(4), 0.1512(3) Al2: 0.4745(5), 0.8809(4), 0.8581(3) A13: 0.9593(5), 0.2510(4), 0.4986(3) D1: 0.6057(14), 0.5722(12), 0.1782(9) D2: 0.6523(14), 0.5907(11), 0.0190(6) D3: 0.7843(17), 0.8088(9), 0.1721(10) D4: 0.9475(12), 0.5201(10), 0.2158(9) D5: 0.4888(15), 0.7127(10), 0.8153(9) D6: 0.6918(11), 0.9294(11), 0.9554(8) D7: 0.3783(15), 0.9895(12), 0.7474(8) D8: 0.3312(15), 0.8752(13), 0.8981(10) D9: 0.9500(15), 0.3124(13), 0.3908(8) D10: 0.7599(14), 0.1597(12), 0.4549(10) D11: 1.1293(13), 0.1222(10), 0.5635(8) D12: 0.9941(14), 0.3727(11), 0.5902(7)
$LiMgAlD_6$	*P321* (No. 150) [290] a = b = 7.985550(2) c = 4.378942(7) α = β = 90, γ = 120	Mg: 1, 0.3570(13), 0 Li: 0, 0.686(6), 1/2 Al1: 0, 0, 0 Al2: 1/3, 2/3, 0.492(10) D1: 0.540(3), 0.763(2), 0.278(3) D2: 0.119(3), 0.576(2), 0.734(3) D3: 0.904(2), 0.117(2), 0.228(3)

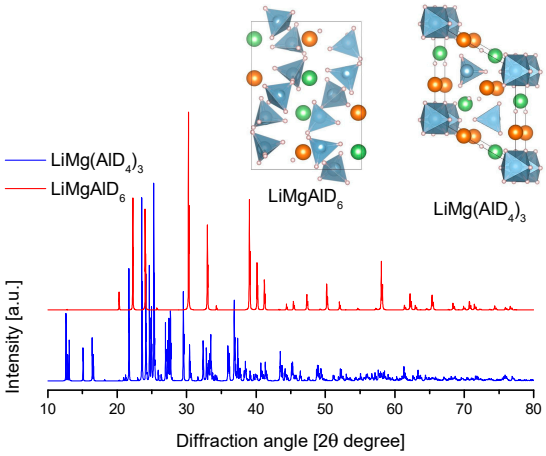

Figure 24. Crystal structure of Li-Mg alanates and its calculated diffraction patterns (λ = $Cu_{k\alpha 1}$)

4.4. Li-Ca Alanates

$LiCa(AlH_4)_3$ has a total hydrogen content of 8.6 wt.%; thus, it appears as a very attractive hydrogen storage material. $LiCa(AlH_4)_3$ was produced by the metathesis reaction between $LiAlH_4$ and $CaCl_2$, utilizing mechanical milling [292]:

$$3LiAlH_4 + CaCl_2 \rightarrow LiCa(AlH_4)_3 + 2LiCl. \quad (93)$$

$LiCa(AlH_4)_3$ (plus LiCl) starts decomposing at 120 °C and it ends at about 180 °C. Liu et al. proposed the formation of $LiCaAlH_6$ in the first dehydrogenation step [292]. In the second step (180–300 °C), $LiCaAlH_6$ decomposed to form Al, CaH_2, and LiH. The two steps released 6 wt.% of hydrogen [292]:

$$LiCa(AlH_4)_3 \rightarrow LiCaAlH_6 + 2Al + 3H_2 \quad (94)$$

$$LiCaAlH_6 \rightarrow CaH_2 + LiH + Al + 3/2\ H_2 \quad (95)$$

In the second step, some $CaH_{2-x}Cl_x$ was detected. No information regarding possible re-hydrogenation was found. The crystal structure of $LiCa(AlH_4)_3$ was experimentally determined as the space group *P6₃/m* (Table 17 and Figure 25) [292]. Theoretical research confirmed this symmetry and contributed to determining the hydrogen atomic positions (Table 17) [293]. The complete crystal structure of $LiCaAlH_6$ was predicted from the theoretical calculations [294].

Table 17. Crystallographic data of Li-Ca mixed alanates.

Compound	Space Group, Cell Dimensions [Å]	Atomic Coordinates
$LiCa(AlH_4)_3$ (experimental)	*P6₃/m* (No. 176) [292] a = b = 8.91978(12); c = 5.8887(7) α = γ = 90, β = 120	Li: 0, 0, 0 Ca: 2/3, 1/3, 1/4 Al: 0.2805(3), 0.9027(4), 1/4
$LiCa(AlH_4)_3$ (theoretical)	*P6₃/m* (No. 176) [293] a = b = 9.093 c = 5.996 α = γ = 90, β = 120	Li: 0, 0, 0 Ca: 2/3, 1/3, 1/4 Al: 0.3, 0.9, 1/4 H1: 0.544, 0.501, 1/4 H2: 0.807, 0.815, 1/4 H3: 0.535, 0.754, 0.029
$LiCaAlH_6$ (theoretical)	*P–4* (No. 81) [294] a = b = 6.6652 c = 16.5607 α = γ = β= 90	Li1: 0, 0, 0 Li2: 0, 0, 1/2 Li3: 1/2, 1/2, 0 Li4: 1/2, 1/2, 1/2 Li5: 0, 1/2, 0.4843 Li6: 0, 1/2, 0.0085 Ca1: 0.3119, 0.2730, 0.1937 Ca2: 0.2380, 0.1803, 0.6978 Al1: 0.2812, 0.2452, 0.3777 Al2: 0.2812, 0.2398, 0.8264 H1: 0.4729, 0.2445, 0.3245 H2: 0.2947, 0.0386, 0.4346 H3: 0.1523, 0.0958, 0.2964 H4: 0.1623, 0.4222, 0.3053 H5: 0.2861, 0.4340, 0.4450 H6: 0.2449, 0.0032, 0.5840 H7: 0.0609, 0.3014, 0.8263 H8: 0.2532, 0.4729, 0.9283 H9: 0.3881, 0.3663, 0.7959 H10: 0.2891, 0.0307, 0.8161 H11: 0.2130, 0.1039, 0.9599 H12: 0.2158, 0.4740, 0.0859

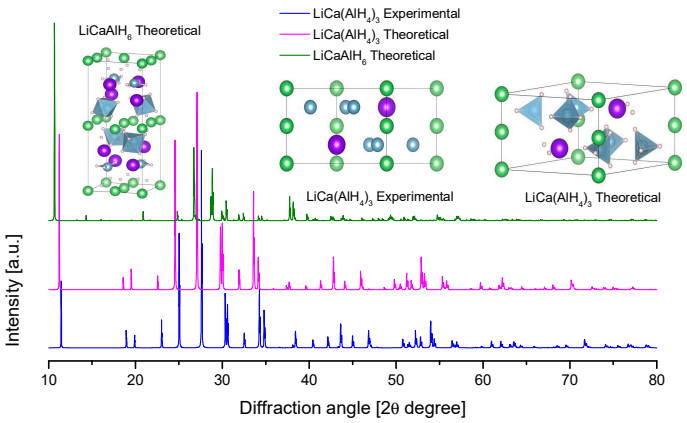

Figure 25. Crystal structure of Li-Ca mixted alanate and its calculated diffraction patterns ($\lambda = Cu_{k\alpha 1}$).

4.5. Na-K Alanates

K_2NaAlH_6 is the only reported mixed Na-K alanate. This material has a total hydrogen content of 4.46 wt.%. K_2NaAlH_6 can be produced by the reaction assisted by ball-milling between KH and $NaAlH_4$ in a 2:1 molar relation, with or without hydrogen pressure (10 bar) [295,296]. K_2NaAlH_6 decomposes into simple hydrides, Al and hydrogen gas at ~352 °C [296,297]:

$$K_2NaAlH_6 \rightarrow 2KH + NaH + Al + 3/2\ H_2 \quad (96)$$

The addition of $TiCl_3$, TiF_3, graphene, or carbon nanotubes slightly reduced the dehydrogenation temperature, with TiF_3 being the most effective material [296]. K_2NaAlH_6 is reported to store hydrogen reversible; however, full capacity was not recovered [295]. K_2NaAlH_6 is reported as a cubic close-packed structure of isolated $[AlH_6]^{3-}$ octahedra; the octahedral interstices are occupied by Na^+ ions, while the tetrahedral interstices are filled with K^+ ions (Table 18, Figure 26) [295].

Table 18. Crystallographic data of Na-K mixed alanates.

Compound	Space Group, Cell Dimensions [Å]	Atomic Coordinates
K_2NaAlD_6	*Fm-3m* (No. 225) [295] a = b = c = 8.118(1) α = β = γ = 90	K: 1/4, 1/4, 1/4 Na: 1/2, 1/2, 1/2 Al: 0, 0, 0 D: 0.2167(8), 0, 0

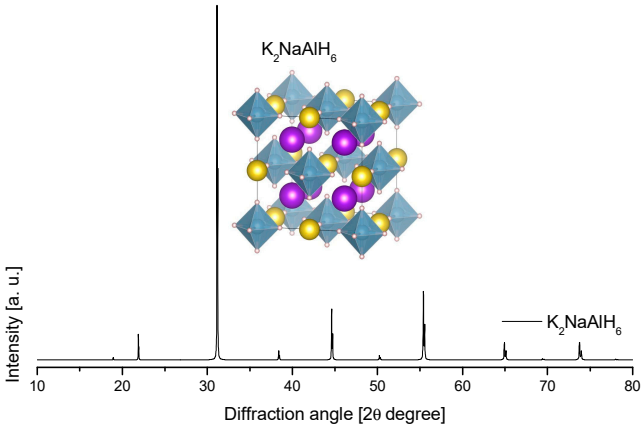

Figure 26. Crystal structure of Na-K mixed alanate and its calculated diffraction pattern ($\lambda = Cu_{k\alpha 1}$).

5. Anion Substitution

Ion size and oxidation state make, in principle, F^- ions suitable for substituting H^- ions in some hydrogen storage compounds, such as hydrides [298], borohydrides, or alanates [299]. The substitution could tune the thermodynamics, with the goal being to reduce the dehydrogenation temperature [299]. Perhaps the clearest example of this is the production of $Na_3AlH_{6-x}F_x$ from NaF and Al [300]. However, despite reducing the enthalpy of the first dehydrogenation, the reversibility of the system was compromised [300]. Other examples of anion substitution, despite being less studied, included $K_3AlH_{6-x}F_x$ [301] and $CaAlF_xH_{5-x}$ [219]. Unfortunately, limited information regarding these systems can be found, thus experimental and/or theoretical studies should be performed in the future.

6. Techniques of Characterization of Alanates

The most common physicochemical characterization techniques for hydrogen storage materials, and thus alanates, are X-ray diffraction (in-situ, ex-situ, with synchrotron or conventional X-ray sources), and spectroscopies, such as Infrared and Raman. Other vibrational spectroscopy techniques, such as Inelastic Neutron Scattering (INS), Nuclear Resonant Inelastic X-ray Scattering Spectroscopy

(NRIXS), or Photoacoustic (PA) Infrared Spectroscopy are far less widespread. The main results of X-ray diffraction studies were presented along with the description of each alanate. Thus, we did not include a special section for it. On the other hand, the characterization of alanates by IR and Raman Spectroscopies is also frequently used due to the relatively low cost of equipment and the relative simplicity of sample preparation for such tests. Therefore, we present IR and Raman spectroscopies in this review.

Fourier Transformed Infrared Spectroscopy (IR) and Raman Spectroscopy

Vibrational transitions can be observed as infrared or Raman spectra. Although frequently, these two techniques are complementary, their physical origins are different [302]. IR absorption spectra originate from photons in the infrared region that are absorbed by transitions between two vibrational levels of the molecule in the electronic ground state. Raman spectra have their origin in the electronic polarization that is caused by ultraviolet, visible, and near-IR light [302]. The observed vibration modes depend on factors, such as the molecular symmetry, identity of atoms, and bond energies, i.e., the kinetic and potential energies of the system. The kinetic energy is determined by the masses of the individual atoms and their geometrical arrangement in the molecule. On the other hand, the potential energy arises from the interaction between the individual atoms and it is described in terms of the force constants [302]. For the alanates, the common structures are the tetrahedral $[AlH_4]^-$ and octahedral $[AlH_6]^{3-}$ units. Figure 27 illustrates the four normal modes of vibration of a tetrahedral $[AlH_4]^-$. All four vibrations are Raman-active, whereas only ν_3 and ν_4 are infrared active [302]. Octahedral molecules have six normal modes of vibration; of these, vibrations ν_1, ν_2, and ν_5 are Raman-active, whereas only ν_3 and ν_4 are infrared-active (Figure 28) [302].

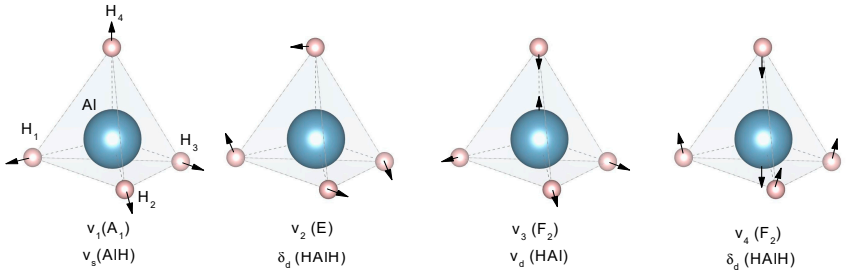

Figure 27. Normal modes of vibration of tetrahedral $[AlH_4]^-$. Adapted from reference [302].

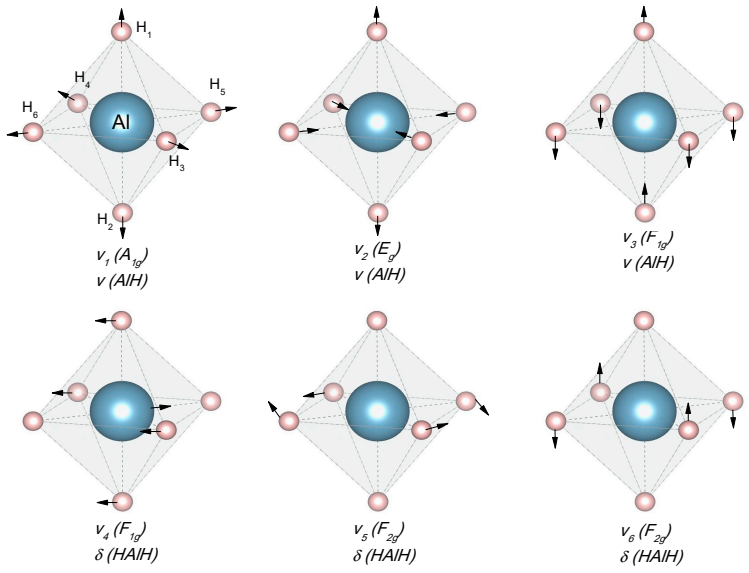

Figure 28. Normal modes of vibration of octahedral $[AlH_6]^{3-}$. Adapted from reference [302].

The vibrational spectra of alanates are frequently classified as external and internal. The external vibrations are due to the vibration of the whole crystal structure. Meanwhile, the internal vibrations are due to the $[AlH_4]^-$ ion, which has four active vibrational modes in Raman and only two in infrared [303]. Some of these features are shared with other materials of similar structure, for example, the borohydrides [304]. The infrared active modes of the $[AlH_4]^-$ ion are the asymmetric stretching modes in the region 1600–2000 cm^{-1} and the bending modes in the region 700–900 cm^{-1} [305]. Some representative data are collected in Tables 19 and 20. As a generally accepted trend of infrared vibrations in the alanates of group 1, the stretching modes, in wavenumbers, roughly decrease with increasing mass of the cation [306]. Meanwhile, the bending modes are unaffected by the counter-ion [305,306]. Other correlations between the stretching and bending peaks (or regions) versus ionization energy, electronegativities, or bond distance have been proposed [302]. Indeed, we tried to find correlations with these parameters. However, we obtained the best results by using the difference in the electronegativities between Al and the counter-cation or the counter-cation ion size. In Figure 29 we present a correlation between the most intense stretching and bending IR peak of $MAlH_4$ (M = group 1 metals, $[AlH_4]^-$ tetrahedra) versus the difference in electronegativities of Al and the metal. The electronegativity scale was the Allred–Rochow [307]. The IR data that were obtained by Adicks et al. in pure crystalline materials [177] were complemented by data published in several experimental and theoretical reports compiled in this review [167,308–320]. The data reflects the significant dispersion of results. The $NaAlH_4$ data are the most common and particularly disperse, which is probably due to the diversity in the material history, such as milling, doping, or cycling [318]. The quantity of available IR data on K, Rb, and Cs- alanates is rather scarce. Still, some tendencies were found; there is a bell-shape dispersion of the Al-H stretching frequency (most intense peak) versus the difference of electronegativity between Al and the group 1 metal. Meanwhile, there is an almost linear increase of the Al-H bending frequency (most intense peak). This can be related to the changes in the geometry of the alanates, along with the group.

Table 19. Representative infrared frequencies of Al-H bonds reported for different alanates.

Alanate	Mode/Peak Position [cm^{-1}]			Comments/Reference
	Stretching	Bending	Librational	
$LiAlH_4$	1779, 1642	885, 811, 715	465	Pure crystalline material [177]
	1800, 1780, 1645	890, 810, 700		[306] and Refs. within
	1757, 1615	900, 830		[310] and Refs. within
Li_3AlH_6	1410, 1300	1000, 960, 854		[321]
	1386, 1276	1000, 950, 850		[310] and Refs. within
Li_3AlD_6	1020, 915	740, 700, 635		[321]
$NaAlH_4$	1680	900, 811, 730, 680		Pure crystalline material [177]
	1680	900, 800, 735, 690		[306] and Refs. within
Na_3AlH_6	1440, 1290	930, 842, 690		[321]
$KAlH_4$	1715	811, 729		Pure crystalline material [177]
$RbAlH_4$	1715	811, 763, 739		Pure crystalline material [177]
	1715	811, 769, 729		[306] and Refs. within
$CsAlH_4$	1711	741		Pure crystalline material [177], Ref. [306] and Refs. within
$Mg(AlH_4)_2$	1935	800, 625		Ref. [306] and Refs. within
	642, 1937			[43]
	1620, 1700–1800			[39]
	2013, 1905, 1850, 716, 663, 620, 360, 302, 282			[210]
$Ca(AlH_4)_2$	600, 1780			[40]
	1788	816, 653	482	[306] and Refs. within

Table 20. Representative Raman frequencies of Al-H bonds reported for different alanates.

Alanate	Assignation/Peaks Position [cm^{-1}]					Comments/Reference
	Combination	Stretching	Bending	Librational	Translational	
$LiAlH_4$		1837, 1762, 1722	950, 882, 830, 780, 690	510, 438, 322	220, 165, 151, 143, 112, 95	[306]
Li_3AlH_6	2090, 1974	1604, 1311	1014, 975	577, 510		[321]
Li_3AlD_6	1478, 1397	1137, 940	730, 686	412, 360		[321]
$NaAlH_4$		1762, 1681,	848, 817, 770	521, 429	180, 125, 117	[306]
Na_3AlH_6		1556, 1465, 1152, 1070	990, 815, 760	560, 480		[321]
$KAlH_4$		1779, 1711	790			[306]
$Mg(AlH_4)_2$		1969, 1944, 1808	824, 768, 736			[306]
		2077, 1852, 1845, 812, 758, 742, 298, 232, 87				[310]

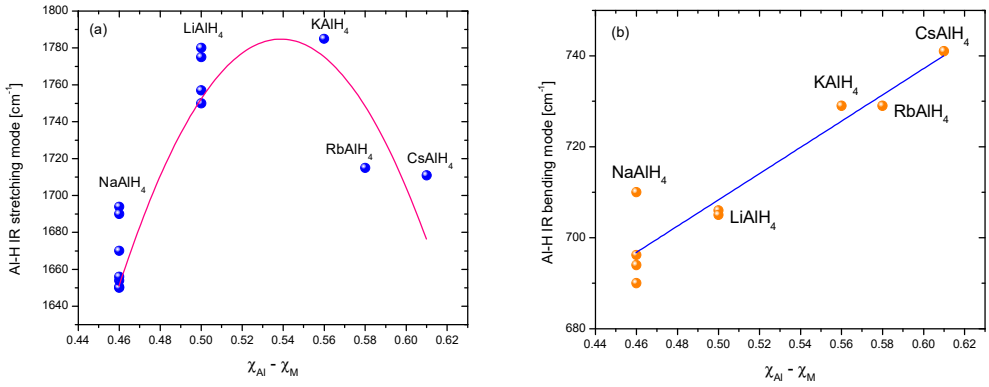

Figure 29. Most intense peak of infrared vibrations in the group 1 alanates, $MAlH_4$. (**a**) Stretching, (**b**) Bending.

The octahedral ion $[AlH_6]^{3-}$ that is present in the so-called intermediaries of alanates also shows infrared and Raman active modes. From the 15 normal vibration modes of a group with octahedral symmetry, two modes are active in the infrared, and three modes are active in the Raman [321]. In Figure 30, we present a correlation between the stretching IR most intense peak of M_3AlH_6 (M = group 1, $[AlH_6]^{3-}$ octahedra) versus the effective ionic radii [307]. The available data for the so-called intermediaries of alanates of group 1 (M_3AlH_6) are scarcer than for the tetrahedral alanates, i.e., $MAlH_4$. Thus, the correlation was constructed with data of Li, Na, and K [167,307,318,322–327]. The red dots of Rb_3AlH_6 and Cs_3AlH_6 are an extrapolation based on the fitted curve.

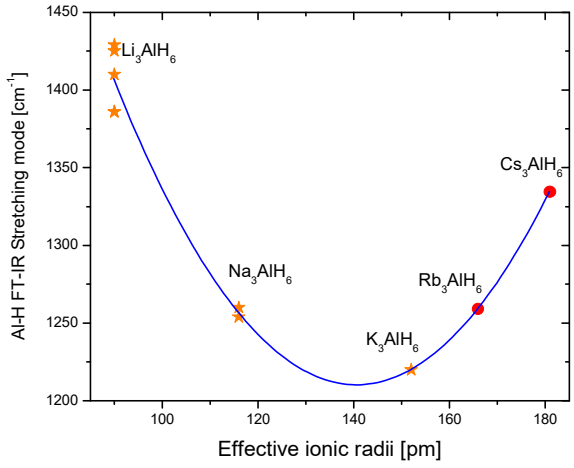

Figure 30. Most intense peak of infrared vibrations in the group 1 intermediaries, M_3AlH_6. The red dots are an extrapolation based on the fitted curve.

In Figure 31, we present a correlation between the stretching and bending Raman most intense peak versus the difference in electronegativities between Al and the metal of $MAlH_4$ (M = group 1). In general, there are less Raman data available than IR data. In both stretching and bending Raman modes, the correlation with the difference in electronegativity is not linear. The reported data were found only for Li, Na, and K-alanates. Thus, the Rb and Cs-alanates data are an extrapolation, pending future reports to corroborate this forecast.

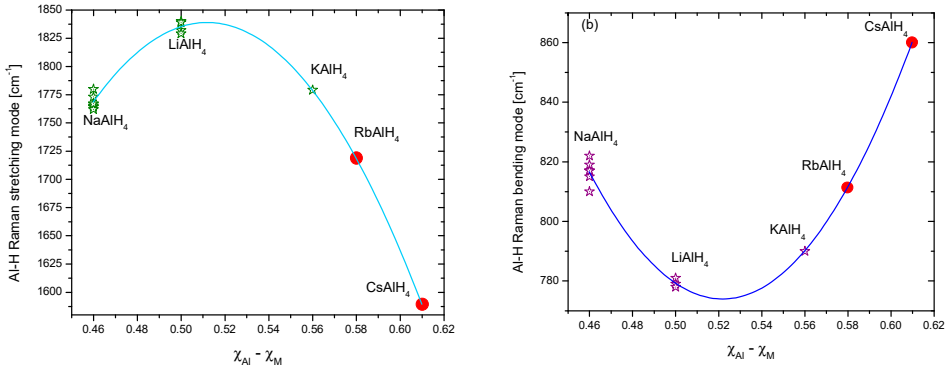

Figure 31. Most intense Raman peak in the group 1 alanates. (**a**) Stretching and (**b**) Bending modes. The red dots are an extrapolation based on the fitted curve.

Not enough IR or Raman data are available for group 2 (apart from Mg and Ca) and the rest of alanates of the periodic table. Additionally to the Figures 29–31, an attempt to find trends that include the double-metal alanates of groups 1 and 2 was performed; no clear trends were found. This can open the possibility of theoretical and experimental studies to obtain these missing data and to obtain general rules that correlate structure and spectroscopic properties.

7. Thermodynamics

A dehydrogenation enthalpy of about 40 kJ/mol is required in order to meet the dehydrogenation temperature compatible with PEMFCs [328]. This enthalpy value roughly means an equilibrium pressure of 1 bar at room temperature. The equilibrium pressure is a function of the temperature, the dehydrogenation enthalpy, and entropy. It is described by the Van't Hoff equation [328]:

$$\ln\left(\frac{p_{eq}}{p^0_{eq}}\right) = \frac{\Delta H}{R} \times \frac{1}{T} - \frac{\Delta S}{R} \quad (97)$$

ΔS mostly corresponds to the change from molecular hydrogen gas to dissolved solid hydrogen [328]. It amounts approximately to the standard entropy of hydrogen (130 $J{\cdot}K^{-1}mol^{-1}$) and is, therefore, frequently taken as a constant for all metal-hydrogen systems [328]. ΔH must be the dehydrogenation reaction enthalpy and each material must report it. However, the formation enthalpy is sometimes used instead, particularly if the material is a metal and its hydride. The enthalpies of formation and dehydrogenation have been related, directly or indirectly, to the bond energy, i.e., the stability of the compound [328,329]. The reported dehydrogenation enthalpies were used to construct the phase diagrams that are presented in this review. The representative values are condensed in Table 21, altogether with formation enthalpies and the activation energies. The thermodynamic data is concentrated mainly in the alanates of group 1, a lot of data is missing on other alanates. The calculated and experimental data of formation enthalpy and dehydrogenation enthalpy show good correlation. However, an in-deep comment on the dispersion of the thermodynamic data is needed. Along with the several consulted papers, different experimental techniques and conditions were used to determine the thermodynamic data. The most used techniques are the differential

scanning calorimetry (with variations, such as high-pressure, with or without hydrogen flow, different of values of flows, etc.), pressure-composition isotherms, and theoretical calculations (different levels of theory, programs, basis sets, etc.). Thus, the natural result is the dispersion of data. Perhaps, a standard method will be advisable. Meanwhile, the activation energies present the most disperse values, which is due to the additive and the history of the materials (mechanical milling, purification, recrystallization, cycling, etc.). Additionally, some of the original data are explicitly related to the released mol of H_2, meanwhile, other data is not clearly reported of mol of which compound is related.

Table 21. Thermodynamic data of alanates.

Alanate	Formation Enthalpy ΔH_f^0 [kJ/mol]	Dehydrogenation Reaction/Dehydrogenation Enthalpy [kJ/mol]		Apparent Activation Energy [kJ/mol]
$LiAlH_4$	−107.1 [330] −113.42 [81] ‖ −114.8 [87] ‡ −118.9 [331] −119 [71]	(15)	−10 [26] −9.79 [81] ‖	102 [75], 103 [332] (pure) 42.6 [73] ($TiCl_3$-1/3$AlCl_3$ 2 mol%) 67 [74] (NbF_3 1 mol%) 81.5 [333] ($FeCl_2$ 2 mol%) 87.4 [308] (TiN 2 mol%)
Li_3AlH_6	−310.89 [81] ‖ −298.5 to −311.0 [81,87,330]	(16)	15.72 [81] ‖ 25 [26]	54.8 [73] ($TiCl_3$-1/3$AlCl_3$ 2 mol%) 77 [74] (NbF_3 1 mol%)
$NaAlH_4$	−78.9 [334] −105.6 [268] −113.0 [331] −116.3 [335] ‡	(25)	36.7 [335] ‡ 37 [88] ϴ 36–40.9 [71] ❁ ❁	114.2 [336] (pure) 113.8 ($NiFe_2O_4$ 3 mol%) [315], and ($MnFe_2O_4$) [317] 86.4 [336] ($LaCl_3$ 2 mol%)
Na_3AlH_6	−238.8 [335] ‡ −172.8 [334] ‖ −260 [337]	(26)	69.6 [335] ‡ 47 [88] ϴ 46.8–47 [71] ❁ ❁	162.6 [336] (pure) 86.4 [336] ($LaCl_3$ 2 mol%)
$KAlH_4$	−166.6 [331] −183.7 [161] ❁ −128 [175] ‖	(34)	70 [167] ❁ ~55 [168] ‖ ❁	140 [164] (pure) ❁ 80 [164] ($TiCl_3$ 2% mol) ❁
K_3AlH_6	−224.7 [175] ‖	(35)	81 [167] ❁	?
$CsAlH_4$	−164.9 [330]	(39)	?	?
$Mg(AlH_4)_2$	−79 [338] ("assessed value")	(42)	20.4 [43] (at 0 K, ab-initio)	123.8 [199] (pure not milled) 123.6 [195] (with $LiCl_2$) 123 [197] (submicron rods) 82.3 [200], 85.5 [208] (TiF_4 doped)
$Ca(AlH_4)_2$	−214 [192] ‖	(45)	−7 [224] ❁, −7.4 [220]	?
$CaAlH_5$	−224 [192] ‖	(46)	26 [41] 32 [224] ❁, 31.1 [220]	161 [41], 153.4 [219] (pure) 57.4 [219] (TiF_3 10 wt.%)
$SrAlH_5$	−248 [192] ‖	(54)	?	?
$BaAlH_5$	−224 [207] ‖	–	?	?
$LaAlH_6$ [261]	?	?	~30 ‖, ❁	?
$MAlH_6$, M=Ce, Pr, Nd [261]	?	(82)	~28-32 ‖, ❁	?
$Eu(AlH_4)_2$ [44]	?	?	−4.4 and 57 (for 2 consecutive reactions of hydrogen release, ❁).	?
Na_2LiAlH_6	−84.5 [268] ❁ ‖ −55.26 [297] ❁ (‖, 300 K) −53.5 [267] ❁	(88)	53.5 [267] ❁, 63.8 [274] ❁ 56.4 [276] ❁ TiF_3 doped 57.3 [285] TiF_4 doped	173 [274] 143.6 [285] TiF_4 doped
K_2LiAlH_6	−100.5 [268] ❁ ‖ −102.42 [297] ❁ (‖, 300 K) −82 [267] ❁	?	82 [267] ❁	?
$LiMg(AlH_4)_3$	−192.6 [206] (‖, 0 K)	(91)	−4.16 [289] ❁, −5 [339] ❁	~66 277
$LiMgAlH_6$	−184.8 [206] (‖, 0 K)	(92)	8.89 [289] ❁, 9 [339] ❁	?
K_2NaAlH_6	−107.66 [297] ❁ (‖, 300 K) −97 [267] ❁	(96)	97 [267] ❁ 98 [295] TiF_3 doped ❁	124.43 [296] 88.05 TiF_3 catalyzed [296]

‡ CALPHAD ‖ DFT ϴ Ti-doped ❁ (and references within) ❁ Explicitly reported per mole of H_2, i.e., kJ/mol H_2, ? Unknown.

8. Conclusions and Perspectives

$NaAlH_4$ and $KAlH_4$ stand out among all of the alanates due to their acceptable hydrogen content and reversibility. Perhaps for light-duty vehicles applications, an option will be the $NaAlH_4$, where the catalyst performance is essential. In that subject, along with the consulted papers, the Ti-based catalyst could be limited in the long-term because of the progressive change in the oxidation state of Ti, associated with the decay of performance. Perhaps, lanthanide-metals compounds could be the solution. However, more research on extensive cycling must be done: There is not enough data up to now on the long-term performance of Ce-catalysts on $NaAlH_4$. On the other hand, $KAlH_4$ can be suitable for niche applications where the high-temperature dehydrogenation is not an issue. However, there is no data regarding extensive cycling.

During the preparation of this review, the compilation of alanates beyond the group 1 and 2 was a good surprise. Many of them have a reasonable good dehydrogenation temperature and hydrogen content. Others can be viewed just as a chemical curiosity. In general, the reports of the alanates of transition metals and main group are very old. Perhaps, re-visiting and updating the information of these alanates with new synthesis and characterization techniques could provide new approaches for solving the hydrogen storage problem.

Despite that the formation of reactive composite materials has proven useful in other hydrogen storage materials, this approach seems not so useful in the alanate family. However, the formation of double cation alanates seems to be attractive for improving the dehydrogenation temperature without the sacrifice of the hydrogen content. The anion substitution is explored to a limited extent in the alanates family, and this modification should be studied deeply.

Author Contributions: Conceptualization, writing—review and editing, K.S.-A.; Crystal structures, X-ray diffraction and Infrared data compilement, J.R.T.-G.; Thermodinamic data and figures, R.G.-O.

Funding: This research was funded by CONACyT, Ciencia Básica 251347-ALANATOS CONVENCIONALES Y NO CONVENCIONALES PARA ALMACENAMIENTO DE HIDROGENO, grant number 251347.

Acknowledgments: All authors are very gratefully to Teresa Vásquez Mejía for the support during bibliographic compilation.

Conflicts of Interest: The authors declare no conflict of interest.

References

1. Sandrock, G.A. Panoramic overview of hydrogen storage alloys from a gas reaction point of view. *J. Alloys Compd.* **1999**, *293–295*, 877–888. [CrossRef]
2. Wiswall, R.H., Jr.; Reilly, J.J. Metal Hydrides for Energy Storage. Office of Scientific & Technical Information Technical Reports, Brookhaven National Laboratory, Upton, N.Y. 1972. Available online: https://www.osti.gov/servlets/purl/6051964 (accessed on 2 July 2019).
3. Vigeholm, B.; Kjøller, J.; Larsen, B. Magnesium for hydrogen storage. *J. Less Common Met.* **1980**, *74*, 341–350. [CrossRef]
4. Zhang, D.L. Processing of advanced materials using high-energy mechanical milling. *Prog. Mater. Sci.* **2004**, *49*, 537–560. [CrossRef]
5. Suryanarayana, C. Mechanical alloying and milling. *Prog. Mater. Sci.* **2001**, *46*, 1–184. [CrossRef]
6. Yu, X.; Tang, T.; Sun, D.; Ouyang, L.; Zhu, O. Recent advances and remaining challenges of nanostructured materials for hydrogen storage applications. *Prog. Mater. Sci.* **2017**, *88*, 1–48. [CrossRef]
7. Bogdanović, B.; Schwickardi, M. Ti-doped alkali metal aluminium hydrides as potential novel reversible hydrogen storage materials. *J. Alloys Compd.* **1997**, *253*, 1–9. [CrossRef]
8. Gross, K.; Majzoub, E. Direct Synthesis of Catalyzed Hydride Compounds. U.S. Patent No. US2003 0143154 A1, 31 July 2003.
9. Milanese, C.; Garroni, S.; Gennari, F.; Marini, A.; Klassen, T.; Dornheim, M.; Pistidda, C. Solid state hydrogen storage in alanates and alanate-based compounds: A review. *Metals* **2018**, *8*, 567. [CrossRef]

10. Na Ranong, C.; Hoehne, M.; Franzen, J.; Hapke, J.; Fieg, G.; Dornheim, M.; Eigen, N.; Bellosta von Colbe, J.M.; Metz, O. Concept, design and manufacture of a prototype hydrogen storage tank based on sodium alanate. *Chem. Eng. Technol.* **2009**, *32*, 1154–1163. [CrossRef]
11. Ley, M.B.; Meggouh, M.; Moury, R.; Peinecke, K.; Felderhoff, M. Development of hydrogen storage tank systems based on complex metal hydrides. *Materials* **2015**, *8*, 5891–5921. [CrossRef]
12. Johnson, T.A.; Jorgensen, S.W.; Dedrick, D.E. Performance of a full-scale hydrogen-storage tank based on complex hydrides. *Faraday Discuss.* **2011**, *151*, 327–352. [CrossRef]
13. Reid, W.E.; Bish, J.M.; Brenner, A. Electrodeposition of metals from organic solutions III. Preparation and electrolysis of titanium and zirconium compounds in nonaqueous media. *J. Electrochem. Soc.* **1957**, *104*, 21–29. [CrossRef]
14. Wiberg, E.; Usón, R. Zur Kenntnis eines Titan-aluminium-wassertsoffs $Ti(AlH_4)_4$. *Z. Nat.* **1951**, *6*, 392–393.
15. DOE technical targets for onboard hydrogen storage for ligh-duty vehicles. Available online: https://www.energy.gov/eere/fuelcells/doe-technical-targets-onboard-hydrogen-storage-light-duty-vehicles (accessed on 12 August 2019).
16. Bergemann, N.; Pistidda, C.; Milanese, C.; Girella, A.; Hanse, B.R.S.; Wurr, J.; Bellosta von Colbe, J.M.; Jepsen, J.; Jensen, T.R.; Marini, A.; et al. $NaAlH_4$ production from waste aluminum by reactive ball milling. *Int. J. Hydrogen Energy* **2014**, *39*, 9877–9882. [CrossRef]
17. Guerrero-Ortiz, R.; Tena-Garcia, J.R.; Flores-Jacobo, A.; Suarez-Alcantara, K. From the can to the tank: $NaAlH_4$ from recycled aluminum. *Int. J. Hydrogen Energy* **2019**, *44*, 20183–20190. [CrossRef]
18. Bellosta von Colbe, J.; Ares, J.R.; Barale, J.; Baricco, M.; Buckley, C.; Capurso, G.; Gallandat, N.; Grant, D.M.; Guzik, M.N.; Jacob, I.; et al. Application of hydrides in hydrogen storage and compression: Achievements, outlook and perspectives. *Int. J. Hydrogen Energy* **2019**, *44*, 7780–7808. [CrossRef]
19. Abdalla, A.M.; Hossaina, S.; Nisfindya, O.B.; Azad, A.T.; Dawood, M.; Azada, A.K. Hydrogen production, storage, transportation and key challenges with applications: A review. *Energy Convers. Manag.* **2018**, *165*, 602–627. [CrossRef]
20. Sanjeev, L. Process for Preparing Dry Sodium Aluminum Hydride. U.S. Patent No. 5,295,581, 22.03, 22 March 1994.
21. Ashby, E.C.; Brendel, G.J.; Redman, H.E. Direct synthesis of complex metal hydrides. *Inorg. Chem.* **1963**, *2*, 499–504. [CrossRef]
22. Møller, K.T.; Sheppard, D.; Ravnsbæk, D.B.; Buckley, C.E.; Akiba, E.; Li, H.W.; Jensen, T.J. Complex metal hydrides for hydrogen, thermal and electrochemical energy storage. *Energies* **2017**, *10*, 1645. [CrossRef]
23. Finholt, A.E.; Bond, A.C., Jr.; Schlesinger, H.I. Lithium aluminum hydride, aluminum hydride and lithium gallium hydride, and some of their applications in organic and inorganic chemistry. *J. Am. Chem. Soc.* **1947**, *69*, 1199–1203. [CrossRef]
24. Barton, L. 1.7.4.2. of Compounds of Aluminum. In *Inorganic Reactions and Methods: The Formation of the Bond to Hydrogen (Part 2), Volume 2*; Zuckerman, J.J., Hagen, A.P., Eds.; VCH Publishers, Inc.: Oklahoma, OK, USA, 1987; pp. 136–137.
25. Wiberg, E.; Bauer, R. Zur Kenntnis eines Magnesium-aluminium-wasserstoffs $Mg(AlH_4)_2$. *Z. Nat.* **1950**, *5*, 397–398.
26. Jain, I.P.; Jain, P.; Jain, A. Novel hydrogen storage materials: A review of lightweight complex hydrides. *J. Alloys Compd.* **2010**, *503*, 303–339. [CrossRef]
27. Wiberg, E.; Bauer, R. Neues zur Kenntnis des Magnesium-aluminium-wasserstoffs $Mg(AlH_4)_2$. *Z. Nat.* **1952**, *7*, 131–132. [CrossRef]
28. Schwab, W.; Wintersberger, K. Über Darstellung und Eigenschaften von Calciumaluminiumhydrid $Ca(AlH_4)_2$. *Z. Nat.* **1953**, *8*, 690–691. [CrossRef]
29. Schwarz, M.; Haiduc, A.; Stil, H.; Paulus, P.; Geerlings, H. The use of complex metal hydrides as hydrogen storage materials: Synthesis and XRD-studies of $Ca(AlH_4)_2$ and $Mg(AlH_4)_2$. *J. Alloys Compd.* **2005**, *404–406*, 762–765. [CrossRef]
30. Fichtner, M.; Fuhr, O. Synthesis and structures of magnesium alanate and two solvent adducts. *J. Alloys Compd.* **2002**, *345*, 286–296. [CrossRef]
31. Komiya, K.; Morisaku, N.; Shinzato, Y.; Ikeda, K.; Orimo, S.; Ohki, Y.; Tatsumi, K.; Yukawa, H.; Morinaga, M. Synthesis and dehydrogenation of $M(AlH_4)_2$ (M = Mg, Ca). *J. Alloys Compd.* **2007**, *446–447*, 237–241. [CrossRef]

32. Bellosta von Colbe, J.M.; Felderhoff, M.; Bogdanović, B.; Schüth, F.; Weidenthaler, C. One-step direct synthesis of a Ti-doped sodium alanate hydrogen storage material. *Chem. Commun.* **2005**, *41*, 4732–4734. [CrossRef] [PubMed]
33. Bogdanović, B.; Schwickardi, M. Method for Reversibly Storing Hydrogen on the Basis of Alkali Metals and Aluminum. U.S. Patent No. US 2003/0053948 A1, 20 March 2003.
34. Huot, J.; Ravnsbæk, D.B.; Zhang, J.; Cuevas, F.; Latroche, M.; Jensen, T.R. Mechanochemical synthesis of hydrogen storage materials. *Prog. Mater. Sci.* **2013**, *58*, 30–75. [CrossRef]
35. Eigen, N.; Gosch, F.; Dornheim, M.; Klassen, T.; Bormann, R. Improved hydrogen sorption of sodium alanate by optimized processing. *J. Alloys Compd.* **2008**, *465*, 310–316. [CrossRef]
36. Hlova, I.; Goldston, J.F.; Gupta, S.; Kobayashi, T.; Pruski, M. A benign synthesis of alane by the composition-controlled mechanochemical reaction of sodium hydride and aluminum chloride. *J. Mater. Sci.* **2017**, *52*, 11900–11910. [CrossRef]
37. Hlova, I.; Gupta, S.; Goldston, J.E.; Kobayashi, T.; Pruski, M.; Pecharsky, V.K. Dry mechanochemical synthesis of alane from LiH and $AlCl_3$. *Faraday Discuss.* **2014**, *170*, 137–153. [CrossRef] [PubMed]
38. Hlova, I. Mechanochemical Synthesis of Hydrogen-Storage Materials Based on Aluminum, Magnesium and Their Compounds. Ph.D. Thesis, Iowa State University, Ames, IA, USA, 2015.
39. Dymova, T.N.; Mal'Tseva, N.N.; Konoplev, V.N.; Golovanova, A.I.; Aleksandrov, D.P.; Sizareva, A.S. Solid-phase solvate-free formation of magnesium hydroaluminates $Mg(AlH_4)_2$ and $MgAlH_5$ upon mechanochemical activation or heating of magnesium hydride and aluminum chloride mixtures. *Russ. J. Coord. Chem.* **2003**, *29*, 385–398. [CrossRef]
40. Kabbour, H.; Ahn, C.C.; Hwang, S.-J.; Bowman, C.R.; Graetz, J. Direct synthesis and NMR characterization of calcium alanate. *J. Alloys Compd.* **2007**, *445–447*, 264–266. [CrossRef]
41. Iosub, V.; Matsunaga, T.; Tange, K.; Ishikiriyama, M. Direct synthesis of $Mg(AlH_4)_2$ and $CaAlH_5$ crystalline compounds by ball milling and their potential as hydrogen storage materials. *Int. J. Hydrogen Energy* **2009**, *34*, 906–912. [CrossRef]
42. Sato, T.; Ikeda, K.; Li, H.-W.; Yukawa, H.; Morinaga, M.; Orimo, S. Direct dry syntheses and thermal analyses of a series of aluminum complex hydrides. *Mater. Trans.* **2009**, *50*, 182–196. [CrossRef]
43. Kim, Y.; Lee, E.-K.; Shim, J.-H.; Cho, Y.W.; Yoon, K.B. Mechanochemical synthesis and thermal decomposition of $Mg(AlH_4)_2$. *J. Alloys Compd.* **2006**, *422*, 283–287. [CrossRef]
44. Pommerin, A.; Wosylus, A.; Felderhoff, M.; Schüth, F.; Weidenthaler, C. Synthesis, crystal structures, and hydrogen-storage properties of $Eu(AlH_4)_2$ and $Sr(AlH_4)_2$ and their decomposition intermediates, $EuAlH_5$ and $SrAlH_5$. *Inorg. Chem.* **2012**, *51*, 4143–4150. [CrossRef]
45. Graetz, J.; Reilly, J.J.; Yartys, V.A.; Maehlen, J.P.; Bulychev, B.M.; Antonov, V.E.; Tarasov, B.P.; Gabis, I.E. Aluminum hydride as a hydrogen and energy storage material: Past, present and future. *J. Alloys Compd.* **2011**, *509*, S517–S528. [CrossRef]
46. Brower, F.M.; Matzek, N.E.; Reigler, P.F.; Rinn, H.W.; Roberts, C.B.; Schmidt, D.L.; Snover, J.A.; Terada, K. Preparation and properties of aluminum hydride. *J. Am. Chem. Soc.* **1976**, *98*, 2450–2454. [CrossRef]
47. Brinks, H.W.; Istad-Lem, A.; Hauback, B.C. Mechanochemical synthesis and crystal structure of α'-AlD_3 and α-AlD_3. *J. Phys. Chem. B* **2006**, *110*, 25833–25837. [CrossRef]
48. Paskevicius, M.; Sheppard, D.A.; Buckley, C.E. Characterization of mechanochemically synthesized alane (AlH_3) nanoparticles. *J. Alloys Compd.* **2009**, *487*, 370–376. [CrossRef]
49. Gupta, S.; Kobayashi, T.; Hlova, I.Z.; Goldston, J.F.; Pruski, M.; Pecharsky, V.K. Solvent-free mechanochemical synthesis of alane, AlH_3: Effect of pressure on the reaction pathway. *Green Chem.* **2014**, *16*, 4378–4388. [CrossRef]
50. Martínez-Rodríguez, M.J.; García-Díaz, B.L.; Teprovich, J.A., Jr.; Knight, D.A.; Zidan, R. Advances in the electrochemical regeneration of aluminum hydride. *Appl. Phys. A* **2012**, *106*, 545–550. [CrossRef]
51. Zidan, R. Electrochemical Process and Production of Novel Complex Hydrides. U.S. Patent No. US 8,470,156 B2, 25 June 2013.
52. Zidan, R. Enhancing Electrochemical Methods for Producing and Regenerating Alane by Using Electrochemical Catalytic Additive. U.S. patent No. US 9, 850,585 B1, 26 December 2017.
53. Graetz, J.; Reilly, J.J. Thermodynamics of the α, β and γ polymorphs of AlH_3. *J. Alloys Compd.* **2006**, *424*, 262–265. [CrossRef]

54. Graetz, J.; Hauback, B.C. Recent developments in aluminum-based hydrides for hydrogen storage. *MRS Bull.* **2013**, *38*, 473–479. [CrossRef]
55. Graetz, J.; Chaudhuri, S.; Lee, Y.; Vogt, T.; Muckerman, J.T.; Reilly, J.J. Pressure-induced structural and electronic changes in α-AlH_3. *Phys. Rev. B* **2006**, *74*, 214114. [CrossRef]
56. Wang, L.; Rawal, A.; Aguey-Zinsou, K.F. Hydrogen storage properties of nanoconfined aluminium hydride (AlH_3). *Chem. Eng. Sci.* **2019**, *194*, 64–70. [CrossRef]
57. Orimo, S.; Nakamori, Y.; Kato, T.; Brown, C.; Jensen, C.M. Intrinsic and mechanical modified thermal stabilities of α-, β- and γ-aluminum trihydries AlH_3. *Appl. Phys. A* **2006**, *83*, 5–8. [CrossRef]
58. Sandrock, G.; Reilly, J.; Graetz, J.; Zhou, W.-M.; Johnson, J.; Wegrzyn, J. Alkali metal hydride doping of α-AlH_3 for enhanced H_2 desorption kinetics. *J. Alloys Compd.* **2006**, *421*, 185–189. [CrossRef]
59. Graetz, J.; Reilly, J.J. Decomposition kinetics of the AlH_3 polymorphs. *J. Phys. Chem. B* **2005**, *47*, 22181. [CrossRef]
60. Ikeda, K.; Muto, S.; Tatsumi, K.; Menjo, M.; Kato, S.; Bielmann, M.; Züttel, A.; Jensen, C.M.; Orimo, S. Dehydriding reaction of AlH_3: In situ microscopic observations combined with thermal and surface analyses. *Nanotechnology* **2009**, *20*, 204004. [CrossRef] [PubMed]
61. Liu, H.; Wang, X.; Dong, Z.; Cao, G.; Liu, Y.; Chen, L.; Yan, M. Dehydriding properties of γ-AlH_3. *Int. J. Hydrogen Energy* **2013**, *38*, 10851–10865. [CrossRef]
62. Sartori, S.; Opalka, S.M.; Løvvik, O.M.; Guzik, M.N.; Tang, X.; Hauback, B.C. Experimental studies of α-AlD_3 and α'-AlD_3 *versus* first-principles modeling of the alane isomorphs. *J. Mater. Chem.* **2008**, *18*, 2361–2370. [CrossRef]
63. Sandrock, G.; Reilly, J.; Graetz, J.; Zhou, W.-M.; Johnson, J.; Wegrzyn, J. Accelerated thermal decomposition of AlH_3 for hydrogen-fueled vehicles. *Appl. Phys. A.* **2005**, *80*, 687–690. [CrossRef]
64. Liu, H.; Wang, X.; Liu, Y.; Dong, Z.; Ge, H.; Li, S.; Yan, M. Hydrogen desorption properties of the MgH_2–AlH_3 composites. *J. Phys. Chem. C* **2014**, *118*, 37–45. [CrossRef]
65. Liu, H.; Wang, X.; Zhou, H.; Gao, S.; Ge, H.; Li, S.; Yan, M. Improved hydrogen desorption properties of $LiBH_4$ by AlH_3 addition. *Int. J. Hydrogen Energy* **2016**, *41*, 22118–22127. [CrossRef]
66. Goncharenko, I.N.; Glazkov, V.P.; Irodova, A.V.; Somenkov, V.A. Neutron diffraction study of crystal structure and equation of state AlD_3 up to the pressure of 7.2 GPa. *Physica B* **1991**, *174*, 117–120. [CrossRef]
67. Brinks, H.W.; Brown, C.; Jensen, C.M.; Graetz, J.; Reilly, J.J.; Hauback, B.C. Synthesis and crystal structure of β-AlD_3. *J. Alloys Compd.* **2007**, *433*, 180–183. [CrossRef]
68. Brinks, H.W.; Langley, W.; Jensen, C.M.; Graetz, J.; Reilly, J.J.; Hauback, B.C. The crystal structure of γ-AlD_3. *J. Alloys Compd.* **2007**, *441*, 364–367. [CrossRef]
69. Kojima, Y.; Kawai, Y.; Haga, T.; Matsumoto, M.; Koiwai, A. Direct formation of $LiAlH_4$ by a mechanochemical reaction. *J. Alloys Compd.* **2007**, *441*, 189–191. [CrossRef]
70. Block, J.; Gray, A.P. The thermal decomposition of lithium aluminum hydride. *Inorg. Chem.* **1965**, *4*, 304–305. [CrossRef]
71. Orimo, S.I.; Nakamori, Y.; Eliseo, J.R.; Züttel, A.; Jensen, C.M. Complex hydrides for hydrogen storage. *Chem. Rev.* **2007**, *107*, 4111–4132. [CrossRef] [PubMed]
72. Ares, J.R.; Aguey-Zinsou, F.; Porcu, M.; Sykes, J.M.; Dornheim, M.; Klassen, T.; Bormann, R. Thermal and mechanically activated decomposition of $LiAlH_4$. *Mater. Res. Bull.* **2008**, *43*, 1263–1275. [CrossRef]
73. Chen, J.; Kuriyama, N.; Xu, Q.; Takeshita, H.T.; Sakai, T. Reversible hydrogen storage via titanium-catalyzed $LiAlH_4$ and Li_3AlH_6. *J. Phys. Chem. B* **2001**, *105*, 11214–11220. [CrossRef]
74. Ismail, M.; Zhao, Y.; Yu, X.B.; Dou, S.X. Effects of NbF_5 addition on the hydrogen storage properties of $LiAlH_4$. *Int. J. Hydrogen Energy* **2010**, *35*, 2361–2367. [CrossRef]
75. Blanchard, D.; Brinks, H.W.; Hauback, B.C.; Norby, P.; Muller, J. Isothermal decomposition of $LiAlD_4$ with and without additives. *J. Alloys Compd.* **2005**, *404–406*, 743–747. [CrossRef]
76. Vajeeston, P.; Ravindran, P.; Vidya, R.; Fjellvåg, H.; Kjekshus, A. Huge-pressure-induced volume collapse in $LiAlH_4$ and its implications to hydrogen storage. *Phys. Rev. B* **2003**, *68*, 212101. [CrossRef]
77. Sklar, N.; Post, B. The crystal structure of lithium aluminum hydride. *Inorg. Chem.* **1967**, *6*, 669–671. [CrossRef]
78. Hauback, B.C.; Brinks, H.W.; Fjellvåg, H. Accurate structure of $LiAlD_4$ studied by combined powder neutron and X-ray diffraction. *J. Alloys Compd.* **2002**, *346*, 184–189. [CrossRef]

79. Sato, T.; Tomiyasu, K.; Ikeda, K.; Otomo, T.; Feygenson, M.; Neuefeind, J.; Yamada, K.; Orimo, S.I. Local atomic structural investigations of precursory phenomenon of the hydrogen release from $LiAlD_4$. *J. Alloys Compd.* **2014**, *586*, 244–247. [CrossRef]
80. Pitt, M.P.; Blanchard, D.; Hauback, B.C.; Fjellvåg, H.; Marshall, W.G. Pressure-induced phase transitions of the $LiAlD_4$ system. *Phys. Rev. B* **2005**, *72*, 214113. [CrossRef]
81. Løvvik, O.; Opalka, S.; Brinks, W.H.; Hauback, B.C. Crystal structure and thermodynamic stability of the lithium alanates $LiAlH_4$ and Li_3AlH_6. *Phys. Rev. B* **2004**, *69*, 134117. [CrossRef]
82. Liu, X.; McGrady, G.S.; Langmi, H.W.; Jensen, C.M. Facile cycling of Ti-doped $LiAlH_4$ for high performance hydrogen storage. *J. Am. Chem. Soc.* **2009**, *131*, 5032–5033. [CrossRef] [PubMed]
83. Liu, X.; Langmi, H.W.; Beattie, S.D.; Azenwi, F.F.; McGradyc, S.; Jensen, C.M. Ti-doped $LiAlH_4$ for hydrogen storage: Synthesis, catalyst loading and cycling performance. *J. Am. Chem. Soc.* **2011**, *133*, 15593–15597. [CrossRef] [PubMed]
84. Graetz, J.; Wegrzyn, J.; Reilly, J.J. Regeneration of lithium aluminum hydride. *J. Am. Chem. Soc.* **2008**, *130*, 17790–17794. [CrossRef] [PubMed]
85. Brinks, H.W.; Fossdal, A.; Fonneløp, J.E.; Hauback, B.C. Crystal structure and stability of $LiAlD_4$ with TiF_3 additive. *J. Alloys Compd.* **2005**, *397*, 291–295. [CrossRef]
86. Ke, X.; Chen, C. Thermodynamic functions and pressure-temperature phase diagram of lithium alanates by ab initio calculations. *Phys. Rev. B* **2007**, *76*, 024112. [CrossRef]
87. Jang, J.-W.; Shim, J.-H.; Cho, Y.C.; Lee, B.-J. Thermodynamic calculation of $LiH \leftrightarrow Li_3AlH_6 \leftrightarrow LiAlH_4$ reactions. *J. Alloys Compd.* **2006**, *420*, 286–290. [CrossRef]
88. Bogdanović, B.; Brand, R.A.; Marjanović, A.; Schwickardi, M.; Tölle, J. Metal-doped sodium aluminium hydrides as potential new hydrogen storage materials. *J. Alloys Compd.* **2000**, *302*, 36–58. [CrossRef]
89. Vajo, J.J.; Skeith, S.L.; Mertens, F. Reversible storage of hydrogen in destabilized $LiBH_4$. *J. Phys. Chem. B* **2005**, *109*, 3719–3722. [CrossRef]
90. Mao, J.; Guo, Z.; Yu, X.; Ismail, M.; Liu, H. Enhanced hydrogen storage performance of $LiAlH_4$–MgH_2–TiF_3 composite. *Int. J. Hydrogen Energy* **2011**, *36*, 5369–5374. [CrossRef]
91. Wan, Q.; Li, P.; Li, Z.; Zhai, F.; Qu, X.; Volinsky, A.V. Improved hydrogen storage performance of MgH_2-$LiAlH_4$ composite by the addition of $MnFe_2O_4$. *J. Phys. Chem. C* **2013**, *117*, 26940–26947. [CrossRef]
92. Lin, I.C.; Tsai, W.-T. In situ synchrotron X-ray diffraction study on the rehydrogenation behavior of MgH_2-$LiAlH_4$ composites. In Proceedings of the 2017 IEEE International Conference on Applied System Innovation: Applied System Innovation for Modern Technology, ICASI, Sapporo, Japan, 13–17 May 2017; Volume 2017, pp. 1918–1921.
93. Ismail, M.; Zhao, Y.; Yu, X.B.; Dou, S.X. Effect of different additives on the hydrogen storage properties of the MgH_2-$LiAlH_4$ destabilized system. *RSC Adv.* **2011**, *1*, 408–414. [CrossRef]
94. Chen, R.; Wang, X.; Xu, L.; Chen, L.; Li, S.; Chen, C. An investigation on the reaction mechanism of $LiAlH_4$–MgH_2 hydrogen storage system. *Mater. Chem. Phys.* **2010**, *124*, 83–87. [CrossRef]
95. Mustafa, N.S.; Ismail, M. Enhanced hydrogen storage properties of $4MgH_2$-$LiAlH_4$ composite system by doping with Fe_2O_3 nanopowder. *Int. J. Hydrogen Energy* **2014**, *39*, 7834–7841. [CrossRef]
96. Sun, W.; Zhang, Y.; Zhu, Y.; Zhuang, X.; Dong, J.; Qu, Y.; Guo, X.; Chen, J.; Wang, Z.; Li, L. The hydrogen storage performance of a $4MgH_2$-$LiAlH_4$-TiH_2 composite system. *J. Alloys Compd.* **2016**, *676*, 557–564. [CrossRef]
97. Meggouh, M.; Grant, D.M.; Walker, G.S. Optimizing the destabilization of $LiBH_4$ for hydrogen storage and the effect of different Al sources. *J. Phys. Chem. C* **2011**, *115*, 22054–22061. [CrossRef]
98. Jin, A.-S.; Shim, J.-H.; Cho, Y.W.; Yi, K.-W.; Zabara, O.; Fichtner, M. Reversible hydrogen storage in $LiBH_4$–Al–LiH composite powder. *Scr. Mater.* **2008**, *58*, 963–965. [CrossRef]
99. Mao, J.F.; Guo, Z.P.; Liu, H.K.; Yu, X.B. Reversible hydrogen storage in titanium-catalyzed $LiAlH_4$–$LiBH_4$ system. *J. Alloys Compd.* **2009**, *487*, 434–438. [CrossRef]
100. Sridechprasat, P.; Phuitot, L.; Rangsunvigit, P.; Kitiyanna, B.; Kulprathipanja, S. A revisit to the hydrogen desorption/absorption behaviors of $LiAlH_4$/$LiBH_4$: Effects of catalysts. *Energies* **2012**, *5*, 3691–3700. [CrossRef]
101. Gu, R.; Wang, C.Y.; Liu, D.M.; Gao, C.; Li, Y.T.; Si, T.Z. De-/rehydrogenation properties and reaction mechanisms of $4LiBH_4$–$LiAlH_4$–MgF_2 system. *Int. J. Hydrogen Energy* **2015**, *40*, 10536–10541. [CrossRef]
102. Mao, J.F.; Yu, X.B.; Guo, Z.P.; Poh, C.K.; Liu, H.K.; Wu, Z.; Ni, J. Improvement of the $LiAlH_4$–$NaBH_4$ system for reversible hydrogen storage. *J. Phys. Chem. C* **2009**, *113*, 10813–10818. [CrossRef]

103. Xia, G.; Meng, Q.; Guo, Z.; Gud, Q.; Liu, H.; Liu, Z.; Yu, X. Nanoconfinement significantly improves the thermodynamics and kinetics of co-infiltrated $2LiBH_4$–$LiAlH_4$ composites: Stable reversibility of hydrogen absorption/resorption. *Acta Mater.* **2013**, *61*, 6882–6893. [CrossRef]
104. Huang, Y.; Xia, G.; Zhang, J.; Guo, Z.; Yu, X. Graphene-tailored molecular bonds for advanced hydrogen and lithium storage performance. *Energy Storage Mater.* **2019**, *17*, 178–185. [CrossRef]
105. Carr, C.L.; Jayawardana, W.; Zou, H.; White, J.L.; Gabaly, F.E.; Corandi, M.S.; Stavila, V.; Allendorf, M.D.; Majzoub, E.H. Anomalous H_2 desorption rate of $NaAlH_4$ confined in nitrogen-doped nanoporous carbon frameworks. *Chem. Mater.* **2018**, *30*, 2930–2938. [CrossRef]
106. De Jongh, P.E.; Adelhelm, P. Nanosizing and nanoconfinement: New strategies towards meeting hydrogen storage goals. *ChemSusChem* **2010**, *3*, 1332–1348. [CrossRef] [PubMed]
107. Fichtner, M. Nanoconfinement effects in energy storage materials. *Phys. Chem. Chem. Phys.* **2011**, *13*, 21186–21195. [CrossRef]
108. Xiong, Z.; Wu, G.; Hu, J.; Chen, P. Investigation on chemical reaction between $LiAlH_4$ and $LiNH_2$. *J. Power Sources* **2006**, *159*, 167–170. [CrossRef]
109. Varin, R.A.; Zbroniec, L.; Jang, M. Mechano-chemical synthesis of nanostructured hydride composites based on Li-Al-N-Mg for solid state hydrogen storage. *Eng. Rev.* **2011**, *31*, 111–123.
110. Chen, R.; Wang, X.; Chen, L.; Li, S.; Ge, H.; Lei, Y.; Chen, C. An investigation on the reaction pathway between $LiAlH_4$ and $LiNH_2$ via gaseous ammonia. *J. Alloys Compd.* **2010**, *495*, 17–22. [CrossRef]
111. Dolotko, O.; Kobayashi, T.; Wiench, J.W.; Pruski, M.; Pecharsky, V. Investigation of the thermochemical transformations in the $LiAlH_4$-$LiNH_2$ system. *Int. J. Hydrogen Energy* **2011**, *36*, 10626–10634. [CrossRef]
112. Lu, J.; Fang, Z.Z. Dehydrogenation of a combined $LiAlH_4$/$LiNH_2$ system. *J. Phys. Chem. B* **2005**, *109*, 20830–20834. [CrossRef] [PubMed]
113. Jepsen, L.H.; Ranvsbæk, D.B.; Grundlach, C.; Besenbacher, F.; Skibsted, J.; Jensen, T.R. A novel intermediate in the $LiAlH_4$–$LiNH_2$ hydrogen storage system. *Dalton Trans.* **2014**, *43*, 3095–3103. [CrossRef] [PubMed]
114. Naik, M.; Rather, S.; So, C.S.; Hwang, S.W.; Kim, A.R.; Nahm, K.S. Thermal decomposition of $LiAlH_4$ chemically mixed with lithium amide and transition metal chlorides. *Int. J. Hydrogen Energy* **2009**, *34*, 8937–8943. [CrossRef]
115. Bogdanović, B.; Felderhoff, M.; Kaskel, S.; Pommerin, A.; Schlichte, K.; Schüth, F. Improved hydrogen storage properties of Ti-doped sodium alanate using titanium nanoparticles as doping agents. *Adv. Mater.* **2003**, *15*, 1012–1015. [CrossRef]
116. Gross, K.J.; Guthrie, S.; Takara, S.; Thomas, G. In-situ X-ray diffraction study of the decomposition of $NaAlH_4$. *J. Alloys Compd.* **2000**, *297*, 270–281. [CrossRef]
117. Jensen, C.; Wang, Y.; Chou, M.Y. Alanates as hydrogen storage materials. In *Solid-State Hydrogen Storage: Materials and Chemistry*; Walker, G., Ed.; Woodhead Publishing: Boca Raton, FL, USA, 2008; pp. 381–419.
118. Lauher, J.W.; Dougherty, D.; Herley, P.J. Sodium tetrahydroaluminate. *Acta Crystallogr. Sect. B* **1979**, *35*, 1454–1456. [CrossRef]
119. Hauback, B.C.; Brinks, H.W.; Jensen, C.M.; Murphy, K.; Maeland, A.J. Neutron diffraction structure determination of $NaAlD_4$. *J. Alloys Compd.* **2003**, *358*, 142–145. [CrossRef]
120. Vajeeston, P.; Fjellvåg, H. Crystal structures of aluminum-based hydrides. *Emerg. Mater. Res.* **2015**, *4*, 192–217. [CrossRef]
121. Canton, P.; Fichtner, M.; Frommen, C.; Léon, A. Synchrotron X-ray studies of Ti-doped $NaAlH_4$. *J. Phys. Chem. B* **2006**, *110*, 3051–3054. [CrossRef]
122. Rönnebro, E.; Noréus, D.; Kadir, K.; Reiser, A.; Bogdanović, B. Investigation of the perovskite related structures of $NaMgH_3$, $NaMgF_3$ and Na_3AlH_6. *J. Alloys Compd.* **2000**, *299*, 101–106. [CrossRef]
123. Li, L.; Xu, C.; Chen, C.; Wang, Y.; Jiao, L.; Yuan, H. Sodium alanate system for efficient hydrogen storage. *Int. J. Hydrogen Energy* **2013**, *38*, 8798–8812. [CrossRef]
124. Pitt, M.P.; Vullum, P.E.; Sørby, M.H.; Emerich, H.; Paskevicius, M.; Buckley, C.E.; Walmsley, J.C.; Holmestad, R.; Hauback, B.C. Hydrogen absorption kinetics of the transition-metal-chloride-enhanced $NaAlH_4$ system. *J. Phys. Chem. C* **2012**, *116*, 14205–14217. [CrossRef]
125. Lee, G.-J.; Shim, J.-H.; Whan, Y.C.; Lee, K. Reversible hydrogen storage in $NaAlH_4$ catalyzed with lanthanide oxides. *Int. J. Hydrogen Energy* **2007**, *32*, 1911–1915. [CrossRef]
126. Li, L.; Wang, Y.; Wang, Y.; Liu, G.; Han, Y.; Qiu, F.; Yan, C.; Song, D.; Jiao, L.; Yuan, H. Direct synthesis of sodium alanate with novel catalytic TiB_2. *J. Alloys Compd.* **2011**, *509S*, S747–S749. [CrossRef]

127. Liu, C.; Jiang, J.; Huang, S.; Wang, P.; Tian, H. Electronic and dehydrogenation properties of TiB_2 cluster-doped $NaAlH_4$ (101) surface: A first-principle approach. *Int. J. Hydrogen Energy* **2014**, *39*, 14178–14183. [CrossRef]
128. Li, L.; Wang, Y.; Qiu, F.; Wang, Y.; Xu, Y.; An, C.; Jiao, L.; Yuan, H. Reversible hydrogen storage properties of $NaAlH_4$ enhanced with TiN catalyst. *J. Alloys Compds.* **2013**, *566*, 137–141. [CrossRef]
129. Mosher, D.A.; Tang, X.; Brown, R.J.; Saitta, S.; Laube, B.L.; Dold, R.H.; Anton, D.L. *High Density Hydrogen Storage System Demonstration Using NaAlH4 Based Complex Compound Hydrides. 1–161*; United Technologies Research Center: East Hartford, CT, USA, 2007.
130. Bogdanović, B.; Felderhoff, M.; Pommerin, A.; Schüth, F.; Spielkamp, N.; Stark, A. Cycling properties of Sc-and Ce-doped $NaAlH_4$ hydrogen storage materials prepared by the one-step direct synthesis method. *J. Alloys Compd.* **2009**, *471*, 383–386. [CrossRef]
131. Berseth, P.A.; Harter, A.G.; Zidan, R.; Blomqvist, A.; Araújo, C.M.; Scheicher, R.H.; Ahuja, R.; Jena, P. Carbon nanomaterials as catalysts for hydrogen uptake and release in $NaAlH_4$. *Nano Lett.* **2009**, *4*, 1501–1505. [CrossRef]
132. Rongeat, C.; Scheerbaum, N.; Schultz, L.; Gutfleisch, O. Catalysis of H_2 sorption in $NaAlH_4$: General description and new insights. *Acta Mater.* **2011**, *59*, 1725–1733. [CrossRef]
133. Lozano, G.A.; Na Ranong, C.; Bellosta von Colbe, J.M.; Bormann, R.; Fieg, G.; Hapke, J.; Dornheim, M. Empirical kinetic model of sodium alanate reacting system (I). Hydrogen absorption. *Int. J. Hydrogen Energy* **2010**, *35*, 6763–6772. [CrossRef]
134. Frankcombe, T.J. Proposed mechanisms for the catalytic activity of Ti in $NaAlH_4$. *Chem. Rev.* **2012**, *112*, 2164–2178. [CrossRef] [PubMed]
135. Beattie, S.D.; Mcgrady, G.S. Hydrogen desorption studies of $NaAlH_4$ and $LiAlH_4$ by in situ heating in an ESEM. *Int. J. Hydrogen Energy* **2009**, *34*, 9151–9156. [CrossRef]
136. Singh, S.; Eijt, S.W.H.; Huot, J.; Kockelmann, W.A.; Wagemaker, M.; Mulder, F.M. The $TiCl_3$ catalyst in $NaAlH_4$ for hydrogen storage induces grain refinement and impacts on hydrogen vacancy formation. *Acta Mater.* **2007**, *55*, 5549–5557. [CrossRef]
137. Løvvik, O.M.; Opalka, S.M. Density functional calculations of Ti-enhanced $NaAlH_4$. *Phys. Rev. B* **2005**, *71*, 054103. [CrossRef]
138. Løvvik, O.M.; Opalka, S.M. Stability of Ti in $NaAlH_4$. *Appl. Phys. Lett.* **2006**, *88*, 161917. [CrossRef]
139. Michel, K.J.; Ozoliņš, V. Site substitution of Ti in $NaAlH_4$ and Na_3AlH_6. *J. Phys. Chem C* **2011**, *115*, 21454–21464. [CrossRef]
140. Marashdeh, A.; Versluis, J.-W.I.; Valdés, A.; Olsen, R.A.; Løvvik, O.M.; Kroes, G.-J. Effect of transition metal dopants on initial mass transport in the dehydrogenation of $NaAlH_4$: Density functional theory study. *J. Phys. Chem. C* **2013**, *117*, 3–14. [CrossRef]
141. Al-Mahboob, A.; Muller, E.; Karim, A.; Muckerman, J.T.; Ciobanu, C.V.; Sutter, P. Site-dependent activity of atomic Ti catalysts in Al-based hydrogen storage materials. *J. Am. Chem. Soc.* **2012**, *134*, 10381–10384. [CrossRef]
142. Wang, Y.; Zhang, F.; Stumpf, R.; Lin, P.; Chou, M.Y. Catalytic effect of near-surface alloying on hydrogen interaction on the aluminum surface. *Phys. Rev. B* **2011**, *83*, 195419. [CrossRef]
143. Zhang, F.; Wang, Y.; Chou, M.Y. Hydrogen interaction with the Al surface promoted by subsurface alloying with transition metals. *J. Phys. Chem. C* **2012**, *116*, 18663–18668. [CrossRef]
144. Xiong, R.; Sang, G.; Zhang, G.; Yan, X.; Li, P.; Yao, Y.; Luo, D.; Chen, C.; Tang, T. Evolution of the active species and catalytic mechanism of Ti doped $NaAlH_4$ for hydrogen storage. *Int. J. Hydrogen Energy* **2017**, *42*, 6088–6095. [CrossRef]
145. Léon, A.; Kircher, O.; Rothe, J.; Fichtner, M. Chemical state and local structure around titanium atoms in $NaAlH_4$ doped with $TiCl_3$ using X-ray absorption spectroscopy. *J. Phys. Chem. B* **2004**, *108*, 16372–16376. [CrossRef]
146. Haiduc, A.G.; Stil, H.A.; Schwarz, M.A.; Paulus, P.; Geerlings, J.J.C. On the fate of the Ti catalyst during hydrogen cycling of sodium alanate. *J. Alloys Compd.* **2005**, *393*, 252–263. [CrossRef]
147. Kang, X.D.; Wang, P.; Song, X.P.; Yao, X.D.; Lu, G.Q.; Cheng, H.M. Catalytic effect of Al_3Ti on the reversible dehydrogenation of $NaAlH_4$. *J. Alloys Compd.* **2006**, *424*, 365–369. [CrossRef]
148. Brinks, H.W.; Hauback, B.C.; Srinivasan, S.S.; Jensen, C.M. Synchrotron X-ray studies of $Al_{1-y}Ti_y$ formation and re-hydriding inhibition in Ti-enhanced $NaAlH_4$. *J. Phys. Chem. B* **2005**, *109*, 15780–15785. [CrossRef] [PubMed]

149. Liu, J.; Ge, Q. A precursor state for formation of $TiAl_3$ complex in reversible hydrogen desorption/adsorption from Ti-doped $NaAlH_4$. *Chem. Commun.* **2006**, *42*, 1822–1824. [CrossRef]
150. Dathara, G.K.P.; Mainardi, D.S. Structure and dynamics of Ti-Al-H compounds in Ti-doped $NaAlH_4$. *Mol. Simul.* **2008**, *34*, 201–210. [CrossRef]
151. Liu, J.; Han, Y.; Ge, Q. Effect of doped transition metal on reversible hydrogen release/uptake from $NaAlH_4$. *Chem. Eur. J.* **2009**, *15*, 1685–1695. [CrossRef]
152. Ismail, M.; Zhao, Y.; Yu, X.B.; Mao, J.F.; Dou, S.X. The hydrogen storage properties and reaction mechanism of the MgH_2-$NaAlH_4$ composite system. *Int. J. Hydrogen Energy* **2011**, *36*, 9045–9050. [CrossRef]
153. Bendyna, J.K.; Dyjak, S.; Notten, P.H.L. The influence of ball-milling time on the dehydrogenation properties of the $NaAlH_4$-MgH_2 composite. *Int. J. Hydrogen Energy* **2015**, *40*, 4200–4206. [CrossRef]
154. Ismail, M.; Zhao, Y.; Yu, X.B.; Dou, S.X. Improved hydrogen storage performance of MgH_2-$NaAlH_4$ composite by the addition of TiF_3. *Int. J. Hydrogen Energy* **2012**, *37*, 8395–8401. [CrossRef]
155. Rafi-ud-Din; Qu, X.; Zahid, G.H.; Asghar, Z.; Shahzad, M.; Iqbal, M.; Ahmad, E. Improved hydrogen storage performances of MgH_2-$NaAlH_4$ system catalyzed by TiO_2 nanoparticles. *J. Alloys Compd.* **2014**, *604*, 317–324. [CrossRef]
156. Cheng, H.; Chen, Y.; Sun, W.; Lou, H.; Liu, Y.; Qi, Q.; Zhang, J.; Liu, J.; Yan, K.; Jin, H.; et al. The enhanced de/re-hydrogenation performance of $4MgH_2$-$NaAlH_4$ composite by doping with TiH_2. *J. Alloys Compd.* **2017**, *698*, 1002–1008. [CrossRef]
157. Plerdseanoy, P.; Meethon, S.; Utke, R. Dehydrogenation kinetics, reversibility, and reaction mechanisms of reversible hydrogen storage material based on nanoconfined MgH_2-$NaAlH_4$. *J. Phys. Chem. Solids* **2015**, *87*, 16–22. [CrossRef]
158. Bhatnagar, A.; Pandey, S.K.; Dixit, V.; Shukla, V.; Shahi, R.R.; Shaz, M.A.; Srivastava, O.N. Catalytic effect of carbon nanostructures on the hydrogen storage properties of MgH_2-$NaAlH_4$ composite. *Int. J. Hydrogen Energy* **2014**, *39*, 14240–14246. [CrossRef]
159. Ismail, M.; Zhao, Y.; Dou, S.X. An investigation on the hydrogen storage properties and reaction mechanism of the destabilized MgH_2-Na_2AlH_6 (4:1) system. *Int. J. Hydrogen Energy* **2013**, *38*, 1478–1483. [CrossRef]
160. Ranvsbæk, D.B.; Jensen, T.R. Tuning the hydrogen storage properties and reactivity: Investigation of the $LiBH_4$-$NaAlH_4$ system. *J. Phys. Chem. Solids* **2010**, *71*, 144–1149. [CrossRef]
161. Morioka, H.; Kakizaki, K.; Chung, S.C.; Yamada, A. Reversible hydrogen decomposition of $KAlH_4$. *J. Alloys Compd.* **2003**, *353*, 310–314. [CrossRef]
162. Dymova, T.N.; Eliseeva, N.G.; Bakum, S.I.; Dergachev, Y.M. Direct synthesis of alkali metal aluminum hydrides in the melt. *Dokl. Akad. Nauk SSSR* **1974**, *215*, 1369–1372.
163. Pukazhselvan, D.; Fagg, D.P.; Srivastava, O.N. On step high pressure mechanochemical synthesis of reversible alanates $NaAlH_4$ and $KAlH_4$. *Int. J. Hydrogen Energy* **2015**, *40*, 4916–4924. [CrossRef]
164. Ares, J.R.; Zhang, J.; Charpentier, T.; Cuevas, F.; Latroche, M. Asymmetric reaction path and hydrogen sorption mechanism in mechanochemically synthesized potassium alanate (KAlH4). *J. Phys. Chem. C* **2016**, *120*, 21299–21308. [CrossRef]
165. Mamatha, M.; Weidenhaler, C.; Pommerin, A.; Felderhoff, M.; Schüth, F. Comparative studies of the decomposition of alanates followed by in situ XRD and DSC methods. *J. Alloys Compd.* **2006**, *416*, 303–314. [CrossRef]
166. Matysina, Z.A.; Zaginaichenko, S.Y.; Schur, D.V.; Zolotarenko, A.D.; Zolotarenko, A.D.; Gabdulin, M.T. Hydrogen sorption properties of potassium alanate. *Russ. Phys. J.* **2018**, *61*, 253–263. [CrossRef]
167. Ares, J.R.; Aguey-Zinsou, K.-F.; Leardini, F.; Jímenez Ferrer, I.; Fernandez, J.-F.; Guo, Z.-X.; Sánchez, C. Hydrogen absorption/desorption mechanism in potassium alanate ($KAlH_4$) and enhancement by $TiCl_3$ doping. *J. Phys. Chem. C* **2009**, *113*, 6845–6851. [CrossRef]
168. Arroyo y de Dompablo, M.E.; Ceder, G. First principles investigations of complex hydrides AMH_4 and A_3MH_6 (A = Li, Na, K, M = B, Al, Ga) as hydrogen storage systems. *J. Alloys Compd.* **2004**, *364*, 6–12. [CrossRef]
169. Santhanam, R.; McGrady, G.S. Synthesis of alkali metal hexahydroaluminate complexes using dimethyl ether as a reaction medium. *Inorg. Chim. Acta* **2008**, *361*, 473–478. [CrossRef]
170. Dymova, T.N.; Selivokhina, M.S.; Eliseeva, N.G. Thermal stability of potassium alumohydride. *Dokl. Akad. Nauk* **1963**, *153*, 1330–1332.

171. Sorte, E.G.; Emery, S.B.; Majzoub, E.H.; Ellis-Caleo, T.; Ma, Z.L.; Hammann, B.A.; Hayes, S.E.; Bowman, R.C., Jr.; Conradi, M.S. NMR study of anion dynamics in solid $KAlH_4$. *J. Phys. Chem. C* **2014**, *118*, 5725–5732. [CrossRef]
172. Arnbjerg, L.M.; Jensen, T.R. New compounds in the potassium-aluminium-hydrogen system observed during release and uptake of hydrogen. *Int. J. Hydrogen Energy* **2012**, *37*, 345–356. [CrossRef]
173. Hauback, B.C.; Brinks, H.W.; Heyn, R.H.; Blom, R.; Fjellvag, H. The crystal structure of $KAlD_4$. *J. Alloys Compd.* **2005**, *394*, 35–38. [CrossRef]
174. Vajeeston, P.; Ravindran, P.; Kjekshus, A.; Fjellvag, H. Crystal structure of $KAlH_4$ from first principle calculations. *J. Alloys Compds.* **2004**, *363*, L7–L11. [CrossRef]
175. Vajeeston, P.; Ravindran, P.; Kjekhus, A.; Fjellvåg, H. First-principles investigations of aluminum hydrides: M_3AlH_6 (M = Na, K). *Phys. Rev. B* **2005**, *71*, 092103. [CrossRef]
176. Weindenthaler, C.; Felderhoff, M.; Bernert, T.; Sørby, M.H.; Hauback, B.C.; Krech, D. Synthesis, crystal structure analysis and decomposition of $RbAlH_4$. *Crystals* **2018**, *8*, 103. [CrossRef]
177. Adkis, T.G.; Gavrilenko, V.V.; Zahartin, I.I.; Ignat'eva, I.A. Study of the infrared spectra of alkali metal aluminum hydrides. *Zhural Prikl. Spektrosk.* **1967**, *6*, 806–812. [CrossRef]
178. Bestide, J.P.; Hajri, J.E.; Claudy, P.; Hajbi, A.E. A new route to alkali metal aluminum hydrides $MAlH_4$ with M = Na, K, Rb, Cs and structural features for the whole family with M = Li to Cs. *Synth. React. Inorg. Met. Org. Chem.* **1995**, *25*, 1037–1047. [CrossRef]
179. Dymova, T.N.; Bakum, S.I.; Mirsaidov, U. Phase States of Alkaly Aluminum Hydrides. *Dokl. Akad. Nauk SSSR* **1974**, *216*, 87–90.
180. Vajeeston, P.; Ravindran, P.; Vidya, R.; Fjellvåg, H.; Kjeshus, A. Design of potential hydrogen-storage materials using first-principle density-functional calculations. *Cryst. Growth Des.* **2004**, *4*, 471–477. [CrossRef]
181. Adimi, S.; Arabi, H.; Ghorbani, S.R.; Pourarin, F. AB-initio study of pressure-induced aluminum hydrides $AAlH_4$ (A = Li, Na, K, Rb, Cs). *Int. J. Hydrogen Energy* **2017**, *42*, 25303–25309. [CrossRef]
182. Ravindan, P.; Vajeeston, P.; Vidya, R.; Fjellvåg, H.; Kjekshus, A. Modeling of hydrogen storage materials by density-functional calculations. *J. Power Sources* **2006**, *159*, 88–99. [CrossRef]
183. Krech, D.; Zibrowius, B.; Weidenthaler, C.; Felderhoff, M. On the preparation and structure of cesium aluminum tetrahydride. *Eur. J. Inorg. Chem.* **2014**, *2014*, 5683–5688. [CrossRef]
184. Bakum, S.I.; Kuznetsova, S.F.; Tarasov, V.P. $CsAlH_4$ thermolysis. *Russ. J. Inorg. Chem.* **2013**, *58*, 1547–1549. [CrossRef]
185. Bernert, T.; Krech, D.; Kockelmann, W.; Felderhoff, M.; Frankcombe, T.J.; Weidenthaler, C. Crystal structure relation between tetragonal and orthorhombic $CsAlD_4$: DFT and time-of-flight neutron powder diffraction studies. *Eur. J. Inorg. Chem.* **2015**, *2015*, 5545–5550. [CrossRef]
186. Graetz, J. Metastable metal hydrides for hydrogen storage. *ISRN Mater. Sci.* **2012**, *2012*, 863025. [CrossRef]
187. Mackay, K.M. *Hydrogen Compounds of the Metallic Elements*; E. & F. N. Spon Ltd.: London, UK, 1966; p. 177.
188. Schlesinger, H.I.; Brown, H.C.; Abraham, B.; Bond, A.C.; Davidson, N.; Finholt, A.E.; Gilbreath, J.R.; Hoekstra, H.; Horvitz, L.; Hyde, E.K.; et al. New developments in the chemistry of diborane and the borohydrides. I. General summary. *J. Am. Chem. Soc.* **1953**, *75*, 186–190. [CrossRef]
189. Schlesinger, H.I.; Brown, H.C.; Hyde, E.K. The preparation of other borohydrides by metathetical reactions utilizing the alkali metal borohydrides. *J. Am. Chem. Soc.* **1953**, *75*, 209–213. [CrossRef]
190. Ashby, E.C.; Sanders, J.R.; Claudy, P.; Schwartz, R.D. A study of the reactions of lithium aluminum hydride and sodium aluminum hydride with beryllium chloride in diethyl ether and tetrahydrofuran. A report questioning the existence of $Be(AlH_4)_2$ in solution. *Inorg. Chem.* **1973**, *12*, 2860–2868. [CrossRef]
191. Wiberg, E.; Bauer, R. Zur Kenntnis eines Berylliumwasserstoffs BeH_2. *Z. Nat.* **1951**, *6*, 171. [CrossRef]
192. Klaveness, A.; Vajeeston, P.; Ravindran, P.; Fjellvåg, H.; Kjekshus, A. Structure and bonding in $BAlH_5$ (B = Be, Ca, Sr) from first-principle calculations. *J. Alloys Compd.* **2007**, *443*, 225–232. [CrossRef]
193. Santhosh, M.; Rajeswarapalanichamy, R.; Priyanga, G.S.; Kanagaprabha, S.; Cinthia, A.J.; Iyakutti, K. A first principles study of structural stability, electronic structure and mechanical properties of beryllium alanate $BeAlH_5$. *AIP Conf. Proc.* **2015**, *1665*, 090032. [CrossRef]
194. He, L.; Wang, S.; Li, Z.; Liu, X.; Jlang, L. Synthesis of magnesium alanate by ball milling MgH_2 and $AlCl_3$ mixtures. *Rare Met.* **2011**, *30*, 55–58. [CrossRef]
195. Xiao, X.; Qin, T.; Jiang, Y.; Jiang, F.; Li, M.; Fan, X.; Li, S.; Ge, H.; Wang, Q.; Chen, L. Significantly enhanced hydrogen desorption properties of $Mg(AlH_4)_2$ nanoparticles synthesized using solvent free strategy. *Prog. Nat. Sci.* **2017**, *27*, 112–120. [CrossRef]

196. Fichtner, M.; Fuhr, O.; Kircher, O. Magnesium alanate—A material for reversible hydrogen storage? *J. Alloys Compd.* **2003**, *356–357*, 418–422. [CrossRef]
197. Liu, Y.; Pang, Y.; Zhang, X.; Zhou, Y.; Gao, M.; Pan, H. Synthesis and hydrogen storage thermodynamics and kinetics of $Mg(AlH_4)_2$ submicron rods. *Int. J Hydrog. Energy* **2012**, *37*, 18148–18154. [CrossRef]
198. Fossdal, A.; Brinks, H.W.; Fichtner, M.; Hauback, B.C. Thermal decomposition of $Mg(AlH_4)_2$ studied by in situ synchrotron X-Ray diffraction. *J. Alloys Compd.* **2005**, *404–406*, 752–756. [CrossRef]
199. Pang, Y.; Liu, Y.; Zhang, X.; Gao, M.; Pan, H. Role of particle size, grain size, microstrains and lattice distortion in improved dehydrogenation properties of the ball-milled $Mg(AlH_4)_2$. *Int. J. Hydrogen Energy* **2013**, *38*, 1460–1468. [CrossRef]
200. Pang, Y.; Liu, Y.; Zhang, X.; Gao, M.; Pan, H. TiF_4-doped $Mg(AlH_4)_2$ with significantly improved dehydrogenation properties. *Int. J. Hydrogen Energy* **2013**, *38*, 13343–13351. [CrossRef]
201. Gremaud, R.; Borgschulte, A.; Lohstroh, W.; Schreuders, H.; Züttel, A.; Dam, B.; Griessen, R. Ti-Catalyzed $Mg(AlH_4)_2$: A reversible hydrogen storage material. *J. Alloys Compd.* **2005**, *404–406*, 775–778. [CrossRef]
202. Fossdal, A.; Brinks, H.W.; Fichtner, M.; Hauback, B.C. Determination of the crystal structure of $Mg(AlH_4)_2$ by combined X-ray and neutron diffraction. *J. Alloys Compd.* **2005**, *387*, 47–51. [CrossRef]
203. Fichtner, M.; Engel, J.; Fuhr, O.; Glöss Rubner, O.; Ahlrichs, R. The structure of magnesium alanate. *Inorg. Chem.* **2003**, *42*, 7060–7066. [CrossRef]
204. Vajeeston, P.; Ravindran, P.; Kjekshus, A.; Fjellvag, H. High hydrogen content complex hydrides: A density-functional study. *Appl. Phys. Lett.* **2006**, *89*, 071906. [CrossRef]
205. Van Setten, M.J.; de Wijs, G.A.; Popa, V.A.; Brocks, G. Ab initio study of $Mg(AlH_4)_2$. *Phys. Rev. B* **2005**, *72*, 073107. [CrossRef]
206. Akbarzadeh, A.R.; Wolverton, C.; Ozolins, V. First-principles determination of crystal structures, phase stability and reaction thermodynamics in the Li-Mg-Al-H hydrogen storage system. *Phys. Rev. B* **2009**, *79*, 184102. [CrossRef]
207. Klaveness, A.; Vajeeston, P.; Ravindran, P.; Fjellvåg, H.; Kjekshus, A. Structural phase stability and bonding behavior of $BAlH_5$ (B = Mg, Ba) from first-principles calculations. *Phys. Rev. B* **2006**, *73*, 094122. [CrossRef]
208. Pang, Y.; Li, Q. Insight into the kinetic mechanism of the first-step dehydrogenation of $Mg(AlH_4)_2$. *Scr. Mater.* **2017**, *130*, 223–228. [CrossRef]
209. Løvvik, O.M.; Molin, P.N. Density-functional band-structure calculations of magnesium alanate $Mg(AlH_4)_2$. *Phys. Rev. B* **2005**, *72*, 073201. [CrossRef]
210. Spanò, E.; Bernasconi, M. Ab initio of the vibrational properties of $Mg(AlH_4)_2$. *Phys. Rev. B* **2005**, *71*, 174301. [CrossRef]
211. Yang, C.H.; Chen, T.T.; Tsai, W.T.; Liu, B.H. In situ synchrotron X-ray diffraction study on the improved dehydrogenation performance of $NaAlH_4$-$Mg(AlH_4)_2$ mixture. *J. Alloys Compd.* **2013**, *577*, 6–10. [CrossRef]
212. Hudson, M.S.L.; Pukazhselvan, D.; Scheeja, I.G.; Srivastava, O.N. Studies on synthesis and dehydrogenation behavior of magnesium alanate and magnesium-sodium alanate mixture. *Int. J. Hydrogen Energy* **2007**, *32*, 4933–4938. [CrossRef]
213. Wang, Y.; Wang, Y.; Wang, X.; Zhang, H.; Jiao, L.; Yuan, H. Destabilization effects of $Mg(AlH_4)_2$ on MgH_2: Improved desorption performance and its reaction mechanism. *Int. J. Hydrogen Energy* **2014**, *39*, 17747–17753. [CrossRef]
214. Liu, D.; Liu, Q.; Si, T.; Zhang, Q.; Fang, F.; Sun, D.; Ouyang, L.; Zhu, M. Superior hydrogen storage properties of $LiBH_4$ catalyzed by $Mg(AlH_4)_2$. *Chem. Commun.* **2011**, *47*, 5741–5743. [CrossRef] [PubMed]
215. Pang, Y.; Liu, Y.; Zhang, X.; Li, Y.; Gao, M.; Pan, H. New insights into the effects of NaCl and LiCl on the hydrogen storage behaviors of a $6LiBH_4$-$Mg(AlH_4)_2$ composite. *RSC Adv.* **2015**, *5*, 12144–12151. [CrossRef]
216. Huang, J.; Gao, M.; Li, Z.; Cheng, X.; Gu, J.; Liu, Y. Destabilization of combined $Ca(BH_4)_2$ and $Mg(AlH_4)_2$ for improved hydrogen storage properties. *J. Alloys Compd.* **2016**, *670*, 135–143. [CrossRef]
217. Finholt, E.; Barbaras, G.D.; Barbaras, G.K.; Urry, G.; Wartik, T.; Schlesinger, H.I. The preparation of sodium and calcium aluminum hydrides. *J. Inorg. Nucl. Chem.* **1955**, *1*, 317–325. [CrossRef]
218. Fichtner, M.; Frommen, C.; Fuhr, O. Synthesis and properties of calcium alanate and two solvent adducts. *Inorg. Chem.* **2005**, *44*, 3479–3484. [CrossRef]
219. Li, C.; Xiao, X.; Ge, P.; Xue, J.; Li, S.; Ge, H. Investigation on synthesis, structure and catalytic modification of $Ca(AlH_4)_2$ complex hydride. *Int. J. Hydrogen Energy* **2012**, *37*, 936–941. [CrossRef]

220. Mamatha, M.; Bogdanović, B.; Felderhoff, M.; Pommerin, A.; Schmidt, W.; Schüth, F.; Weidenthaler, C. Mechanochemical preparation and investigation of properties of magnesium, calcium and lithium-magnesium alanates. *J. Alloys Compds.* **2006**, *407*, 78–86. [CrossRef]
221. Sato, T.; Sørby, M.H.; Ikeda, K.; Sato, S.; Hauback, B.C.; Orimo, S. Syntheses, crystal structures, and thermal analyses of solvent-free $Ca(AlD_4)_2$ and $CaAlD_5$. *J. Alloys Compd.* **2009**, *487*, 472–478. [CrossRef]
222. Weidenthaler, C.; Frankcombe, T.J.; Felderhoff, M. First crystal structure studies of $CaAlH_5$. *Inorg. Chem.* **2006**, *45*, 3849–3851. [CrossRef]
223. Løvvik, O.M. Crystal structure of $Ca(AlH_4)_2$ predicted from density-functional band-structure calculations. *Phys. Rev. B* **2005**, *71*, 144111. [CrossRef]
224. Wolverton, C.; Ozoliņš, V. Hydrogen storage in calcium alanate: First-principles thermodynamics and crystal structures. *Phys. Rev. B* **2007**, *75*, 064101. [CrossRef]
225. Liu, D.M.; Gao, C.; Qian, Z.X.; Si, T.Z.; Zhang, Q.A. Reversible hydrogen storage in $LiBH_4/Ca(AlH_4)_2$ systems. *Int. J. Hydrogen Energy* **2013**, *38*, 3291–3295. [CrossRef]
226. Hanada, N.; Lohstroh, W.; Fichtner, M. Comparison of the calculated and experimental scenarios for solid-state reactions involving $Ca(AlH_4)_2$. *J. Phys. Chem. C* **2008**, *112*, 131–138. [CrossRef]
227. Alapati, S.V.; Johnson, J.K.; Sholl, D.S. Large-scale screening of metal hydride mixtures for high-capacity hydrogen storage from first-principles calculations. *J. Phys. Chem. C* **2008**, *112*, 5258–5262. [CrossRef]
228. Dymova, T.N.; Aleksandrov, D.P.; Konoplev, V.N.; Silina, T.A.; Sizareva, A.S. Peculiarities of the solid-phase formation of strontium pentahydroaluminate from binary hydrides by mechanochemical activation and modeling of theprocess on the basis of thermo gasovolumetry data. *Russ. J. Coord. Chem.* **2000**, *26*, 531–537.
229. Sato, T.; Takagi, S.; Sørby, M.H.; Deledda, S.; Hauback, B.C.; Orimo, S.I. Crystal structural determination of $SrAlD_5$ with corner-sharing AlD_6 octahedron chains by X-ray and neutron diffraction. *Crystals* **2018**, *8*, 89. [CrossRef]
230. Zhang, Q.A.; Makamura, Y.; Oikawa, K.I.; Kamiyama, T.; Akiba, E. Synthesis and crystal structure of Sr_2AlH_7: A new structural type of alkaline earth aluminum hydride. *Inorg. Chem.* **2002**, *41*, 6547–6549. [CrossRef]
231. Zhang, Q.A.; Akiba, E. Synthesis of Sr_2AlH_7 by ball milling followed by hydrogenation. *J. Alloys Compd.* **2005**, *394*, 308–311. [CrossRef]
232. Zhang, Q.A.; Enoki, H.; Akiba, E. Formation mechanism of Sr_2AlH_7. *J. Alloys Compd.* **2007**, *427*, 153–159. [CrossRef]
233. Gingl, F.; Vogt, T.; Akiba, E. Trigonal $SrAl_2H_2$: The first zintl phase hydride. *J. Alloys Compod.* **2000**, *306*, 127–132. [CrossRef]
234. Zhang, Q.A.; Nakamura, Y.; Oikawa, K.I.; Kamiyama, T.; Akiba, E. New alkaline earth aluminum hydride with one-dimensional zigzag chains of $[AlH_6]$: Synthesis and crystal structure of $BaAlH_5$. *Inorg. Chem.* **2002**, *41*, 6941–6943. [CrossRef] [PubMed]
235. Zhang, Q.A.; Nakamura, Y.; Oikawa, K.; Kamiyama, T.; Akiba, E. Hydrogen-induced phase decomposition of Ba_7Al_{13} and the crystal structure of Ba_2AlH_7. *J. Alloys Compd.* **2003**, *316*, 180–186. [CrossRef]
236. Liu, X.; Asano, K.; Sakaki, K.; Nakamura, Y.; Enoki, H.; Akiba, E. Investigations on the formation and decomposition behaviors of $BaAlH_5$ and Ba_2AlH_7. *J. Phys. Chem. C* **2008**, *112*, 17423–17426. [CrossRef]
237. Liu, X.; Asano, K.; Akiba, E. Direct synthesis of $BaAlH_5$ and Ba_2AlH_7 from BaH_2 and Al system and their hydriding/dehydriding characteristics. *J. Alloys Compd.* **2009**, *477*, 744–748. [CrossRef]
238. Chahrkin, O.P. Theoretical study of metal tetrahydroborates and alanates $L(MH_4)_3$, $HL(MH_4)_2$, and $H_2L(MH_4)$ (L = Be, Mg, Al, Sc, Ti, V, Zn, M = B, Al). *Russ. J. Inorg. Chem.* **2008**, *53*, 1910–1919. [CrossRef]
239. Kost, M.E.; Golovanova, A.I. Interaction of LiH and Al with transition metal halogens. *Izv. Akad. Nauk SSSR* **1978**, *14*, 1732–1734.
240. Cao, Z.; Ouyang, L.; Wang, H.; Liu, J.; Felderhoff, M.; Zhu, M. Reversible hydrogen storage in yttrium aluminum hydride. *J. Mater. Chem. A* **2017**, *5*, 6042–6046. [CrossRef]
241. Kost, M.E.; Golovanova, A.L. Interaction of titanium and iron halides with lithium aluminum hydride in diethyl ether. Translated from *Izv. Akad. Nauk SSSR* **1975**, *5*, 991–994. [CrossRef]
242. Ramzan, M.; Ahuja, R. $M_{N+1}AX_N$ (M = Ti, A = Al. X = H) phase class materials with hydrogen: Ti_4AlH_3 and Ti_3AlH_2. *Appl. Phys. Lett.* **2010**, *96*, 261906. [CrossRef]
243. Maeland, A.J.; Hauback, B.C.; Fjellvåg, H.; Sørby, M.H. The structures of hydride phases in the Ti_3Al/H system. *Int. J. Hydrogen Energy* **1999**, *24*, 163–168. [CrossRef]

244. Epshteyn, A.; Miller, J.B.; Pettigrew, K.A.; Stroud, R.M.; Purdy, A.P. Surface passivated air and moisture stable mixed zirconium aluminum metal-hydride nanoparticles. *Mater. Res. Soc. Symp. Proc.* **2008**, *1056*, HH03–HH16. [CrossRef]
245. Matsubara, E.; Waseda, Y.; Li, X.G.; Aoki, K.; Masumoto, T. X-Ray diffraction study of amorphous Zr_3InH_4 and Zr_3AlH_4 alloys produced by hydrogen-induced amorphization method. *J. Mater. Sci. Lett.* **1990**, *9*, 1017–1019. [CrossRef]
246. Wiberg, E.; Neumaier, H. Zur Kenntnis von Doppel-und Tripelhydriden der Übergangsmetalle. I. Über die Umsetzung von Niob(v)-chlorid mit Lithiumalanat. *Z. Anorg. Allg. Chem.* **1965**, *340*, 189–200. [CrossRef]
247. Aubry, J.; Monnier, G.; Hackspill, M.J. Sur la preparation de quelques aluminohydrures métalliques. *Comptes Rendus* **1954**, *238*, 2534–2535.
248. Monnier, G. Contribution a l'étude de l´éther oxyde d´éthyle, milieu réactionel, en chimie minérale. *Ann. Chim.* **1957**, *13*, 14–57.
249. Neumaier, H.; Büchel, D.; Ziegelmaier, G. Über die Umsetzung von Eisen(III)-chlorid mit Lithiumalanat bei tiefen Temperaturen. *Z. Anorg. Allg. Chem.* **1996**, *345*, 46–51. [CrossRef]
250. Scheaffer, G.W.; Roscoe, J.S.; Stewart, A.C. The reduction of iron(III) chloride with lithium aluminohydride and lithium borohydride: Iron(II) borohydride. *J. Am. Chem. Soc.* **1956**, *78*, 729–733. [CrossRef]
251. Ashby, E.C.; Kovar, R.A. Reaction of lithium aluminum hydride with copper(I) and mercury(II) salts. Nature of the reactive species in the conjugate reducing agent $LiAlH_4$-CuI. *Inorg. Chem.* **1977**, *16*, 1437–1440. [CrossRef]
252. Wiberg, E.; Henle, W. Über eine neue Darstellungsweise des Kupferwasserstoffs CuH. *Zeitschrift für Naturforschung B* **1952**, *7*, 250. [CrossRef]
253. Wiberg, E.; Henle, W. Zur Kenntnis eines Silber-aluminium-wasserstoffs $AgAlH_4$. *Z. Nat.* **1952**, *7*, 250–251. [CrossRef]
254. Zhizhin, K.Y.; Mal´tseva, N.N.; Buzanov, G.A.; Kunetsov, N.T. Hydride compounds of zinc. *Russ. J. Inorg. Chem.* **2014**, *59*, 1665–1678. [CrossRef]
255. Wiberg, E.; Schmidt, M. Zur Kenntnis eines Gallium-aluminium-wasserstoffs $Ga(AlH_4)_3$ und eines Galliumwasserstoff-Ätherats GaH_3*OR_2. *Z. Nat.* **1951**, *6*, 172.
256. Wiberg, E. Neuere Ergebnisse der präparativen Hydrid-Forschung. *Angew. Chem.* **1953**, *65*, 16–34. [CrossRef]
257. Wiberg, E.; Dittmann, O.; Nöth, H.; Schmidt, M. Über Wasserstoff-Verbindungen des Thalliums, V. Zur Kenntnis eines Thallium(I)-boranats $TlBH_4$ und Thallium(I)-alanats $TlAlH_4$. *Z. Nat.* **1957**, *12*, 62–63.
258. Wiberg, E.; Nöth, H. Über Wasserstoff-Verbindungen des Thalliums VI. Zur Kenntnis eines Thallium(III)-boranats $TlCl(BH_4)_2$. *Z. Nat.* **1957**, *12*, 63–65.
259. Wiberg, E.; Schmidt, M. Zur Kenntnis eines Thallium-aluminium-wasserstoffs $TlCl(AlH_4)_2$. *Z. Nat.* **1951**, *6*, 334–335. [CrossRef]
260. Wiberg, E.; Bauer, R. Zur Kenntnis eines Zinn-aluminium-wasserstoffs $Sn(AlH_4)_4$. *Z. Nat.* **1951**, *6*, 392. [CrossRef]
261. Weidenthaler, C.; Pommerin, A.; Felderhoff, M.; Sun, W.; Wolverton, C.; Bogdanović, B.; Schüth, F. Complex rare-earth aluminum hydrides: Mechanochemical preparation, crystal structure and potential for hydrogen storage. *J. Am. Chem. Soc.* **2009**, *131*, 16735–16743. [CrossRef]
262. Mueller, W.M.; Blackledge, J.P.; Libowitz, G.G. *Metal Hydrides*; Academic Press: Moscow, Russia, 1968; pp. 435–436.
263. Bergsma, J.; Goedkoop, J.A.; Vucht, J.H.N. Neutron diffraction investigation of solid solutions $AlTh_2Dn$. *Acta Cryst.* **1961**, *14*, 223–228. [CrossRef]
264. Sørby, M.H.; Fjellvåg, H.; Hauback, B.C.; Maeland, A.J.; Yartys, V.A. Crystal structure of Th_2Al deuterides. *J. Alloys Compd.* **2000**, *309*, 154–164. [CrossRef]
265. Vajeeston, P.; Vidya, R.; Ravindran, P.; Fjellvåg, H.; Kjekshus, A.; Skjeltorp, A. Electronic structure, phase stability, and chemical bonding in Th_2Al and Th_2AlH_4. *Phys. Rev. B* **2002**, *65*, 075101. [CrossRef]
266. Rude, L.H.; Nielsen, T.K.; Ravnsbæk, D.B.; Bösenberg, U.; Ley, M.B.; Richter, B.; Arnbjerg, L.M.; Dornheim, M.; Filinchuk, Y.; Besenbacher, F.; et al. Tailoring properties of borohydrides for hydrogen storage: A review. *Phys. Status Solidi A* **2011**, *208*, 1754–1773. [CrossRef]
267. Graetz, J.; Lee, Y.; Reilly, J.J.; Park, S.; Vogt, T. Structures and thermodynamics of the mixed alkali alanates. *Phys. Rev. B* **2005**, *71*, 184115. [CrossRef]

268. Løvvik, O.M.; Swang, O.; Opalka, S.M. Modeling alkali alanates for hydrogen storage by density-functional band-structure calculations. *J. Mater. Res.* **2005**, *20*, 3199–3213. [CrossRef]
269. Majzoub, E.H.; Ozoliņš, V. Prototype electrostatic ground state approach to predicting crystal structures of ionic compounds: Application to hydrogen storage materials. *Phys. Rev. B* **2008**, *77*, 104115. [CrossRef]
270. Claudy, P.; Bonnetot, B.; Bastide, J.P.; Letoffe, J.M. Reactions of lithium and sodium aluminum hydride with sodium or lithium hydride. Preparation of a new alumino-hydride of lithium and sodium LiN_2AlH_6. *Mater. Res. Bull.* **1982**, *17*, 1499–1504. [CrossRef]
271. Huot, J.; Boily, S.; Güther, V.; Schulz, R. Synthesis of Na_3AlH_6 and Na_2LiAlH_6 by mechanical alloying. *J. Alloys Compd.* **1999**, *383*, 304–306. [CrossRef]
272. Okada, N.; Genma, R.; Nishi, Y.; Uchida, H.H. RE-oxide doped alkaline hydrogen storage materials prepared by mechanical activation. *J. Mater. Sci.* **2004**, *39*, 5503–5506. [CrossRef]
273. Genma, R.; Uchida, H.H.; Okada, N.; Nishi, Y. Hydrogen reactivity of Li-containing hydrogen storage materials. *J. Alloys Compd.* **2003**, *356*, 358–362. [CrossRef]
274. Wang, F.; Liu, Y.; Gao, M.; Luo, K.; Pan, H.; Wang, Q. Formation reactions and the thermodynamics and kinetics of dehydrogenation reaction of mixed alanate Na_2LiAlH_6. *J. Phys. Chem. C* **2009**, *113*, 7978–7984. [CrossRef]
275. Genma, R.; Okada, N.; Sobue, T.; Uchida, H.H. Mechanically milled alanates as hydrogen storage materials. *Int. J. Hydrogen Energy* **2006**, *31*, 309–311. [CrossRef]
276. Fossdal, A.; Brinks, H.W.; Fonneløp, J.E.; Hauback, B.C. Pressure-composition isotherms and thermodynamic properties of TiF_3-enhanced Na_2LiAlH_6. *J. Alloys Compd.* **2005**, *397*, 135–139. [CrossRef]
277. Fan, X.; Xiao, X.; Chen, L.; Li, S.; Ge, H.; Wang, Q. Direct synthesis and hydrogen storage behaviors of nanocrystalline Na_2LiAlH_6. *J. Mater. Sci.* **2011**, *46*, 3314–3318. [CrossRef]
278. Teprovich, J.A., Jr.; Zhang, J.; Colón-Mercado, H.; Cuevas, F.; Peters, B.; Greenway, S.; Zidan, R.; Latroche, M. Li-driven electrochemical conversion reaction of AlH_3, $LiAlH_4$, and $NaAlH_4$. *J. Phys. Chem. C* **2015**, *119*, 4666–4674. [CrossRef]
279. Nakamura, Y.; Fossdal, A.; Brinks, H.W.; Hauback, B.C. Characterization of Al–Ti phases in cycled TiF_3-enhanced Na_2LiAlH_6. *J. Alloys Compd.* **2006**, *416*, 274–278. [CrossRef]
280. Ma, X.Z.; Martinez-Franco, E.; Dornheim, M.; Klassen, T.; Bormann, R. Catalyzed Na_2LiAlH_6 for hydrogen storage. J. Alloys Compd. **2005**, *404–406*, 771–774. [CrossRef]
281. Fonneløp, J.E.; Løvvik, O.M.; Sørby, M.H.; Brinks, H.W.; Hauback, B.C. Adjustment of the decomposition path for Na_2LiAlH_6 by TiF_3 addition. *Int. J. Hydrogen Energy* **2011**, *36*, 12279–12285. [CrossRef]
282. Løvvik, O.M.; Swang, O. Crystal structures and electronic structures of alkali aluminohexahydrides from density functional calculations. *J. Alloys Compd.* **2005**, *404–406*, 757–761. [CrossRef]
283. Løvvik, O.M.; Swang, O. Structure and stability of possible new alanates. *Europhys. Lett.* **2004**, *67*, 607–613. [CrossRef]
284. Brinks, H.W.; Huback, B.C.; Jensen, C.M.; Zidan, R. Synthesis and crystal structure of Na_2LiAlD_6. *J. Alloys Compd.* **2005**, *392*, 27–30. [CrossRef]
285. Liu, Y.; Wang, F.; Cao, Y.; Gao, M.; Pan, H.; Wang, Q. Mechanisms for the enhanced hydrogen desorption performance of the TiF_4-catalyzed Na_2LiAlH_6 used for hydrogen storage. *Energy Environ. Sci.* **2010**, *3*, 645–653. [CrossRef]
286. Rönnebro, E.; Majzoub, E.H. Crystal structure, Raman spectroscopy and Ab initio calculations of a new bialkali alanate K_2LiAlH_6. *J. Phys. Chem. B* **2006**, *110*, 25686–25691. [CrossRef] [PubMed]
287. Bulychev, B.M.; Semenenko, K.N.; Bitcoev, K.B. Synthesis and investigation of complex compounds of magnesium alanate. *Koord Khim* **1978**, *4*, 374–380.
288. Grove, H.; Brinks, H.W.; Heyn, R.H.; Wu, F.-J.; Opalka, S.M.; Tang, X.; Laube, B.L.; Hauback, B.C. The structure of $LiMg(AlD_4)_3$. *J. Alloys Compd.* **2008**, *455*, 249–254. [CrossRef]
289. Grove, H.; Løvvik, O.M.; Huang, W.; Opalka, S.M.; Heyn, R.H.; Hauback, B.C. Decomposition of lithium magnesium aluminum hydride. *Int. J. Hydrogen Energy* **2011**, *36*, 7602–7611. [CrossRef]
290. Grove, H.; Brinks, H.W.; Løvvik, O.M.; Heyn, R.H.; Hauback, B.C. The crystal structure of $LiMgAlD_6$ from combined neutron and synchrotron X-ray powder diffraction. *J. Alloys Compds.* **2008**, *460*, 64–68. [CrossRef]
291. Hudson, M.S.L.; Raghubanshi, H.; Pukazhselvan, D.; Srivastava, O.N. Effects of helical GNF on improving the dehydrogenation behavior of $LiMg(AlH_4)_3$ and $LiAlH_4$. *Int. J. Hydrogen Energy* **2010**, *35*, 2083–2090. [CrossRef]

292. Liu, D.M.; Qian, Z.X.; Si, T.Z.; Zhang, Q.A. Synthesis, crystal structure and thermal decomposition of $LiCa(AlH_4)_3$. *J. Alloys. Compd.* **2012**, *520*, 202–206. [CrossRef]
293. Wang, H.C.; Zheng, J.; Wu, D.H.; Wei, L.T.; Tang, B.Y. Crystal feature and electronic structure of novel mixed alanate $LiCa(AlH_4)_3$: A density functional theory investigation. *RSC Adv.* **2015**, *5*, 16439–16445. [CrossRef]
294. Sato, T.; Takagi, S.; Deledda, S.; Hauback, B.C.; Orimo, S.I. Extending the applicability of the Goldschmidt tolerance factor to arbitrary ionic compounds. *Sci. Rep.* **2016**, *6*, 23592. [CrossRef]
295. Sørby, M.H.; Brinks, H.W.; Fossdal, A.; Thorshaung, K.; Hauback, B.C. The crystal structure and stability of K_2NaAlH_6. *J. Alloys Compd.* **2006**, *415*, 284–287. [CrossRef]
296. Bhatnagar, A.; Pandey, S.K.; Shahi, R.R.; Hudson, M.S.L.; Shaz, M.A.; Srivastava, O.N. Synthesis, characterization and hydrogen sorption studies of mixed sodium-potassium alanate. *Cryst. Res. Technol.* **2013**, *48*, 520–531. [CrossRef]
297. Pan, R.K.; Yao, J.G.; Ji, R.L.; Liu, W.W.; Yin, D.F. First principles study on elastic and electronic properties of bialkali alanates $M_2M'AlH_6$. *Int. J. Hydrogen Energy* **2018**, *43*, 3862–3870. [CrossRef]
298. Fonneløp, J.E.; Corno, M.; Pinatel, E.R.; Sørby, M.H.; Ugliengo, P.; Baricco, M.; Hauback, B.C. Experimental and computational investigations on the AlH_3/AlF_3 system. *J. Alloys Compd.* **2011**, *509*, 10–14. [CrossRef]
299. Yin, L.C.; Wang, P.; Kang, X.D.; Sun, C.H.; Cheng, H.M. Functional anion concept: Effect of fluorine anion on hydrogen storage of sodium alanate. *Phys. Chem. Chem. Phys.* **2007**, *9*, 1499–1502. [CrossRef] [PubMed]
300. Eigen, N.; Bösenberg, U.; Bellosta von Colbe, J.; Jensen, T.R.; Cerenius, Y.; Dornheim, M.; Klassen, T.; Bormann, R. Reversible hydrogen storage in NaF-Al composites. *J. Alloys Compd.* **2009**, *477*, 76–80. [CrossRef]
301. Brinks, H.W.; Fossdal, A.; Hauback, B.C. Adjustment of the stability of complex hydrides by anion substitution. *J. Phys. Chem. C* **2008**, *112*, 5658–5661. [CrossRef]
302. Nakamoto, K. *Infrared and Raman Spectra of Inorganic and Coordination Compounds. Part A: Theory and Applications in Inorganic Chemistry*; John Wiley & Sons, Inc.: Hoboken, NJ, USA, 2009; pp. 192–236.
303. Biliskov, N. Infrared spectroscopy as a convenient tool for investigation of hydrogen sorption mechanisms and bonding in complex hydrides. In *Infrared Spectroscopy: Theory, Advances and Development*; Cozzolino, D., Ed.; Nova Science Publishers: Hauppauge, NY, USA, 2014; pp. 1–42.
304. Zavorotynska, O.; Corno, M.; Damin, A.; Spoto, G.; Ugliengo, P.; Barico, M. Vibrational properties of MBH_4 and MBF_4 crystals (M = Li, Na, K): A combined DFT, infrared, and Raman study. *J. Phys. Chem. C* **2011**, *115*, 18890–18900. [CrossRef]
305. Tsumuraya, T.; Shishidou, T.; Oguchi, T. Ab initio study on the electronic structure and vibration modes of alkali and alkaline-earth amides and alanates. *J. Phys.* **2009**, *21*, 185501. [CrossRef]
306. Parker, S.F. Spectroscopy and bonding in ternary metal hydride complexes-potential hydrogen storage media. *Coord. Chem. Rev.* **2010**, *254*, 215–234. [CrossRef]
307. Huheey, J.E.; Keiter, E.A.; Keiter, R.L. *Inorganic Chemistry. Principles of Structure and Reactivity*; Harper Collins: New York, NY, USA, 1993; pp. 187–190.
308. Li, L.; Qiu, F.; Wang, Y.; Xu, Y.; An, C.; Liu, G.; Jiao, L.; Yuan, H. Enhanced hydrogen storage properties of TiN–$LiAlH_4$ composite. *Int. J. Hydrogen Energy* **2013**, *38*, 3695–3701. [CrossRef]
309. Zang, L.; Cai, J.; Zhao, L.; Gao, W.; Liu, J.; Wang, Y. Improved hydrogen storage properties of $LiAlH_4$ by mechanical milling with TiF_3. *J. Alloys Compd.* **2015**, *647*, 756–762. [CrossRef]
310. Ares Fernandez, J.R.; Aguey-Zinsou, F.; Elsaesser, M.; Ma, X.Z.; Dornheim, M.; Klassen, T.; Bormann, R. Mechanical and thermal decomposition of $LiAlH_4$ with metal halides. *Int. J. Hydrogen Energy* **2007**, *32*, 1033–1040. [CrossRef]
311. Liu, S.S.; Sun, L.-X.; Zhang, Y.; Xu, F.; Zhang, J.; Chu, H.-L.; Fan, M.-Q.; Zhang, T.; Song, X.-Y.; Grolier, J.P.E. Effect of ball milling time on the hydrogen storage properties of TiF_3-doped $LiAlH_4$. *Int. J. Hydrogen Energy* **2009**, *34*, 8079–8085. [CrossRef]
312. Li, Z.; Zhai, F.; Wan, Q.; Liu, Z.; Shan, J.; Li, P.; Volinsky, A.A.; Qu, X. Enhanced hydrogen storage properties of $LiAlH_4$ catalyzed by $CoFe_2O_4$ nanoparticles. *RSC Adv.* **2014**, *4*, 18989–18997. [CrossRef]
313. Li, Z.; Li, P.; Wan, Q.; Zhai, F.; Liu, Z.; Zhao, K.; Wang, L.; Lü, S.; Zou, L.; Qu, X.; et al. Dehydrogenation improvement of $LiAlH_4$ catalyzed by Fe_2O_3 and Co_2O_3 nanoparticles. *J. Phys. Chem. C* **2013**, *117*, 18343–18352. [CrossRef]
314. Cheng, H.; Xu, L.; Fan, X.; Huang, X.; Liu, J.; Yan, K.; Zhang, Y. Synergistic effects played by CMK-3 and NbF_5 Co-additives on de/re-hydrogenation performances of $NaAlH_4$. *Int. J. Hydrogen Energy* **2018**, *43*, 9705–9712. [CrossRef]

315. Huang, Y.; Li, P.; Wan, Q.; Zhang, J.; Li, Y.; Li, R.; Dong, X.; Qu, X. Improved dehydrogenation performance of $NaAlH_4$ using $NiFe_2O_4$ nanoparticles. *J. Alloys Compd.* **2017**, *709*, 850–856. [CrossRef]
316. Kumar, S.; Kain, V.; Kojima, Y. Remarkably improved dehydrogenation of $ZrCl_4$ doped $NaAlH_4$ for hydrogen storage application. *Int. J. Hydrogen Energy* **2017**, *42*, 15299–15307. [CrossRef]
317. Wan, Q.; Li, P.; Li, Z.; Zhao, K.; Liu, Z.; Wang, L.; Zhai, F.; Qu, X.; Volinsay, A.A. $NaAlH_4$ dehydrogenation properties enhanced by $MnFe_2O_4$ nanoparticles. *J. Power Sources* **2014**, *248*, 388–395. [CrossRef]
318. Gomes, S.; Renaudin, G.; Hagemann, H.; Yvon, K.; Sulic, M.P.; Jensen, C.M. Effects of milling, doping and cycling of $NaAlH_4$ studied by vibrational spectroscopy and X-ray diffraction. *J. Alloys Compd.* **2005**, *390*, 305–313. [CrossRef]
319. Rafi-Ud-Din; Qu, X.; Li, P. Superior catalytic effects of Nb_2O_5, TiO_2, and Cr_2O_3 nanoparticles in improving the hydrogen sorption properties of $NaAlH_4$. *J. Phys. Chem.* **2012**, *116*, 11924–11938. [CrossRef]
320. Franke, I.; Flick, T.; Bauer, H. Hydrogen desorption kinetics of $CeCl_3$-doped sodium aluminum hydride compacts measured by parallel in-situ FTIR-ATR-spectroscopy and gravimetry. *Int. J. Hydrogen Energy* **2015**, *40*, 4175–4183. [CrossRef]
321. Bureau, J.C.; Amri, Z.; Létoffé, J.M. Etude comparative des hexahydrido-et des hexadeuteridoaluminates de lithium et de sodium. I-spectres Raman et infrarouge de Li_3-et Na_3AlH_6, et Li_3AlD_6. *Mat. Res. Bull.* **1989**, *24*, 23–31. [CrossRef]
322. Amama, P.B.; Grant, J.T.; Shamberger, P.J.; Voevodin, A.A.; Fisher, T.S. Improved dehydrogenation properties of Ti-doped $LiAlH_4$: Role of Ti precursors. *J. Phys. Chem. C* **2012**, *116*, 21886–21894. [CrossRef]
323. Ismail, N.; Aboud, A.A.; Hamdel-Din, A.; Farghali, A.A.; Khedr, M.H. Influence of LiH and Ti metal additives on milling $LiAlH_4$ compound. *Int. J. Adv. Res.* **2014**, *2*, 307–316.
324. Wu, X.; Wang, X.; Cao, G.; Li, S.; Ge, H.; Chen, L.; Yan, M. Hydrogen storage properties of $LiBH_4$–Li_3AlH_6 composites. *J. Alloys Compd.* **2012**, *517*, 127–131. [CrossRef]
325. Ismail, M.; Zhao, Y.; Yu, X.; Dou, S.X. Improved hydrogen storage property of $LiAlH_4$ by milling with carbon based additives. *Int. J. Electroact. Mater.* **2013**, *1*, 13–22.
326. Halim Yap, F.A.; Ali, N.A.; Idris, N.H.; Ismail, M. Catalytic effect of $MgFe_2O_4$ on the hydrogen storage properties of Na_3AlH_6–$LiBH_4$ composite system. *Int. J. Hydrogen Energy* **2018**, *43*, 20882–20891. [CrossRef]
327. Franke, I.; Bauer, H.D.; Scheppat, B. *OCM 2013. Optical Characterization of Materials. Conference Proceedings*; Beyerer, J., Puente León, F., Längle, T., Eds.; KIT Scientific Publishing: Karlsruhe, Germany, 2013; pp. 78–88.
328. Züttel, A. Hydrogen Storage Methods. *Naturwissenschaften* **2004**, *91*, 157–172. [CrossRef]
329. Yoshino, M.; Komiya, K.; Takahasi, Y.; Shinzato, Y.; Yukawa, H.; Morinaga, M. Nature of the chemical bond in complex hydrides, $NaAlH_4$, $LiAlH_4$, $LiBH_4$ and $LiNH_2$. *J. Alloys Compds.* **2005**, *404–406*, 185–190. [CrossRef]
330. Claudy, P.; Bonnetot, B.; Letoffe, M.J.; Turk, G. Determination des constantes thermodynamiques des hydrures simples et complexes de l'aluminium. IV. Enthalpie de formation de $LiAlH_2$ et Li_3AlH_6. *Thermochim. Acta.* **1978**, *27*, 213–221. [CrossRef]
331. Smith, M.B.; Bass, G.E., Jr. Heats and free energies of formation of the alkali aluminum hydrides and of cesium hydride. *J. Chem. Eng. Data* **1963**, *8*, 342–346. [CrossRef]
332. Sulaiman, N.N.; Ismail, M. Catalytic effect of $SrFe_{12}O_{19}$ on the hydrogen storage properties of $LiAlH_4$. *Int. J. Hydrogen Energy* **2017**, *42*, 19126–19134. [CrossRef]
333. Cai, J.; Zang, L.; Zhao, L.; Liu, J.; Wang, Y. Dehydrogenation characteristics of $LiAlH_4$ improved by in-situ formed catalysts. *J. Energy Chem.* **2016**, *25*, 868–873. [CrossRef]
334. Opalka, S.M.; Anton, D.L. First principles study of sodium–aluminum–hydrogen phases. *J. Alloys Compd.* **2003**, *356–357*, 486–489. [CrossRef]
335. Lee, B.-M.; Jang, J.-W.; Shim, J.-H.; Cho, Y.W.; Lee, B.-J. Thermodynamic assessment of the NaH ↔ Na_3AlH_6 ↔ $NaAlH_4$ hydride system. *J. Alloys Compd.* **2006**, *424*, 370–375. [CrossRef]
336. Fan, X.; Xiao, X.; Chen, L.; Han, L.; Li, S.; Ge, H.; Wang, Q. Hydriding-dehydriding kinetics and the microstructure of La-and Sm-doped $NaAlH_4$ prepared via direct synthesis method. *Int. J. Hydrogen Energy* **2011**, *36*, 10861–10869. [CrossRef]
337. Grochala, W.; Edwards, P.P. Thermal decomposition of the non-interstitial hydrides for the storage and production of hydrogen. *Chem. Rev.* **2004**, *104*, 1283–1315. [CrossRef]

338. Palumbo, M.; Torres, F.J.; Ares, J.R.; Pisani, C.; Fernandez, J.F.; Baricco, M. Thermodynamic and ab initio investigation of the Al–H–Mg system. *Comput. Coupling Phase Diagr. Thermochem.* **2007**, *31*, 457–467. [CrossRef]
339. Cuevas, F. *Advanced Materials and Technologies*; Cuevas, F., Burzo, E., Eds.; Springer: Berlin/Heidelberg, Germany, 2018; pp. 252–260.